The

Geophysical Journal

of the

Royal Astronomical Society

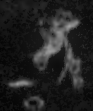

Volume 6 No. 1 December 1961

Published and Sold by the
Royal Astronomical Society
Burlington House, London, W.1, England

Price £1. 12s (US$ 5) Subscription for volume £6. (US$ 18)

The Geophysical Journal
of the Royal Astronomical Society

Editor

S. K. Cook, M.A., Ph.D., F.R.A.S., F.G.S.
(*Geophysical Secretary*)
National Physical Laboratory,
Teddington, Middx.

T. F. Gaskell,
M.A., Ph.D., F.R.A.S.
British Petroleum Company,
London.

The following papers have been accepted for publication:

F. H. Hibberd, An analysis of the position of the Earth's magnetic pole in the geological past.

B. A. Ostenso, Note on the paper of F. F. Evison, C. E. Ingham, H. H. Orr & J. H. Le Fort, "Thickness of the Earth's crust in Antarctica and the surrounding oceans".

D. Van Hilten, A devisting permian pole from rocks in Northern Italy.

J. A. Hudson, Love waves in a heterogeneous medium.

J. A. Miller, K. Shibata & M. Munson, The potassium–argon age of the lava of Killerton Park, Exeter.

J. A. Miller, The potassium–argon age of the Shiddaw and Eskdale granites.

C. Bull, E. Irving & I. Willis, Further palaeomagnetic results from South Victoria Land.

G. D. Garland & D. H. Langon, Heat flow in Western Canada.

E. Irving, Palaeomagnetic directions and pole positions, IV.

E. W. Carpenter, R. A. Savill & J. K. Wright, The dependence of seismic signal amplitudes on the size of underground explosions.

G. E. Cook, Luni-solar perturbations of the orbit of an earth satellite.

R. A. Savill, E. W. Carpenter & J. K. Wright, The derivation and solution of indicator equations for seismometer–galvanometer combinations including the effect of seismometer inductance.

C. W. F. Everitt & J. A. Clegg, A new field test of palaeomagnetic stability.

R. L. Wilson, The palaeomagnetic history of a doubly-baked rock.

W. A. Fowler, J. L. Greenstein & F. Hoyle, Nucleosynthesis during the early history of the solar system.

B. A. Bolt & A. Marussi, Eigenvibrations of the Earth observed at Trieste.

W. D. Parkinson, The influence of continents and oceans on geomagnetic variations.

M. Båth, Direction of approach of microseisms.

I. Abubakar, Disturbance due to a line source in a semi-infinite transversely isotropic elastic medium.

K. O. Whitehead & J. A. Jacobs, Oscillations of the Earth's outer atmosphere and micropulsations.

J. C. Brandsberg, R. J. Wold & T. S. Laughon, Gravity base stations in Antarctica.

K. R. Nag, Disturbance due to shearing-stress discontinuity in a semi-infinite elastic medium.

The Geophysical Journal

of the

ROYAL ASTRONOMICAL SOCIETY

Vol. 6 No. 1 December 1961

Mountain-building Movement in Japan and its Vicinity

Naoto Kawai

(Received 1960 May 25)

Summary

By means of the depth-indicator established on a basis of pressure-temperature equilibrium relationship of ferromagnetic minerals, the depths at which plutonic rocks have been formed are estimated in the Japanese Islands and the surrounding area.

Upheavals of landmasses derived therefrom show that the amount of the upheaval reaches more than 20 km in some places in Japan and is very small in the Asian Continent.

Comparison of the data of gravity anomalies, geological structure and upheavals makes it possible to discuss the mountain-building movement and its mechanism in these regions.

1. Introduction

There are two streams in the recent progress on rock-magnetism in Europe and in Australia: one is the evaluation of continental mass movement invoked by Clegg & others (1956, 1957) and the other, the consolidation of the polar wandering hypothesis suggested by Creer (1957) and Runcorn & others (1956). As suggested by these authors, the comparison of the remanent magnetization of rocks from North America and Europe makes it possible to connect these two subjects with each other. According to their interpretation, a westward drift of the American continent relative to Europe commenced in Precambrian times and the pole position of the Earth was in the Pacific Ocean in Palaeozoic times (Creer & others 1958; Irving 1958a).

During the time in which these advances have been made in Britain and Australia, our group has made another kind of study on rock-magnetism from which the mountain-building mechanism can be clarified. It was found that our

studies bear such a close relationship to the above-mentioned results that the writer would like to offer several suggestions which seem to relate these ideas.

2. Estimation of depth at which plutonic rocks were formed

Recently the author (1957) studied the effect of pressure and temperature upon the formation of ferromagnetic mineral solid-solutions contained in rocks (magnetite-ulvöspinel and hematite-ilmenite solid-solutions) and proposed the $P-T$ equilibrium relationship of these minerals. His results are shown in Figure 1 (a) and (b). As illustrated in the diagrams, the Ti-concentration (or Curie point*)

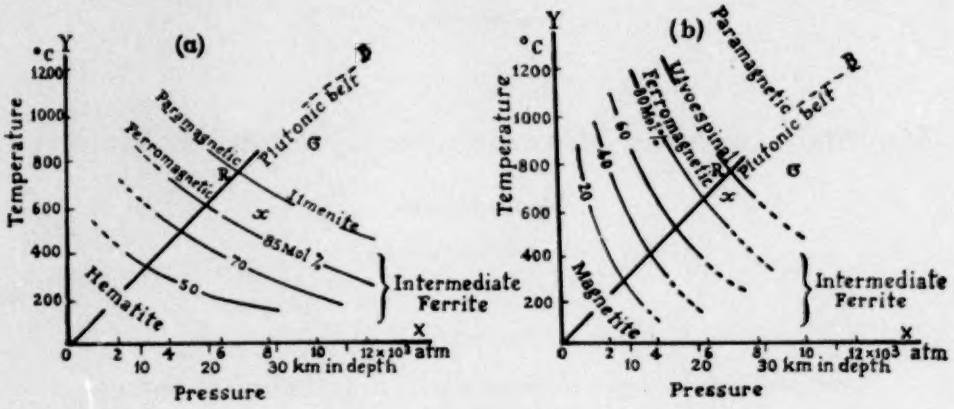

FIG. 1.

(a) $P-T$ equilibrium diagram of ilmenite-hematite solid-solution series. % shows the molecular percentage of ilmenite in the solid-solution.

(b) $P-T$ equilibrium diagram of ulvöspinel-magnetite solid-solution series. % shows the molecular percentage of ulvöspinel in the solid-solution.

in these solid-solutions increases as the pressure and temperature at which the minerals have been formed are increased. This phenomenon was common in normal plutonic rocks which were classified gabbro, diorite and grano-diorite. A line *OB* in the diagram is drawn in such a way that all points on it represent the P—T conditions inside the lithosphere estimated by assuming the average geothermal gradient and the gravitational load of the rock column in the upper part of the Earth's crust. When we draw the section of these diagrams along the line *OB*, the relation of the Ti-contents (or Curie point) *vs* depth from the Earth's surface (or equivalent P—T condition) is to be that shown in Figure 2. Therefore, if enough care is paid to choose suitable rocks in order to get an accurate result of determining depth and when either Curie point or chemical composition of the above-said minerals in a plutonic rock is determined, the curve in Figure 2 will indicate the depth at which rock was initially formed.

We have sampled a number of plutonic rocks from various localities in Japan. By using the above-mentioned Curie point method, depth-estimation has been carried out at various localities in Japan and the surrounding area. The results so far obtained are shown in Table 1 and Figure 3.

* Ti-contents in these minerals can be decided by measuring their Curie point.

Table 1

Locality	*Estimated Depth*	*Locality*	*Estimated Depth*
	km		km
Pokchinsan (Korea)	1·2	Tongre (Korea)	3
Ogi (Saga)	23	Yamaga (Kumamoto)	21
Osada (Shimane)	17	Nagahama (Ehime)	23
Unomachi (Ehime)	23	Besshi (Ehime)	23
Shodoshima (Okayama)	22	Awajishima (Hyogo)	21
Kibi (Okayama)	24	Yakuno (Kyoto)	24
Maizuru (Kyoto)	23	Sakurai (Nara)	23
Kasagi (Nara)	23	Okitsu (Mie)	24
Toba (Mie)	22	Tomioka (Shizuoka)	25
Kofu (Yamanashi)	25	Funabiki (Fukushima)	21
Arizitsu (Fukushima)	12	Gorintoge (Iwate)	7
Omoto (Iwate)	7	Miyamori (Iwate)	9
Erimo (Hokkaido)	25	Karikachi (Hokkaido)	25
Okushibetsu (Hokkaido)	23	Nemuro (Hokkaido)	9

3. The mountain-building mechanism of the Japanese Islands inferred from the depth of plutonic rocks

Assuming that the depth of formation of plutonic rocks distributed at various localities be determined, we can reasonably infer how and when the Earth's crust in that area was deformed. Since we sampled these plutonic rocks from intensely eroded and therefore from nearly horizontal land surface, the figures determined for the depth indicate the amount of vertical upheaval, i.e. the extent of erosion as it differs from place to place in this area.

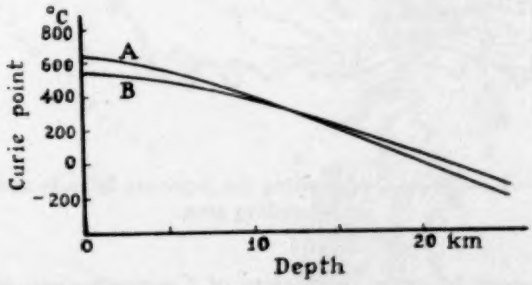

FIG. 2.—Variation of Curie point of ferromagnetic minerals with depth.
(a) for the series of ilmenite-hematite solid-solution.
(b) for the series of ulvöspinel-magnetite solid-solution.

We can see in the figure, that the upheavals are very small in Korea but significantly large along the Median-line in Japan. The values become greater approaching the Japanese Islands from the west and then smaller towards the Pacific Ocean, resulting in maxima upheavals here and there in Japan. There maxima can be seen at the Kyushu Island, the Setouchi Inland-Sea area around Hiroshima, the area around Lake Biwa and the central mountain zone of the Japanese Alps. The upheavals are also great in the area of the Hidaka mountain zone of Hokkaido Island.

Since geological evidence suggests that these rocks are late Palaeozoic in age, the contour lines showing equal upheaval represent the topography of the crustal deformation which has occurred since this time.

The writer used plutonic rocks with ferrite whose TiO_2-concentration is in the range 5–50 per cent as test samples. When the Ti-concentration is out of this range the writer's P—T diagram of titaniferous ferrites is not strictly valid, and his depth scale is unsuitable.

The extent of the erosion subsequently occurring at the above-mentioned maxima is very great and, when averaged out, amounts to 24 km. The total mass of land eroded and probably transported into the Pacific Ocean or the Sea of Japan works out to be more than $1{\cdot}1 \times 10^{16}$ tons. The contour lines in the figure show the topography of the mountains if the amount of erosion is very small.

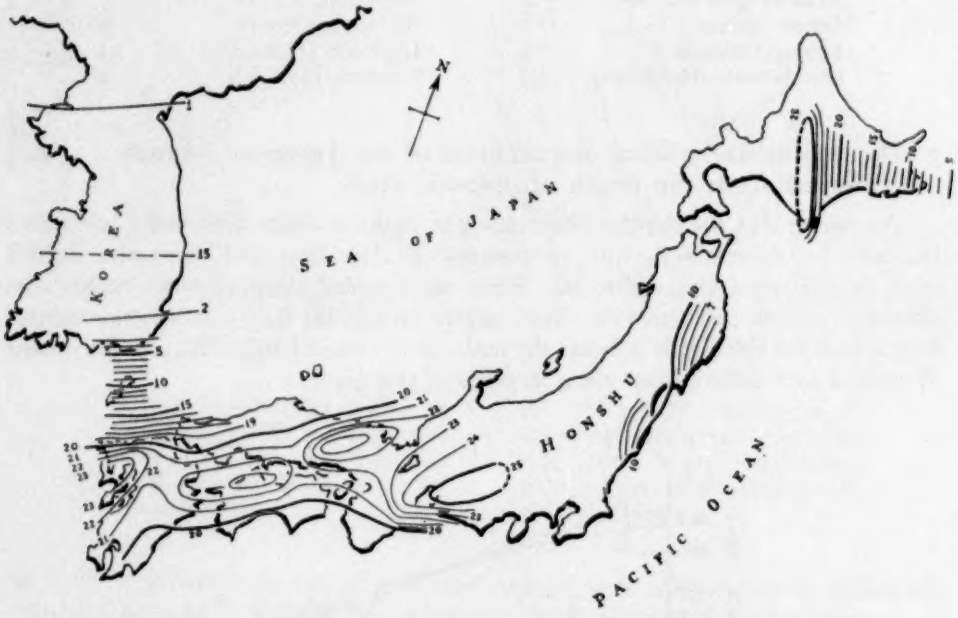

FIG. 3.—Iso-upheaval map along the Japanese Islands and the surrounding area.

During the Annual Meeting of Society of Geomagnetism and Geoelectricity of Japan held in 1958 in Tokyo, when the writer first presented his original map similar to Figure 3, Miyabe of Geographical Survey pointed out a marked resemblance between the configurations of the Bouguer gravity anomaly contour lines as presented by Tsuboi & others (1953/56) and those of the contour lines of the upheavals. Where the maxima of the upheavals appear, there exist fairly large negative gravity anomalies, as shown in Figure 4. This seems to indicate a large mass deficiency beneath the place where the mountain once existed.

As to the negative gravity anomaly in the mountainous region, many authors have focussed their attention on the static model insisting on the necessity for a plane of compensation in the mantle. At the depth of this plane the excess gravity load due to the mountain would be compensated by the mass deficiency beneath. Some authors in interpreting the gravity anomaly found in Japan have adopted

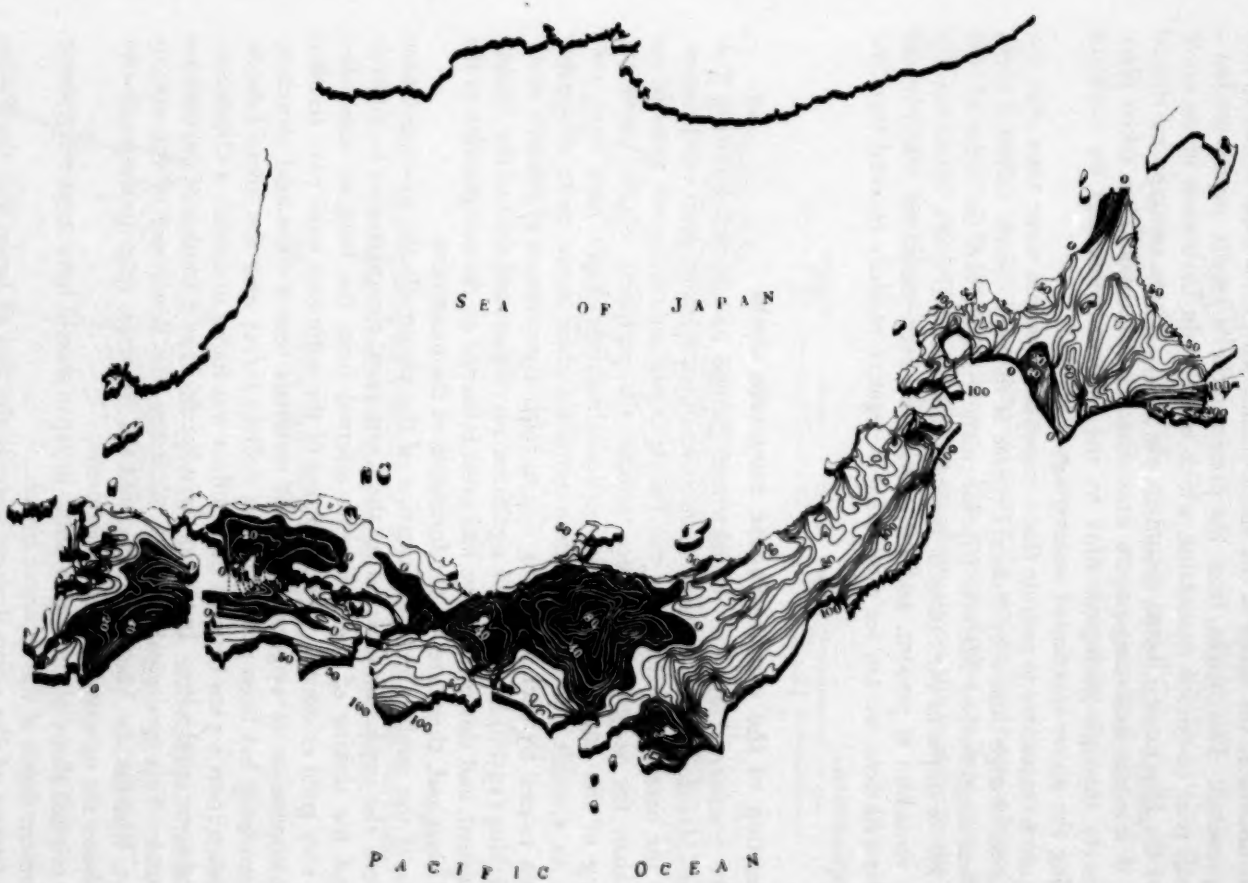

FIG. 4.—Isogal map in Japan.
Numbers in the figure show the amounts of Bouguer anomalies in mgal and black and white lines represent positive and negative anomalies respectively (after Tsuboi).

this kind of compensation and have obtained the depth of the isostasy. Another author has suggested that the negative Bouguer anomaly in the mountainous region in the Middle Honshu Island is an isostatic anomaly.

All these authors, however, in their calculations assumed the present height of the mountains as the cause of the above-mentioned excess mass which should be compensated. This height, from the present writer's results, represents but a very small relic of eroded mountains, which once might have risen up to noble height as the Himalaya–Tibetan mountains do today. These assumptions should be true if isostatic balancing occurs immediately after erosion has taken place continuously through geological time to the present. Virtually no evidence supporting the above-mentioned assumption is known.

It is more reasonable to assume that compensation occurs some time after the surface mass change caused by erosion because of the very viscous nature of rocks as has been suggested by Meinesz (the kinematic viscosity is of the order of 10^{20} c.g.s.). For example in the Setouchi Inland-Sea area and Kyushu Island there is no high mountain at present, and the gravity has been measured nearly at sea level. Nevertheless, we can see a remarkable negative anomaly resulted from the overcompensation.

4. Formation of the circum-Pacific mountain chain

If the continental drift of America and Europe had occurred during Precambrian–Mesozoic times, then the Pacific Ocean experienced great compression. Because the basement rocks under the Pacific Ocean and continental material are harder than the sediment deposited around the periphery of the continent, squeezing of the latter sediment in vertical directions might have been very severe. As a result, the circum-Pacific mountain chain could quite reasonably have been caused by such squeezing due to relative movement of the two continents. Irving (1958b) has reported significant north-eastward drift of the Australian continent, and this would have had great influence on the compression of the Pacific Ocean and, therefore, on the formation of the mountains.

Thus, if the models for the formation of the circum-Pacific mountain zone are correct, the upheavals revealed by the Curie point measurements in plutonic rocks and the sinking of the sediments inferred from the Bouguer anomalies provide very good evidence. The squeezing of the sediments must have resulted in the compression of original basement materials into a sinusoidal structure. Such a tendency has been proved by the drilling survey near the Bikini Islands. A core taken from 1·5 km beneath the sea floor was found to contain a Cretaceous basalt and some coral relics. In the northern Pacific Area, a number of guyots have been found. This geological evidence illustrates the downwarp of the oceanic basement, whereas the Mariana folding and the Albatross ridge in the south-east Pacific shows the upwarping of the basements.

The original shape of the upper bulge in Japan should have some relationship to the present depth of the Japanese trench.

The tangent of the original slope towards the Sea of Japan and the Pacific Ocean might have been reduced by the transportation of the eroded mass from the continental land and its deposition on the original slope (see the schematic diagram Figure 5 illustrating the transfer of sediments). Thus the motive force of the Earth's crustal movement occurring in Japan in the late Palaeozoic times was probably caused by the compression of the Pacific basement.

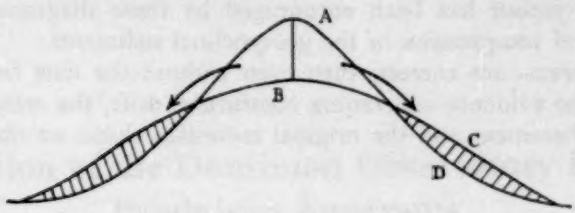

FIG. 5.—Transportation of land mass to the oceans by erosion.
A: original land mass. B: present land surface.
C: present slope. D: original slope.

In Figure 6 (a) and (b), geological structures which have been inferred from a geological survey in Japan are shown. This interpretation has been made by Shiki (1960) and two sections are given, one of which shows the geology at the middle Permian and the other that at the late Permian.

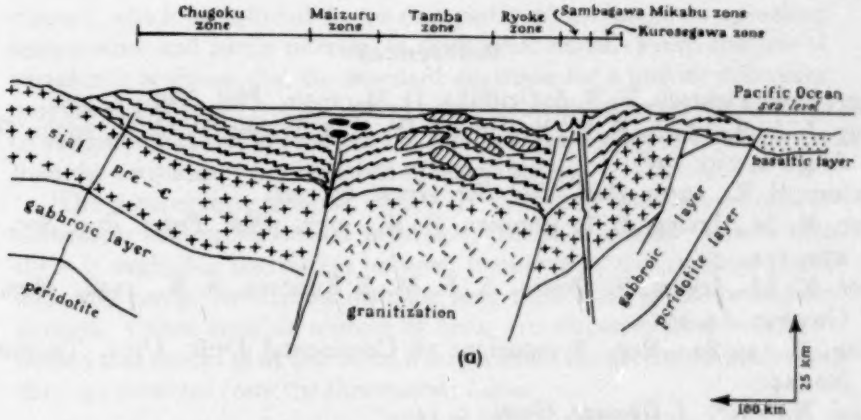

FIG. 6(a).—Geological structure at the middle Permian mountain-building movement of the Japanese Islands (after Shiki).

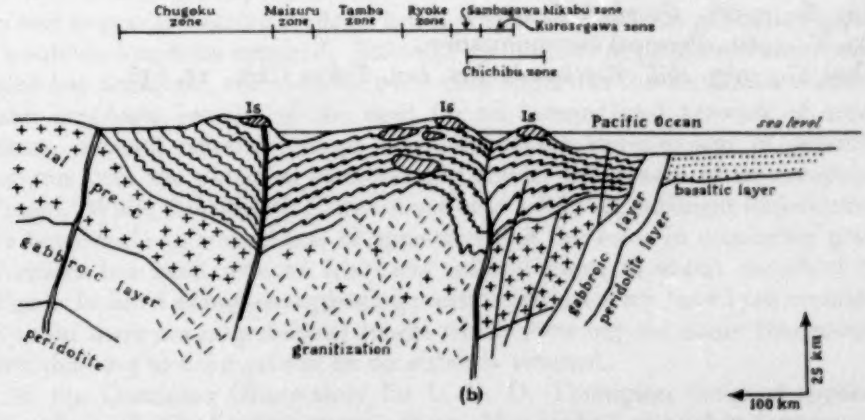

FIG. 6(b).—Geological structure at the upper Permian mountain-building movement of the Japanese Islands (after Shiki).

The present author has been encouraged by these diagrams because they suggest downward compression of the geosynclinal sediments.

If these diagrams are correct, then even without the data from the gravity anomalies and the evidence concerning continental drift, the compression of the Pacific Oceanic basement and the original mountain shape we observed become consistent.

5. Acknowledgments

The author wishes to thank Professor N. Kumagai for his interest and advices throughout the study. He is also indebted to Mr T. Shiki for his valuable discussions and suggestions on the geological structure of the Japanese Islands.

Geological Institute,
Kyoto University,
Japan:
1960 *May.*

References

Clegg, J. A., Deutsch, E. R. & Griffiths, D. H., 1956. *Phil. Mag.*, **1**, 419.

Clegg, J. A., Deutsch, E. R., Everitt, C. W. F. & Stubbs, P. H. S., 1957. *Phil. Mag.*, **6**, 219, 1957.

Runcorn, S. K., 1956. *Bull. Geol. Soc. Amer.*, **67**, 301.

Creer, K. M., Irving, E. & Runcorn, S. K., 1957. *Phil. Trans. Roy. Soc. A.*, **250**, 144.

Creer, K. M., Irving, E., Nairn, A. E. M. & Runcorn, S. K., 1958. *Ann. de Geophys.*, **14**, 492.

Irving, E., 1958a. Rep. Symposium of Continental Drift, Univ. Tasmania, No. 24.

Kawai, N., 1957. *J. Geomag. Geoel.*, **9**, 140.

Tsuboi, C., Jitsukawa, A., Tajima, H. & Okaad, A., 1935/56. *Bull. Earthquake Res. Inst. Tokyo Univ*: Part I (Suppl. 4), 1953; Parts II, III, IV and V, 1954; Part VI, 1955; Parts VIII and IX, 1956.

Irving, E., 1958b. *Geophys. J.*, **1**, 224.

Shiki, T., 1960. Personal communication.

Tsuboi, C., 1937. *Bull. Earthquake Res. Inst. Tokyo Univ.*, **15**, 636.

Evaluation of the Dominion Observatory Bronze Pendulum Apparatus

Angus C. Hamilton

(Received 1961 March 10)

Summary

From an analysis of all the observations on the pendulum pier in Ottawa over a three year period it is shown that there is a long term trend in the periods of the bronze pendulums; there is a gradual increase of some 4×10^{-7}s followed by a decrease of about the same amount which is believed to be due partly to a change in operating temperature and partly to creep in the bronze metal. From analysis of variance it is shown that the standard deviation for a gravity difference may be as low as 0·15 or as high as 0·58 mgal depending on the method of computation; this shows that the internal consistency is much better than the consistency between sets of observations.

The temperature control system is discussed and the record of thermistor resistances for one pendulum pair is presented to show that there is negligible correlation between temperature and residual errors and only partial correlation with the long term drift of the pendulum periods. Other possible sources of error are discussed and it is concluded that shocks of undetermined origin affect the pendulum each time they are removed from the thermostated case.

1. Introduction

When modern gravity meters capable of making sensitive measurements proportional to gravity became available it was at first assumed that pendulum apparatus would no longer be required. Although the number of pendulum observations needed has decreased, the need for pendulum apparatus has continued with even greater emphasis because of the need for an international network of control stations. Several research groups have undertaken development of pendulum apparatus with the objective of measuring gravity differences to an accuracy of 0·1 mgal. While this objective has not yet been achieved, sufficient improvements have been made in several sets of apparatus that the error in measuring gravity differences has been reduced from one milligal down to about one-third of a milligal. Isolated examples suggesting much better accuracy have been mentioned but so far there are no published results which show beyond doubt that accuracy better than 0·3 to 0·4 mgal can be consistently attained.

At the Dominion Observatory Dr L. G. D. Thompson designed apparatus with which to use bronze quarter-metre Mendenhall pendulums constructed about the turn of the century by the United States Coast and Geodetic Survey

Table 1

Observations on the pendulum pier

Room 8, Geophysical Laboratory, Dominion Observatory, Ottawa

(In units of 10^{-7} s, with 4 994 400·0 subtracted from each observation)

Pendulums 4–5		Pendulums 4–6		Pendulums 5–6	
Date	*S*	Date	*S*	Date	*S*
1956					
Oct 3	62·9	Oct 5	56·7	Oct 23	59·9
	59·5		55·0		60·3
	61·3		56·8		60·2
	60·6				
Oct 28	61·5	Oct 27	56·0	Oct 26	59·4
	65·0		57·7		58·6
	63·2		55·9		61·2
	64·1		59·6		60·9
Dec 3	61·7				
	62·7				
	61·6				
1957		Jan 9	60·9		
			60·6		
			60·0		
			61·4		
			60·1		
		Jan 11	64·2	Jan 18	58·4
			63·9		62·4
			63·1		66·2
			61·7		65·6
Mar 12	64·1	Mar 13	65·0	Mar 14	67·2
	65·5		64·5		69·3
	62·9		63·6		68·2
	63·8		64·3		68·3
Mar 21	63·5	Mar 20	64·4	Mar 19	68·5
	64·1		65·8		69·2
	65·1		64·1		68·7
	65·4		63·9		69·2

Pendulums 4–5		Pendulums 4–6		Pendulums 5–6	
Date	*S*	Date	*S*	Date	*S*
1957					
Apr 18	66·4	Apr 17	63·5	Apr 16	67·6
	65·8		65·9		67·8
	66·5		65·9		66·5
	67·5		65·1		69·1
	65·5				
May 23	66·3	May 26	69·0	May 27	67·8
	66·3		67·0		69·1
	66·5		67·0		70·4
				May 30	69·6
					70·6
					68·0
Jun 21	69·4	Jun 19	68·1	Jun 15	69·2
	67·3		68·8		71·4
	68·8		67·6		70·3
			67·3		
Jun 25	66·5	Jun 20	67·3	Jun 24	71·8
	67·8		67·5		70·8
	65·7		68·1		70·8
Jun 28	64·8			Jun 26	67·8
	64·7				69·3
	66·5				
				Jun 27	68·9
					69·9
Aug 2	67·5	Aug 3	66·1	Aug 4	71·0
	66·9		67·0		71·0
	66·0		66·5		70·9
1958					
Feb 21	58·7	Feb 24	63·0	Feb 25	69·0
	60·7		60·8		69·0
	57·8		61·4		70·0
Feb 28	68·2	Feb 27	67·7	Feb 26	69·2
	68·0		68·4		68·9
	68·7		68·5		70·2

Table 1—*continued*

Pendulums 4–5		Pendulums 4–6		Pendulums 5–6	
Date	*S*	Date	*S*	Date	*S*
1958					
Apr 9	63·8	Apr 10	65·0	Apr 11	68·8
	65·7		65·5		68·8
	62·8		68·0		69·2
		Apr 30	69·2	Apr 15	71·6
			71·0		71·6
			72·4		68·6
		May 1	68·7	Apr 16	70·8
			72·5		68·3
			72·0		70·2
		May 7	70·2		
			71·9		
			70·0		
Jun 20	69·0	Jun 17	68·8	Jun 18	71·6
	67·7		71·1		68·9
	66·6		71·4		70·2
Jun 26	66·8				
	67·8				
July 2	65·9	July 3	64·0	July 4	74·2
	65·6		67·5		70·7
	66·6		65·8		72·6
July 9	65·1	July 10	65·6	July 11	74·4
	66·4		64·5		74·0
	65·4		65·6		72·9
Sept 18	63·4	Sept 19	59·9	Sept 20	69·4
	62·1		60·4		70·2
	64·8		58·8		68·6
Oct 27	62·4	Nov 7	63·5	Oct 31	65·2
	64·4		64·2		67·9
	61·3		65·2		65·7
Nov 12	65·5	Nov 14	64·4	Nov 17	70·1
	68·1		65·0		69·4
	66·2		63·1		70·6

Pendulums 4–5		Pendulums 4–6		Pendulums 5–6	
Date	*S*	Date	*S*	Date	*S*
1959					
May 21	68·2	May 26	67·1	May 27	73·5
	68·5		66·5		72·4
	68·2		66·2		74·8
Jun 3	66·4	Jun 4	62·5	Jun 5	72·4
	66·4		63·6		73·4
	66·0		64·8		72·8
July 7	63·0	July 8	62·0	July 9	72·0
	62·2		63·4		71·4
	62·4		63·6		72·2
July 15	62·2	July 16	64·7	July 17	70·5
	62·4		63·0		72·4
	63·6		62·6		69·6
Oct 29	63·2	Oct 30	63·5	Nov 2	65·0
	63·1		62·2		65·6
	62·3		62·6		68·3
Nov 26	58·5	Nov 27	61·6	Nov 30	64·6
	58·9		60·0		65·8
	56·6		61·8		66·2
Dec 1	62·7				
	61·6				
	62·4				
	—		—		—
	$M = 64·6$		$M = 64·67$		$M = 68·76$
	$N = 89$		$N = 95$		$N = 93$

Swick 1921). Tests were begun in 1956 and since then the apparatus has been tested repeatedly on the pier in Ottawa and during three seasons in the field (Thompson 1959; Winter & Valliant 1960; Winter, Valliant & Hamilton, in press 1961). From the start of tests to the end of 1959, no significant changes in procedure were introduced, the only change in equipment was the addition of a second set of pendulums, Numbers 1, 2, and 3, early in 1958. Although there is no significant difference in the performance of the two sets of pendulums, this analysis is limited to observations with pendulums 4, 5, and 6 used throughout the period. These observations provide sufficient data for an objective evaluation of the accuracy of the equipment and of the performance of the temperature control system.

2. The observations

The observations that have been made with pendulums 4, 5 and 6 on the pier in the Geophysical Laboratory at Ottawa are listed in Table 1. This includes all the completed observations; inevitably many observations are classed incomplete due to poor time signals, voltage variations, recorder failure and other difficulties. The symbol, $\bar{S}$, is the conventional term for the mean period of two pendulums swung as a pair.

Usually three swings, each lasting about 50 minutes, were made with a pair of pendulums on one day, although in some of the early tests two, four or five swings were made on one day. At the end of a day the thermostated, evacuated case was opened, one pendulum of the pair was replaced by a new pendulum and the case was sealed, evacuated and allowed to reach thermal equilibrium overnight in preparation for observations the following day.

The average of the mean periods observed on one day is designated P, thus

$$P = (\sum_{i=1}^{n} \bar{S})/n \qquad (1)$$

in which n is the number of swings made in one day. The values of P corresponding to the data in Table 1 are plotted in Figure 1 along with histograms of their distribution.

In appraising the results of these and other pendulums there is always doubt as to the inherent accuracy of the apparatus. Usually some type of analysis for internal consistency is carried out and then some comparisons are made with previously measured and equally uncertain gravity differences. By this approach it is difficult, if not impossible, to arrive at an objective evaluation of the performance of any apparatus. On the other hand the large number of observations under similar conditions on one pier at various intervals over several years can be analysed independently and collectively to give a good picture of the performance of the bronze apparatus.

3. Analysis of the observations

(a) *Long term trend*

From the plot of the points in Figure 1 it was immediately apparent that there was a long term trend in the periods. As a first approximation to this trend the data for each pair were fitted to a curve of the form

$$P = aT^2 + bT + c \qquad (2)$$

in which P is the average period for the swings on one day,

T is time in weeks,

a, b, c are constants to be found.

The curves and equations are shown on Figure 1.

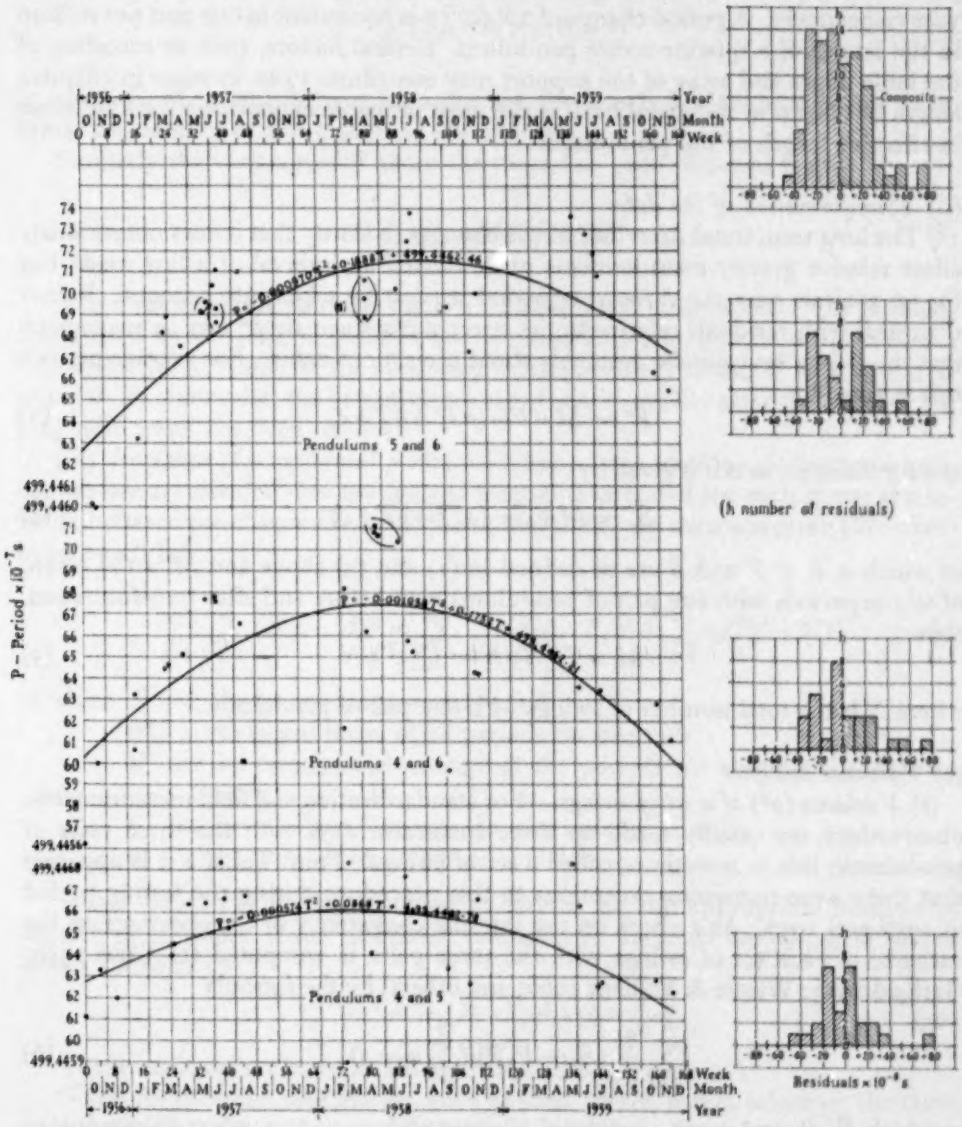

FIG. 1.—Observed periods, Ottawa, 1956–59 for pendulums 4, 5 and 6.

There is no evidence to show conclusively what is causing this long term drift in the pendulum periods. As discussed subsequently and illustrated in Figure 3, the readings of the thermistors that monitor the temperature in the pendulum case are changing gradually but whether this represents a change in temperature or a drift in thermistor characteristics is uncertain. Even if the temperature within

the case is changing as much as indicated by the lid thermistors there is still a drift of some 2×10^{-7} s per year to be explained. It is believed that most of the drift is due to creep in the bronze metal similar to changes that have been noted for length standards (Field 1939). Analysis of the standardization periods of pendulums 1, 2 and 3 for the years 1921 to 1927 (Miller 1929) shows that during those years there was a decrease in period averaging 6·41, 1·65 and $1{\cdot}41 \times 10^{-7}$ s per year respectively. A period change of 2×10^{-7} s is equivalent to one part per million in the length of a quarter-metre pendulum. Several factors, such as rounding of the knife edges and sway of the support may contribute to an increase in effective length but creep in the metal itself is the most probable explanation for a decrease in effective length of the pendulums.

(b) *Transformation of the data*

The long term trend described above changes so slowly that it does not seriously affect relative gravity measurements made during an interval of a few weeks but for an analysis over the three-year period it must be taken into account. Rather than deal with residuals relative to the curve a transformation* can be made such that the points have similar residuals about their mean value. For average periods this is given by

$$P' = M+P-(aT^2+bT+c) \tag{3}$$

and for mean periods it is given by

$$\bar{S}' = M+\bar{S}-(aT^2+bT+c) \tag{4}$$

in which a, b, c, P and $\bar{S}$ are as defined in (1) and (2) above and M is the mean, of all the periods with one pair of pendulums both before and after transformation, thus

$$M = (\sum \bar{S})/N = (\sum \bar{S}')/N \tag{5}$$

where N is the total number of swings with one pair of pendulums.

(c) *Variance analysis*

(i) *Variance* (σ^2) *of a set of swings.*—For standardization and field measurements, observations are usually made on three successive days with the three pairs of pendulums; this is sometimes called a set of swings. From Table 1 it is apparent that there were numerous exceptions to this procedure during the testing period in 1956 and 1957. As a check on the internal consistency of the observations the variance of each set of swings with the three pairs is computed (cf. Cook 1950; Garland 1953; Winter & Valliant 1960; and others) by the formula

$$[\sum_{k=1}^{3} \sum_{i=1}^{n} (\bar{S}_{ki}-P_k)^2]/(\sum_{k=1}^{3} n_k-3) \tag{6}$$

in which $\bar{S}$, P, and n are as defined above and $k = 1, 2, 3$ refers to pendulum pairs 4–5, 4–6 and 5–6.

By this method only one variance is obtained for the periods of the three pendulum pairs in each set. The average for all complete sets is listed in row *A*, Table 2. It follows that some of the incomplete sets of test swings are not included in this average.

* To illustrate the procedure an analytical method of transformation is described although a graphical method was actually used.

This variance is a useful criterion of the care with which the measurements were made and of the performance of the ancillary equipment but as will be shown later it is of negligible value as a measure of the precision of gravity measurements.

(ii) *Variance of observed periods.*—From the data in Table 1 the variance of each pair of pendulums was found by the formula

$$[\sum_{j=1}^{h} \sum_{i=1}^{n} (\bar{S}_{ji} - M)^2]/(N-1) \tag{7}$$

in which $\bar{S}$, M, n and N have been defined above and h is the number of days, hence the number of sub-groups of observations.

Similarly the variance of P about the mean has been obtained from

$$[\sum_{j=1}^{h} (P_j - M)^2]/(h-1). \tag{8}$$

These variances are listed in Table 2, rows B and C respectively. These values are vitiated by the long term effect and consequently are not valid criteria of the day-to-day performance of the apparatus. Comparison of B and C with D and H respectively shows that the variances are significantly smaller after the effect of the long term trend has been removed.

(iii) *Variance of transformed periods.*—When a large number of observations on one variate are divided into groups and a mean is obtained for each group the relation between the observations, the mean, and the group means is given (Weatherburn 1947) by

$$\sum_{j=1}^{h} \sum_{i=1}^{n_j} (\bar{S}'_{ji} - M)^2 = \sum_{j=1}^{h} \sum_{i=1}^{n} (\bar{S}_{ji}' - P_j')^2 + \sum_{j=1}^{h} n_j (P_j' - M)^2 \tag{9}$$

in which $\bar{S}'$ is the transformed mean period
M is the grand mean of all periods for one pair
P' is the transformed average of the periods for one day, i.e. for one group
h is the number of groups, i.e. the number of days
n is the number of swings on one day.

When each term in this equation is divided by the appropriate number of degrees of freedom three unbiased estimates of variance are obtained which satisfy the identity

$$(N-1)\sigma^2 = (N-h)\sigma^2 + (h-1)\sigma^2. \tag{10}$$

These variances are listed in Table 2, rows D, E and G.

If the classification into groups, such as these above, is non-selective, the three estimates of variance will approach equality in the limit; for finite samples we can test for the existence of selective classification by comparing ratios of these variances with ratios predicted by theoretical statistical methods.

(iv) *Variance ratio tests.*—If a large sample, say 1 000, is randomly drawn from a normally distributed population that is several times larger than the sample, one would expect the variance of the sample to differ very little from that of the population; for small samples from much smaller populations an appreciable difference can be expected in the variances hence the ratio of these variances will depend on

Table 2

		Variances (10^{-14} s^2) and degrees of freedom						Average standard deviations (10^{-7} s)			
		4–5		4–6		5–6		Averages		Milligals	
		σ^2	d.f.	σ^2	d.f.	σ^2	d.f.	σ^2	d.f.	$\sigma S'$	$\sigma P'$	$\sigma P'$	$\sigma \Delta g$
A	$\dfrac{\sum_{k=1}^{3}\sum_{j=1}^{n}(S_{kj}-P_k)^2}{\sum_{k=1}^{3}n_k-3}$							1·27	6	1·13	0·65	0·26	0·15
B	$\dfrac{\sum_{j=1}^{h}\sum_{i=1}^{n}(S_{ji}-M)^2}{(N-1)}$	7·72	88	14·40	94	12·88	92						
C	$\dfrac{\sum_{j=1}^{h}(P_j-M)^2}{(h-1)}$	7·39	27	14·26	28	11·15	29						
D	$\dfrac{\sum_{j=1}^{h}\sum_{i=1}^{n_j}(S_{ji'}-M)^2}{(N-1)}$	5·50	88	8·12	94	6·30	92	6·64	91	2·58	1·49	0·60	0·35

E	$\dfrac{\sum_{f=1}^{h}\sum_{i=1}^{n_f}(S_{fi}'-P_f')^2}{(N-h)}$	1·02	61	1·17	66	1·64	63	1·28	63	1·13	0·65	0·26	0·15
G	$\dfrac{\sum_{f=1}^{h}n_f(P_f'-M)^2}{(h-1)}$	15·70	27	24·48	28	16·47	29	18·88	28	4·35	2·51	1·00	0·58
H	$\dfrac{\sum_{f=1}^{h}(P_f'-M)^2}{(h-1)}$	4·98	27	7·81	28	5·22	29	6·00	28	—	2·45	0·98	0·57

	Variance ratios			d.f.	F Significance level	
	4–5	4–6	5–6	average	1 per cent	1 per cent
D/E	5·4	6·9	3·8	91:63	1·8	1·5
G/D	2·9	3·0	2·6	28:91	1·9	1·6
G/E	15·4	20·9	10·0	28:63	2·0	1·7

the size of the sample and of the population. Tables of variance ratios (F) for normal populations have been published by Snedecor (1934). For the number of degrees of freedom of the sample and of the population these tables list two values designated as 5 per cent and 1 per cent points of F. The 5 per cent point for instance is that value which, for the given degrees of freedom, will be exceeded in 5 cases out of a hundred. These values can be used to test the hypotheses that samples are either from the same normal population or are from normal populations of equal variance. A value of F less than the 5 per cent point is not considered significant, a value greater than the 1 per cent point is highly significant and throws doubt on the truth of the hypothesis, hence these points are also known as significance levels.

Using the transformed observations from which the long term trend has been removed we have, for each pendulum pair, the variance from a total population, D, (Table 2) the variance from groups, E, and the variance from group means, G. As shown by (9) and (10) these variances should be equal. By comparing their ratios with predicted values of F we can test whether or not the differences in variance are significant.

In the lower section of Table 2 the variance ratios, degrees of freedom and corresponding significance levels of F are summarized. As all the ratios are much greater than the 1 per cent of F there is no doubt whatever that the differences in variances are highly significant.

(v) *Why do the variances differ so widely?*—As far as physically possible every swing has been made under similar conditions; the same temperature, pressure, initial arc, etc., were maintained for all observations. Yet it is generally assumed—and this analysis confirms it quantitatively since $\sigma_E^2 < \sigma_D^2$—that two swings on any one day tend to differ less than two swings on different days. The variance ratio D/E averages 5 whereas the probability is only 0·01 that it should exceed 1·8. As it should, variance E does not differ greatly from variance A; both are based on deviations from group, or daily, means, hence both are a measure of internal consistency. Variance D is based on deviations from the grand mean, hence it is a measure of external consistency. As shown by equations (9) and (10) variances D and E will be approximately equal if there is no selective classification operative. Obviously the grouping by days is highly selective; in other words there is a discrepancy between internal and external consistency.

The suspected cause of this discrepancy is attributed to shocks received during the transfer of the pendulums from the sealed case to the heated carrying case and back between successive days.

(d) *Serial correlation tests*

From the variance analysis above it was apparent that a pendulum observation is not independent of its predecessor, in other words the observations are serially correlated. To confirm this indication serial correlation tests were made on S, P, S', and P'; these tests are summarized in Table 3.

For these tests it is necessary to compute a coefficient

$$K = \frac{\delta^2}{\sigma^2} \tag{11}$$

in which δ^2 is the mean of the sum of the squares of first differences and σ^2 is the variance.

For example

$$K_P = \frac{\delta_P^2}{\sigma_P^2} = \frac{\sum_{j=1}^{h-1} (P_{j+1} - P_j)^2]/(h-1)}{[\sum_{j=1}^{h-1} (P_j - M)^2]/(h-1)}. \qquad (12)$$

As for variance analysis, tables giving the 5 per cent and 1 per cent points of K for different degrees of freedom are available (Ferber 1949).* In this case a value of K less than 1 per cent significance level indicates the existence of positive serial correlation.

Table 3

Serial correlation tests

	Pendulums			Significance Level	
	4–5	4–6	5–6	1 per cent	5 per cent
S	0·72	0·36	0·28	1·5	1·7
P	0·72	0·53	0·46	1·2	1·4
S'	1·1	0·6	0·6	1·5	1·7
P'	2·5	1·1	0·9	1·2	1·4

In Table 3 significant positive serial correlation is indicated for both S and P. This is to be expected because of the long term trend. Even after the transformation which removes the effect of the long term trend there is still significant correlation for S' and marginal correlation for P'. The significant positive correlation for S' confirms the evidence from variance analysis that on any one day the observations are clustered together. The marginal correlation for P' can be interpreted either as an indication that a more complex curve is needed to describe the long term trend or that some of the clustering effect noted for S' carries over from day to day.

(e) *Comments on the behaviour of the pendulums*

From a study of the information in Figure 1 and Tables 2, and 3, we can make some deductions concerning the behaviour of the bronze pendulums.

(i) As long as the pendulums are left in the thermostated, evacuated case and only raised and lowered between swings the periods are quite consistent. This is confirmed by the low variances A and E.

(ii) The effect of opening the case, removing the pendulums to the heated carrying case, and returning them to the sealed case introduces shocks of unknown origin which tend to increase the variance by a factor of five.

(iii) These shocks are essentially random in size and direction but, as indicated by the serial correlation of P', each one is influenced slightly by its predecessor.

(v) There is no evidence to show that the pendulums will recover from these shocks while in the sealed case. There are insufficient data to test this statistically but when the pendulums have been left in the sealed case between sets of swings

* *Note.*—In Table 3 the values of the significance levels for S and S' have been obtained by extrapolation from the Table on p. 525 of Ferber.

(bracketed groups, Figure 1) regardless of the time lapse they appear to behave as we would expect if the swings had all been made as one large set.

(v) There is also no evidence to show that long field trips or long periods of quiescence have any more effect than a simple transfer to the carrying case and back to the sealed case. This can be interpreted as a tribute to careful handling and constant heating on field trips.

4. Standard deviation for a gravity difference

(a) *Observations at Ottawa*

For each average variance in Table 2, corresponding standard deviations have been tabulated and the standard deviation of P' has been found on the assumption that there are three observations in each group, thus

$$\sigma(P') = \sigma(S')/3^{\frac{1}{2}}. \tag{13}$$

This is not strictly accurate but it is adequate for this type of analysis. The equivalent standard deviation of P' in terms of milligals listed in the second last column of Table 2 has been computed from the approximate relation

$$\sigma(P')\,(\text{mgal}) = 0{\cdot}4\,\sigma(P')\,(\text{s} \times 10^{-7}). \tag{14}$$

In measuring a gravity difference between two stations six pendulums are grouped in two sets of three so that observations are made with six pairs of pendulums. If $\sigma(P')$ is the standard deviation in milligals of the observations with one pair of pendulums at one station then by the laws of error propagation the standard deviation of the difference between two stations is given by

$$\sigma(\Delta g) = \sigma(P')6^{-\frac{1}{2}}2^{\frac{1}{2}}. \tag{15}$$

Values of $\sigma(\Delta g)$ corresponding to the different variances are listed in the last column of Table 2. Using the same observed data, standard deviations differing by a factor of four have been obtained; this illustrates the importance of defining clearly the method by which standard deviations for gravity differences are computed. Unfortunately it is not possible to say that one of these values is correct and the others are wrong; each contains useful information about the apparatus and studying them as a group yields valuable information about the performance of the apparatus.

(i) Standard deviations from rows A and E of Table 2 are equal. This is to be expected as they are derived from residuals of periods S, or S' about group means P and P'. The low value of 0·15 mgal shows that the deviations about the group means are small hence the internal consistency is good. This value of standard deviation would apply if a gravity difference could be measured without exposing the pendulums to the shocks which they apparently receive each time they are removed from the evacuated thermostated case.

(ii) Standard deviations from rows G and H are 0·58 and 0·57 mgal respectively; although both are derived from the residuals of group means, P', about the grand means, M, the small difference arises because the values in row G are weighted proportional to the number of observations in each group whereas in row H each group is given equal weight. This is the order of magnitude for the standard deviation of a gravity difference that would apply if field observations were made without standardization swings before and after each field trip; in other words it is

the value that would apply if field procedure were not designed to utilize the beneficial effects of serial correlation.

(iii) The standard deviation of 0·35 mgal given in row *D* is based on the residuals of the transformed periods, S', about the means, M, for each pair of pendulums. This is the most direct and hence the best method by which to evaluate the inherent accuracy of the apparatus. It is fortuitous that the mean of the values from (i) and (ii) above, is 0·36 mgal.

(b) *Internal analysis of field observations*

In the field usually only one set of observations is made at each station hence only the variance analysis by the formula in row *A*, Table 2, can be applied. This has been done for each season's work and the results summarized in Table 4. It is apparent that the internal consistency of the results in the field is comparable with that on the pier in Ottawa.

(c) *Pair analysis of field observations*

It is customary to compute the gravity difference between two stations independently for each pair of pendulums. The standard deviation can then be computed for a pair and also for the mean gravity difference. Averages for each season are summarized in Table 4.

Table 4

Sammary of standard deviations and comparisons of gravity differences (mgal)

Location	Year	Internal Analysis $\sigma\Delta g$	Pair Analysis $\sigma\Delta g$	Comparisons (without regard to sign)	Ottawa Pier $\sigma\Delta g$
Canada and United States	1957 (Only one set of 3 pendulums used)	0·17*	0·23	0·33	
					0·35
Prairie Provinces	1958	0·16	0·20	0·41	
Canada and Europe	1959	0·14	0·16	0·40	
Ottawa	1956–59	0·15			

* Two erratic observations omitted in computing this value.

(d) *Comparisons with other values*

Each gravity difference that was measured with these pendulums has been measured many times with gravity meters and in some cases with other pendulum apparatus. From these previous measurements a value—usually the mean—has been adopted in order to make a comparison with these results. Individually each of these previous values is of dubious accuracy but on the average they are not likely to be seriously in error. It is interesting to note that these comparisons, listed in Table 4, do not differ significantly from the standard deviation derived from analysis of the results on the Ottawa pier.

(e) *Weighting observations for network adjustments*

From the discussion above and from data in Tables 2 and 4, it follows that there may be several distinctly different values for the standard deviation of a gravity difference. Thus there are several approaches to the weighting of the observations. Weighting frequently is based on the internal consistency of each set of measurements. This appears to be scientifically rigorous but unless it can be shown that the internal analysis takes account of all the factors it is virtually meaningless. From this investigation it appears that the internal analysis takes account of all small errors and omits a large one.

Differences measured with this apparatus have a standard error of the order of 0·35 mgal and there is no way of determining from any one set of measurements whether the error is greater or less than this value. If the measurements have been made with the usual care—$\sigma(\bar{S})$ of the order of $1{\cdot}1 \times 10^{-7}$s—there is no way of deriving a figure for the error in the gravity difference; whether $\sigma(\bar{S})$ is 0·9 or $1{\cdot}3 \times 10^{-7}$s is insignificant when it is known that the whole set may be in error by $2{\cdot}0 \times 10^{-7}$s. Before the results with different apparatus can be weighted validly for adjustment of the first-order world network a similar objective appraisal of each apparatus is needed.

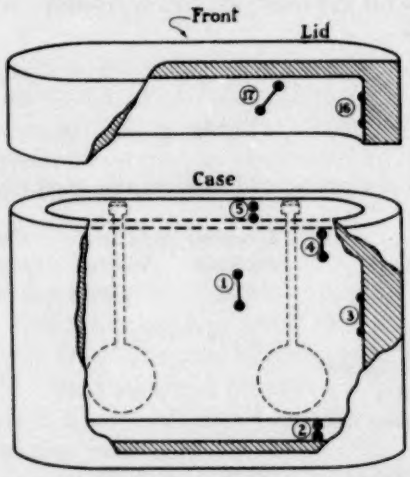

FIG. 2.—Location of thermistors in case wall relative to pendulums.

5. Pendulum temperature tests

(a) *Temperature control and monitoring system*

Variations in temperature inside the pendulum case are limited to 0·01 deg C by a thermistor (Western Electric Type 10A) embedded in the wall of the case acting as a thermostat. Selection of the operating temperature (about 40° C) is arbitrary but once selected must not be allowed to change. To check that the temperature remains stable and uniform within the case seven thermistors (Western Electric Type 12A) are mounted in it; five are on the wall and two on the lid (see Figure 2). The resistance of these thermistors can be measured by a bridge circuit to give the temperature at any sensing point at any time. The coils that supply the heat are wound such that in any horizontal plane the temperature is radially symmetrical but very sensitive adjustments are necessary to eliminate vertical gradients.

(b) *Temperature sensitivity of the pendulums*

A change in temperature of 0·06 deg C will cause a change in period of $2{\cdot}5 \times 10^{-7}$ s, equivalent to an apparent change in gravity of 1 mgal (McDiarmid 1915). As temperature increases, length of the pendulums increases, periods increase and observed g decreases. Thermistor resistance decreases with increase in temperature; for these thermistors the coefficient is very nearly $-0{\cdot}005$ deg C/ohm. Thus for a change in resistance of 1 ohm: change in period is

$$\Delta p = \frac{1 \times -0{\cdot}005}{0{\cdot}024} = -0{\cdot}2 \times 10^{-7}\text{s} \tag{16}$$

and change in gravity is

$$\Delta g = \frac{1 \times -0{\cdot}005}{-0{\cdot}06} = 0{\cdot}08\ \text{mgal.} \tag{17}$$

(c) *Thermistor resistance for pendulum* 5–6, *Ottawa* 1956–59.

In Figure 3 for each thermistor the average resistance recorded during swings with pendulum pair 5–6 at Ottawa is plotted. Fluctuations in resistance recorded during 1956 and early 1957 reflect adjustments that were made in the heat control circuitry to eliminate vertical gradients. Subsequent fluctuations in the record that correspond to case overheat or to a breakdown of the control circuitry are noted on the figure.

(d) *Average deviations in thermistor readings*

For the period of this analysis the average resistance for each thermistor was found and from these averages were found the individual deviations at each point and the average deviation of the case temperature from normal. For this purpose the thermistors were grouped three ways:

(i) All seven thermistors 1, 2, 3, 4, 5, 16, 17,
(ii) Two lid thermistors 16, 17,
(iii) Five case thermistors, 1, 2, 3, 4, 5,

the data from each group are plotted in Figure 3. An analysis to detect a long term trend was made in the same manner as in "Long Term Trend" above. The curves and equations are shown on the Figure. It is apparent that, to a limited extent, the trend corresponds with the long term trend in pendulum periods.

(e) *Correlation between thermistor resistance and pendulum periods*

The temperature deviations for each of the three groupings above were tested for cross correlation with the deviations of pendulum periods (Figure 1). From the temperature sensitivity of the pendulums it might be expected that a large positive (negative) ΔP would correspond to a large negative (positive) ΔR. This was not confirmed. Cross correlation was tested by the formula

$$r = \frac{\sum_{n=1}^{N} \Delta P_n \Delta R_n - \frac{1}{N} \sum_{n=1}^{N} \Delta P_n \sum_{n=1}^{N} \Delta R_n}{\left[\{\sum_{n=1}^{N} \Delta P_n^2 - \frac{1}{N}(\sum_{n=1}^{N} \Delta P_n)^2\}\{\sum_{n=1}^{N} \Delta R_n^2 - \frac{1}{N}(\sum_{n=1}^{N} \Delta R_n)^2\}\right]^{\frac{1}{2}}} \tag{18}$$

in which ΔP is the deviation in pendulum period
ΔR is the deviation in thermistor resistance
$N = 29$.

For the three thermistor groupings we get

$$r_{I} = 0{\cdot}43 \text{ (1 to 17)}$$
$$r_{II} = 0{\cdot}24 \text{ (16 \& 17)}$$
$$r_{III} = 0{\cdot}32 \text{ (1 to 5)}$$

Although all three coefficients indicate negligible correlation it is interesting to note that the value from the lid thermistors is even lower than the others.

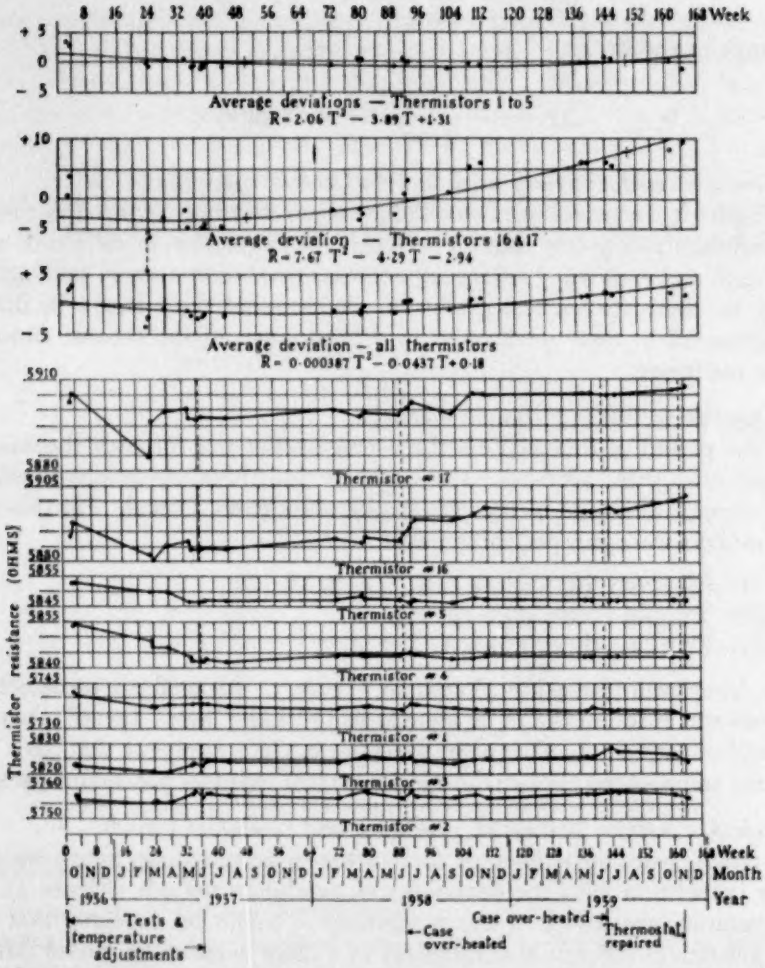

FIG. 3.—Thermistor resistance readings recorded during swings of pendulum pair 5 and 6, 1956–59.

(f) *Assessment of the temperature control system*

The evidence from this analysis indicates that the pendulum periods are affected less by temperature changes than would be predicted using the coefficient for temperature sensitivity. The long term trend in temperature is in the proper direction but not large enough to account for the trend in pendulum periods. There is still the possibility that the thermistors—including the control thermistor

—are drifting in the same direction at the same rate; this seems highly improbable but it could effectively mask a change in operating temperature. An absolute calibration of the thermistors was made at the end of 1959 but due to uncertainty in identification it cannot be correlated with the absolute calibration made in 1956.

From the data for all the thermistors over the entire period the standard deviation of thermistor resistance is 1·8ohm; combining this with the sensitivity factor of 0·08mgal/ohm gives a standard deviation due to temperature changes of 0·14mgal. This figure is high since it includes the fluctuations in lid temperature as well as those due to adjustment in 1956–57. Using the data from the case thermistors only, the standard deviation due to temperature changes for a set of measurements with one pair of pendulums becomes 0·10mgal. This appears to be a fair assessment of the temperature control system.

6. Possible sources of error other than temperature

In addition to temperature changes there are numerous factors which may contribute to the error of an observation. Several of these are discussed and their effect is estimated.

(a) *Recording*

Irregularities in the rotation of the photographic drum and shrinkage or expansion of the photographic paper during processing can contribute at the most only very small errors. The maximum contribution to the standard deviation is estimated at 0·03 mgal.

(b) *Scaling and interpolating records*

These errors are due to small variations in the size of the dots on the record and to the uncertainty in estimating the centre of a dot precisely. The contribution to the standard deviation of a set of swings from errors in recording and scaling is estimated to be 0·09mgal.

(c) *Arc correction*

The initial arc is maintained at $0{\cdot}0075 \pm 0{\cdot}0003$ radian for each swing and a small correction is applied to reduce the period to that of a pendulum swinging with an arc of 0·0075 radian. This correction is determined by measuring photographically the amplitude of a reflected light beam at a distance of one metre from the pendulum case. A pendulum arc of 0·0075 radian gives a deflection of 30·00mm to the light beam. Deviations from 30·00mm are corrected for by application of the empirical formula $C = 1{\cdot}2(30{\cdot}00 - x)$ in which x is the observed deflection of the light beam in millimetres and C is the correction in 10^{-7}s. The term usually amounts to about $0{\cdot}5 \times 10^{-7}$ and never exceeds $1{\cdot}0 \times 10^{-7}$; the error in deriving this correction should not exceed $0{\cdot}1 \times 10^{-7}$s for one swing or $0{\cdot}1/3^{\frac{1}{2}}$, equivalent to $0{\cdot}06 \times 10^{-7}$s, for three swings.

(d) *Knife edges and flats*

When pendulum 5 is swung on knife edge No. 1, its average period is longer by 56×10^{-7}s than when it is swung on knife edge No. 2. This shows that there is a knife edge effect due either to rigidity or rounding. However, since it has not changed appreciably during three years' observations it is fair to assume that it will

not have any significant effect on gravity differences. This subject is discussed in detail by Winter & Valliant (1960).

(e) *Timing*

For time interval measurements a portable frequency standard is aligned with *WWV* several times during a swing. It is obvious that the accuracy of the portable standard can be no better than the value against which it is compared. Ionospheric effects on the sky wave (Shaull 1950) can at times reduce the accuracy of the received frequency to a few parts in 10^7 which can cause errors as large as 0·5 mgal in one swing. This large error could conceivably occur on three successive swings but the probability of this happening is low. In fact, it is more probable that the error during one swing would be compensated during a successive swing. On this basis the standard deviation in a set of three swings is estimated to be no larger than 0·2 mgal.

7. Summary and conclusions

(a) The periods of the bronze pendulums are changing slowly. Part of this change may be due to change in temperature as a result of drift in the control thermistor but it is believed that at least part of the change is due to creep in the bronze metal.

(b) The standard deviation derived by combining the contributions from all known sources of error agrees well with the standard deviation derived from analysis of variance for internal consistency. Using estimates derived from the discussion of error sources yields the following standard deviations in g for a set of three swings with one pair of pendulums:

Temperature	0·10 mgal
Recording	0·03
Scaling and interpolating records	0·06
Arc correction	0·03
Knife edges and flats	0·05
Timing	0·20

from which

$$\sigma g = \left(\sum_{i=1}^{n} \sigma_i^2\right)^{\frac{1}{2}} = 0{\cdot}25 \text{ mgal}. \tag{19}$$

From analysis of variance (Table 2, row *A*) the standard deviation for the same number of swings is 0·26 mgal indicating that there is no serious discrepancy in the assessment of errors.

(c) The standard deviation for a gravity difference measured with all the Dominion Observatory bronze pendulums varies from 0·15 to 0·58 mgal depending on the method by which it is calculated. Thus illustrates the difficulty in getting an objective assessment of any pendulum apparatus; an illusion that very high accuracy is being attained can be created if the analysis is based on internal consistency only. Internal analysis provides a good criterion of observational technique and of the performance of the ancillary equipment but it is virtually valueless as a basis for assessing the accuracy of results. It is suggested that a standard deviation of 0·35 mgal be used for weighting observations made with this apparatus.

(d) From this analysis it appears that the pendulums are quite consistent as long as they are not removed from the thermostated evacuated case whereas even a brief transfer to the carrying case may cause a change in period large enough to account for the fourfold difference in standard deviation that is found. There is no indication of the cause of this effect; whether it is due to thermal, physical, or other shocks there is no way of deciding at present. When the electronic recording and timing system now being developed is completed it is expected that errors other than those due to the pendulums themselves will be negligible; it is then proposed to undertake a program to locate the cause of the erratic behaviour of the pendulums.

Acknowledgments

Mr P. J. Winter assisted with the tabulations and computations for this analysis, Mr H. D. Valliant prepared the material on which the analysis of temperature effects is based, and both contributed to the discussion of sources of error. Dr M. J. S. Innes and Dr J. A. Rottenberg reviewed the manuscript and contributed many valuable suggestions. This assistance and advice is gratefully acknowledged.

Division of Gravity,
Dominion Observatory,
Ottawa:
1961 *March*

References

Cook, A. H., 1950. Measurements of gravity in Ireland, Pendulum observations at Dublin, Sligo, Galway and Cork. *Geophys. Mem.* No. 2., Part 1, (Dublin Inst. for Advanced Studies, School of Cosmic Physics, Dublin).

Ferber, Robert, 1949. Statistical Techniques in market research. McGraw-Hill Book Co. Inc.

Field, R. H., 1939. Note on the permanence of standards of length. *Canad. J. Res.*, **17.**

Fisher, R. A., 1925. *Statistical methods for research workers.* Oliver & Boyd, (2nd rev. ed).

Garland, G. D., 1953. Gravity measurements in North America with the Cambridge pendulum apparatus. *Proc. Roy. Soc. A,* **219,** 215–233.

McDiarmid, F. A., 1915. Gravity. *Pub. Dom. Obs.* **2,** No. 10.

Miller, A. H., 1929. Gravity in Western Canada. *Pub. Dom. Obs.* **8,** No. 9.

Shaulí, J. M., 1950. Adjustment of high-precision frequency and time standards. *Proc. Inst. Radio Eng.* **38.**

Snedecor, G. W., 1934. *Statistical methods.* Iowa Collegiate Press.

Swick, C. H., 1921. Modern methods for measuring the intensity of gravity. *U.S.C. & G.S. Spec. Pub. No.* 69.

Thompson, L. G. D., 1959. An improved bronze pendulum apparatus for relative gravity determinations. *Pub. Dom. Obs.* **21,** No. 3.

Weatherburn, C. E., 1947. *A first course in mathematical statistics.* Cambridge University Press.

Winter, P. J. & Valliant, H. D., 1960. Relative gravity determinations in the Prairie Provinces with Dominion Observatory bronze pendulum apparatus. *Geophys. J.*, 3.

Winter, P. J., Valliant, H. D. & Hamilton, A. C., 1961. Pendulum observations at Ottawa, Gander, Teddington, Paris, Rome and Bad Harzburg. *Bull. Géod, Int., No.* 60.

Interaction Between Tide and Surge in the Thames

J. R. Rossiter

(Received 1961 March 16)

Summary

Observations of storm surges in the Thames reveal an interaction effect between tide and surge which is statistically significant, and takes the form of an amplification of surge height (whether positive or negative) on the rising tide. Representing the estuary by a channel of constant depth and exponentially varying breadth the distributions of elevation and current along the estuary have been computed for different combinations of input (at the seaward end) of tide and surge. The results agree remarkably well with the phenomenon as observed in nature; they provide the basis for a simple physical explanation of the interaction, in which it is argued that the principal mode of interaction is by the surge changing the phase of the tide, and vice-versa. This argument requires the tides in the Thames to be of progressive wave type; this is shown to be true, in general, for tides subject to friction in an exponential estuary of constant depth.

The computations also reveal that maximum levels are propagated upstream so that a higher maximum is amplified less than a lower maximum.

The paper confirms a number of Proudman's earlier theoretical results on interaction in estuaries.

1. Introduction

In continuation of the research programme conducted by the Liverpool Observatory and Tidal Institute into storm surges around the coasts of the British Isles, once the basic surge-forecasting formulae for North Sea stations had been provided to the Advisory Committee on Oceanographic and Meteorological Research of the Ministry of Agriculture, Fisheries and Food (Rossiter 1959), attention was focused upon the problem of propagation of surges up the River Thames.

The Flood Warning Organization, responsible for the practical task of day to day forecasting of danger levels, had early encountered considerable difficulty in estimating the amplification of surges propagated from the North Sea into the Thames. In particular, positive surges observed near high water in the Lowestoft/Harwich area and travelling southwards with the tide, rarely turned out to be as dangerous as might be expected; in consequence there arose the possibility of an excessive number of false alarms being issued.

This problem was considered to be a particular aspect of the larger one of interaction between tide and surge. The hydrodynamical equations governing the propagation of long waves in shallow water, containing, as they do, non-linear

terms, are clearly the reason for secondary oscillations being produced when tide (primarily a continuous oscillation of period 12 h) and surge (a transient oscillation of approximate "period" 24 h) co-exist. Formal expressions of limited scope for the secondary effects in the case of *continuous* oscillations of one or more periods can be obtained (e.g. Proudman 1953, § 145), but when *transients* are involved the most satisfactory approach is by the numerical solution of type problems.

So far as the author is aware only two names have hitherto been associated with this specific problem of interaction, those of Proudman (1955 a and b, 1957, 1958) and Doodson (1956). Proudman's papers developed formal solutions of great interest; most of them included bottom friction proportional to the square of the current; the effects of the non-linear inertia term and the variation in cross-sectional area of an estuary were considered. Despite mathematical complications which prevented a general solution being found, Proudman's principal 1955b result, that for the same sequence of meteorological conditions over the sea the surge up an estuary is less at the time of high water than it is at the time of low water, is confirmed in the present investigation. Doodson's work was primarily numerical in nature; he developed a method of computation and applied it to the case of a uniform gulf of depth 128 ft and length 105 miles. He found no appreciable interaction between a semidiurnal tide and a diurnal surge, almost certainly because the depth chosen was too great.

The present paper is a numerical investigation of the propagation of tide and surge in an estuary similar in dimensions to the River Thames, with a view to explaining specific phenomena observed in that river.

2. The nature of interaction in the Thames

From the head of the tidal Thames (Richmond Lock) to its seaward limit is some 68 miles; Southend is 7 miles within this limit, and tidal records for this station have been taken as typical of the estuary. Hourly values of surge height for all important surges, both positive and negative, which were experienced during the years 1928 to 1938 were available from a previous investigation (Rossiter 1959). From these were extracted the surge height at predicted high water time (H), predicted low water time (L), and at the two intermediate times on the rising (R) and falling (F) tides; care was taken to extract surge heights in multiples of 4 from each tidal cycle within a surge period.

Table 1 tabulates the number of surge heights exceeding chosen values for the four states of tide for (a) positive surges, (b) negative surges and (c) both positive and negative surges.

This table clearly reveals a tendency for surges to be greatest on the rising tide, irrespective of the sign of the surge; there appear to be no significant differences between the distributions at the three other states of tide. These results confirm a similar tendency noted by Doodson (1928) on the basis of many fewer data. It is nevertheless desirable that the uniqueness of surge distribution on the rising tide be proved statistically significant, and this was done by means of the χ^2-test. Assuming that the distribution to be expected at any state of tide be represented by the average of the distributions for H, F, L and R, the test shows that the probability of random errors in sampling being responsible for the observed R distribution is less than 0·1 per cent for negative surges and much less than this for positive surges. It is therefore clear that the observed phenomenon is statistically significant.

Table 1

Number of occasions when surge heights at Southend exceed given values, for four states of tide: high water (H), low water (L), half tide rising (R), half tide falling (F).

Surge ht (ft)	0·0	0·5	1·0	1·5	2·0	2·5	3·0	3·5	4·0	4·5	5·0	5·5	6·0	6·5	7·0
							(a) Positive surges								
H	633	368	186	91	44	23	15	5	2	2	1	1	1		
F	594	339	168	66	36	22	11	5							
L	539	306	161	90	55	31	15	9	2	2	1				
R	579	378	255	156	94	58	39	17	10	7	1				
							(b) Negative surges								
H	425	230	113	62	38	23	15	10	6	3	3	2	1	1	
F	464	233	131	77	41	18	12	7	5						
L	519	274	129	72	30	20	8	3	1						
R	479	301	172	99	60	39	23	17	12	6	4	1	1	1	1
							(c) All surges								
H	1058	598	299	153	82	46	30	15	8	5	4	3	2	1	
F	1058	572	299	143	79	40	23	12	5						
L	1058	580	290	162	85	51	23	12	3	2	1				
R	1058	679	427	255	154	97	62	34	22	13	5	1	1	1	1

In order to arrive at a quantitative estimate of the observed effect, values of surge height (residual) were listed in units of a tidal cycle and grouped according to the mean residual of each cycle. In Figure 1 are plotted the mean residuals for each of the four states of tide as ordinates and the mean residual for the complete tidal cycle as abscissae. Assuming linearity over the range involved, it will be seen that on the rising tide surges are increased by approximately 25 per cent over those at any other state. Consistency between positive and negative surges is maintained.

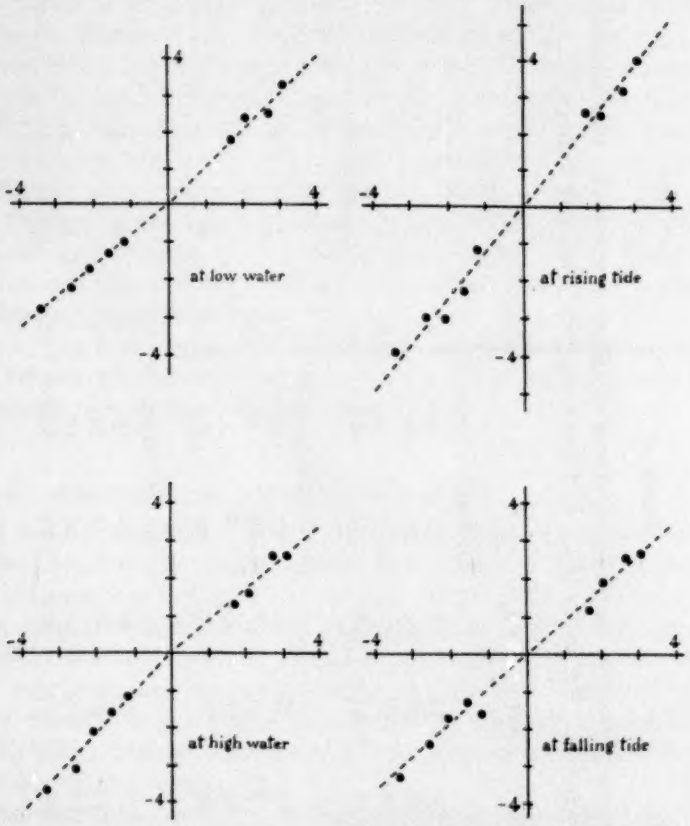

FIG. 1.—Values of surge height at Southend (ordinates) at four states of tide relative to surge height averaged over the tidal cycle (abscissae). Units are feet.

An example of a typical surge which exhibits the interaction effect is given in Figure 2. This diagram (2a) gives the Southend residuals for the surge of 2/3 December 1929, and clearly indicates both the trough and the subsequent peak occurring on the rising tide. Application of a graphical smoothing process to the residuals produces a damped oscillation of period near to 8 h (2b), the first trough of which (21.30 h December 2) gives rise to the very sharp trough in the surge, and the second major crest of which (10.00 h December 3) produces the sharp peak in the surge. This particular example is quite typical of surges at Southend and stations higher up the Thames, and has been chosen because it was preceded by quiet meteorological conditions. The synoptic situation was such that strong

southerly winds spread westwards into the whole of the North Sea on December 2, veering to southwest in the afternoon and moderating by the morning of December 3. The main positive surge may be described as a "return" surge, generated by the return, primarily down the East Coast, of water previously expelled from the North Sea by the southerly winds.

Before considering the most likely physical mechanism for the observed phenomenon, certain possibilities may be excluded. In 1928 Doodson stated: "General reasoning indicates that the effects of an increase of depth of somewhat long duration over a wide area will be to decrease the range of tide; that is, the

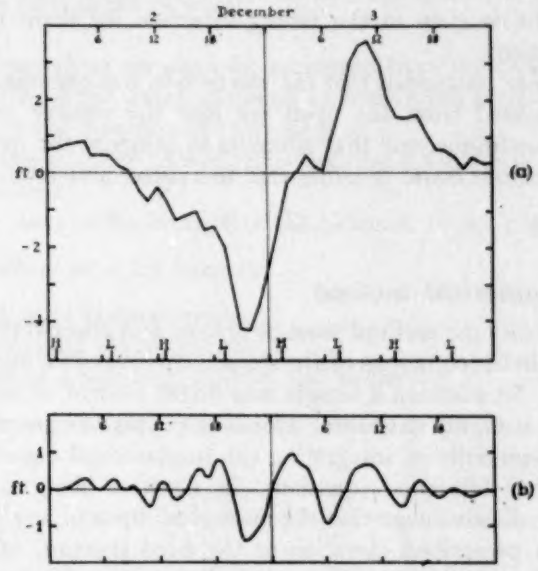

FIG. 2. (a) Surge heights for 1929 December 2 and 3, at Southend; (b) damped oscillatory component of surge. H and L denote tidal high and low waters respectively.

apparent meteorological effects (as shown by the residues) are a general average increment of level, with minima at high water and maxima at low water. These conditions hold when there has been a long-continued NW wind. Apart from this purely tidal effect, the local wind will probably have most influence at low water and will tend to give maximum results between then and high water. Hence there are two theoretical reasons for believing that there is a marked tendency for sea level to be most raised, by meteorological causes, shortly after low water."

With regard to Doodson's first suggestion, residuals at Aberdeen, Tynemouth, Immingham and Lowestoft reveal no evidence of interaction to any perceptible degree, strongly suggesting that the Southend effect is a relatively local one not associated with forces acting over a wide area. Nor does the suggested mechanism seem quantitatively possible in this case. During the exceptional surge of 1953 the mean level of the North Sea as a whole was raised a maximum of approximately 2 ft (Rossiter 1954), so small a proportion of the mean depth of the sea and its approaches that its effect on the range of tide could hardly produce the amount of interaction observed at Southend.

The second of Doodson's suggested mechanisms for interaction is based upon the well-known theory that a wind generated water gradient is inversely proportional to the depth of water. Tomczac (1952a, b) has shown this effect to be of some importance in German North Sea estuaries. For a 25 per cent increase in the water gradient down the North Sea, as observed at Southend on the rising tide, the theory would require a 25 per cent decrease in the mean sea level due to the state of the tide. This effectively restricts the area in which the theory could be considered valid to the mouth of the Thames, where the amplitude of tide varies from about 5 ft at neaps to 9ft at springs, and the mean depth is of the order of 30 ft. But a study of Southend residuals for the years 1928 to 1938 eliminates even this possibility, for there are many instances on record when local winds were slight or even in the wrong direction for them to account for the observed interaction.

It was therefore concluded that the interaction was generated when surge and tide were propagated from the open sea into the estuary under locally quiet meteorological conditions, and that attempts to compute the mode of propagation by numerical methods could possibly lead to a better understanding of the phenomenon.

3. Choice of numerical method

To be satisfactory the method must be able to deal effectively with the principal non-linear terms in the equations of motion and continuity for one-dimensional flow along a channel. In addition a simple and direct control of the numerical input for any problem is highly desirable. Doodson (1956) has described his approach which consists essentially of integrating the fundamental equations, when transformed into finite difference equations, in distance along the channel. This suffered from the disadvantage that the numerical input of any problem had to be in the form of a prescribed elevation at the head (barrier) of the estuary, and iterative methods were then necessary to find an appropriate prescription to produce the required elevation at the mouth. This proved to be a reasonable procedure for the problem chosen, involving a depth of 128 ft, but to carry it out for a depth of 32 ft was found to be impractical due to the generation of large shallow water tides.

It so happened that at the time the choice of method was under consideration the author learned that numerical computations of a somewhat similar nature, but for an entirely different purpose, were in hand for an idealized mathematical model of the Thames. The problem was to determine the effects of a moveable surge barrier on river levels downstream of the barrier site, and this has now been successfully solved by Otter & Day (1960) using a modification of a method originally devised by Hansen (1956), and employing an electronic computer. The essential difference between the methods of Doodson and Hansen was that the latter's consisted of numerical integration of the fundamental equations in *time*.

The potentialities of this method are so great that it was decided to use it for the interaction problem; apart from differences in notation, the development given in the next section is substantially the same as that given by Otter and Day. The mathematical model they used was that of a channel of constant depth and exponentially varying breadth. This is a reasonable representation of the Thames and, most important from the point of view of their preliminary theoretical investigations,

led to a considerable simplification of their formal solution for tides subject to linear bottom friction in the particular case of the Thames (see Appendix). In what follows an exponential channel of constant depth has also been used.

4. The differential equations and their manipulation

We shall denote by:

h the mean depth of water, assumed constant;
ζ the elevation of the surface at time t and position x, measured positive when above the mean level;
$W = h+g$, the total depth of water;
t the time;
x the distance along the channel, measured from the mouth;
u the velocity of the water, assumed uniform from surface to bottom, and positive in the direction of increasing x;
$Q = bWu$ = the quantity of water flowing past a section of channel per unit time at time t;
$b = b_0 \exp(-2ax)$ = the breadth of the channel, where a is a constant;
$x = n\epsilon$, $t = m\tau$ } where m, n are integers;
k a coefficient of bottom friction;
g the acceleration due to gravity;
σ the speed of a harmonic motion, i.e. 2π/period.

The usual differential equations may be written in the form:

continuity:

$$\frac{\partial Q}{\partial x} = -b\frac{\partial \zeta}{\partial t} \tag{1}$$

motion:

$$\frac{\partial u}{\partial t} = -g\frac{\partial W}{\partial x} - \frac{ku|u|}{W}. \tag{2}$$

The non-linear inertia term $u(\partial u/\partial x)$ has been omitted from the equation of motion since it complicates the computations out of all proportion to its importance in the particular model chosen. This was confirmed by preliminary calculations using a desk machine.

If the estuary be partitioned by $N+1$ equidistant sections, commencing at the mouth ($n = 0$) and ending at the barrier ($n = N$), and the origin of time be given by $m = 0$, the finite difference form of (1) at section n and time $(m-\frac{1}{2})\tau$ is

$$\frac{(W_m - W_{m-1})_n}{\tau} = -\frac{1}{b_n}\frac{Q_{m-\frac{1}{2},\, n+\frac{1}{2}} - Q_{m-\frac{1}{2},\, n-\frac{1}{2}}}{\epsilon}.$$

This reduces to

$$W_{m,n} = W_{m-1,n} + pu_{m-\frac{1}{2},n-\frac{1}{2}}\frac{W_{m,n}+W_{m-1,n-1}}{2} - qu_{m-\frac{1}{2},n+\frac{1}{2}}\frac{W_{m,n}+W_{m-1,n+1}}{2},$$

where

$$p = \frac{\tau}{\epsilon}e^{a\epsilon},\ q = \frac{\tau}{\epsilon}e^{-a\epsilon},$$

by replacing $W_{m-\frac{1}{2},n+\frac{1}{2}}$ by the average of $W_{m,n}$ and $W_{m-1,n+1}$, and

$W_{m-\frac{1}{2},n-\frac{1}{2}}$ by the average of $W_{m,n}$ and $W_{m-1,n-1}$.

Then

$$W'_{m,n} = W_{m-1,n} + \gamma_{m,n} W_{m-1,n-1} - \delta_{m,n} W_{m-1,n+1} \tag{3}$$

where

$$W' = W(1-\gamma+\delta),\ \gamma_{m,n} = \tfrac{1}{2} p u_{m-\frac{1}{2},n-\frac{1}{2}},\ \delta_{m,n} = \tfrac{1}{2} q u_{m-\frac{1}{2},n+\frac{1}{2}}. \tag{4}$$

At section $n+\frac{1}{2}$ and time $m\tau$ the finite difference form of (2) becomes

$$\frac{(u_{m+\frac{1}{2}} - u_{m-\frac{1}{2}})_{n+\frac{1}{2}}}{\tau} = -\frac{g}{\epsilon}(W_{m,n+1} - W_{m,n}) - k\left\{\frac{u|u|}{W}\right\}_{m,n+\frac{1}{2}}.$$

If $W_{m,n+\frac{1}{2}}$ is replaced by the average of $W_{m,n}$ and $W_{m,n+1}$, and $(u|u|)_{m,n+\frac{1}{2}}$ by $u_{m+\frac{1}{2},n+\frac{1}{2}}|u_{m-\frac{1}{2},\,n+\frac{1}{2}}|$ it follows that

$$u'_{m+\frac{1}{2},n+\frac{1}{2}} = u_{m-\frac{1}{2}\,n+\frac{1}{2}} + \frac{g\tau}{\epsilon}(W_{m,n} - W_{m,n+1}) \tag{5}$$

where

$$\left.\begin{aligned} u' &= u(1+\alpha),\ \alpha_{m+\frac{1}{2},n+\frac{1}{2}} = w_{m,n+\frac{1}{2}}|u_{m-\frac{1}{2},n+\frac{1}{2}}|, \\ w_{m,n+\frac{1}{2}} &= 2k\tau/(W_{m,n} + W_{m,n+1}). \end{aligned}\right\} \tag{6}$$

Inspection of equation (3) shows that if the values of W are known at all sections of the channel at time $(m-1)\tau$, and the values of u are known at all points midway between sections at time $(m-\frac{1}{2})\tau$, then W can be computed for all n for time $m\tau$. Similarly, equation (5) enables $u_{m+\frac{1}{2}}$ to be calculated for all points midway between sections solely from a knowledge of $u_{m-\frac{1}{2}}$ and W_m. It is to obtain this state of affairs that the approximations leading up to equations (3) and (5) are required.

5. Boundary conditions

At the barrier ($n = N$) the required condition is that $Q_N = 0$ for all m. This affects the use of (3) at the barrier.

In finite difference form the condition may be written

$$(buW)_{N+\frac{1}{2}} = -(buW)_{N-\frac{1}{2}}$$

and hence (3) becomes

$$W'_{m,N} = W_{m-1,N} + 2\gamma W_{m-1,N-1} \tag{7}$$

where

$$W'_N = W_N(1-2\gamma), \qquad \gamma_{m,N} = \tfrac{1}{2} p u_{m-\frac{1}{2},N-\frac{1}{2}}. \tag{8}$$

6. Arrangement of computations for desk machines

To commence the calculations some arbitrary values must be given to W and u, and in the absence of an approximate solution to the problem to be considered the estuary water may be taken to be everywhere at rest with a depth corresponding to low water at the mouth, i.e.

$$u_{m+\frac{1}{2}} = 0 \quad \text{at} \quad m = 0 \quad \text{for all} \quad n+\tfrac{1}{2}$$
$$W_m = W^* \quad \text{at} \quad m = 0 \quad \text{for all} \quad n.$$

For all subsequent m, W^* will be prescribed at $n = 0$ only, and represents a known disturbance of elevation ζ travelling into the estuary from the sea.

Two simple schedules are all that are necessary for the work to proceed. The first is in the form

$$\gamma_m, \delta_m, W'_m, W_m \quad \text{for each of} \quad n = 0 \quad \text{to} \quad n = N,$$

and the second is in the form

$$u'_{m+\frac{1}{2}}, \omega_m, \alpha_{m+\frac{1}{2}}, u_{m+\frac{1}{2}} \quad \text{for each of} \quad n+\tfrac{1}{2}\,(n = 0 \quad \text{to} \quad N-1).$$

With the initial arbitrary conditions listed above, schedule 1 is completed for $m = 1$, using equations (3) and (4) for all sections except the barrier, for which equations (7) and (8) are used. Schedule 2 is then completed for $m = 1$ using equations (5) and (6). The calculations thus proceed alternately for W and u until a solution is reached. For the problem of a continuous oscillatory input of constant amplitude and period the calculations must be continued over a sufficient number of cycles for the effect of the arbitrary initial conditions to have died away. In a typical example (Figure 3) only a little over 2 cycles of calculations were required.

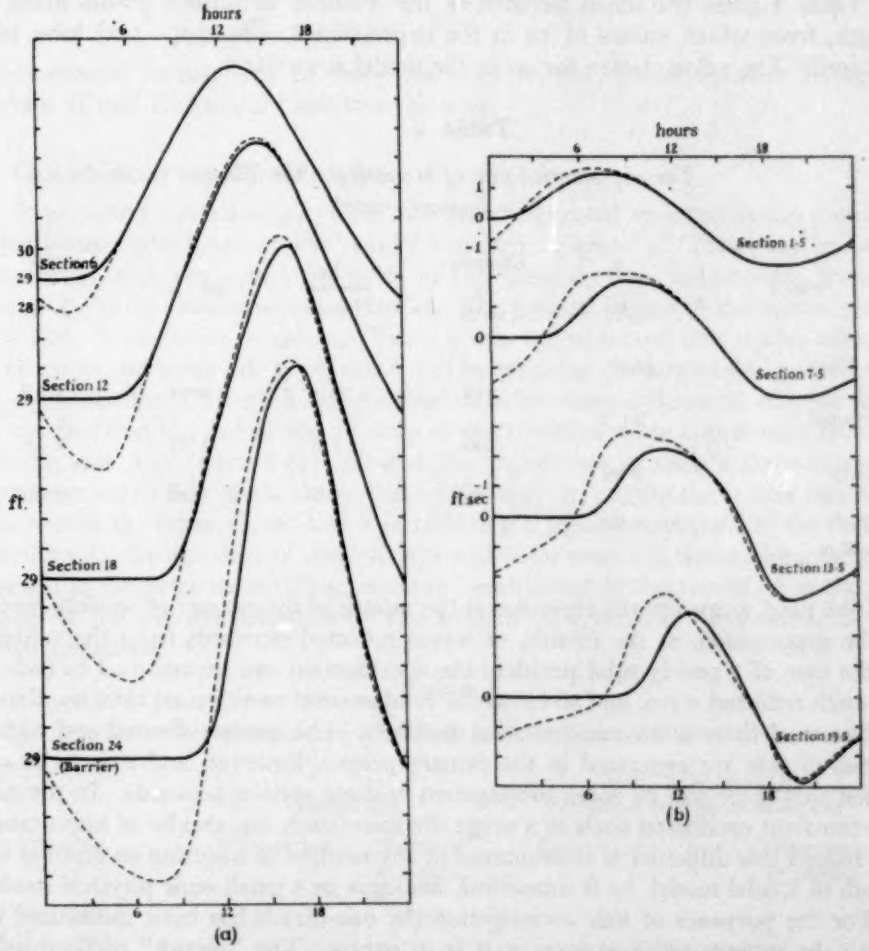

FIG. 3. Computed tidal elevations (a) and currents (b) at sections along an exponential estuary. ——— first cycle of computations, – – – – – second cycle. Prescribed input at the mouth is 3 cos 30°t.

The calculations present no difficulties to experienced computers using desk machines, but suffer from the disadvantage that they are not amenable to summation checks and need to be checked by repetition. The work is therefore most suited to an electronic computer, and it was programmed for the DEUCE machine belonging to the Computer Laboratory of the University of Liverpool by Mr J. M. Watt of that Laboratory, using a tabular interpretive programme. The author's thanks are due to Mr Watt and to the Director of the Laboratory for their assistance in this aspect of the paper.

7. Definition of the mathematical model; numerical data

The average cross-sectional depth of the Thames between Richmond Lock and Southend ranges from 6ft at Richmond Lock to 40ft at Southend. A reasonable mean value of

$$h = 32 \text{ ft.}$$

has been taken.

Table 2 gives the mean breadth of the Thames at various points along its length, from which values of $2a$ in the expression $b = b_0 \exp(-2ax)$ have been deduced. The value chosen for $2a$ in the model is 10^{-5}ft^{-1}

Table 2

The exponential law of breadth for the Thames
$b = b_0 \exp(-2ax)$

Place	b	Distance Δx	$\frac{bx}{b_{x+\Delta x}}$	$2a \,.\, \Delta x$	$2a$
	10^3ft	10^5ft			10^{-5}ft^{-1}
The Naze	26·2				
		21·2	12·3	2·51	1·18
Southend	21·3				
		9·0	7·2	1·97	2·19
Tilbury	2·95				
		1·3	3·6	1·28	0·99
London Bridge	0·82				

The need to specify the elevation at the mouth of the estuary effectively results in the suppression, at the mouth, of waves reflected outwards from the estuary. In the case of a purely tidal problem the specification can be assumed to include any such reflected wave, and so far as the fundamental semidiurnal tidal oscillation is concerned there is no mis-matching problem. The quarter-diurnal and higher species of tide are generated in the estuary proper, however, and it is to be expected that there will be some propagation of these species seawards. In the case of a transient oscillation such as a surge the mis-match can also be of importance, and indeed this difficulty is encountered in any method of injecting an input at the mouth of a tidal model, be it numerical, analogue or a small scale physical model.

For the purposes of this investigation the mis-match has been minimized by taking the estuary twice as long as it is in nature. The "mouth" of the model estuary is thus somewhere in the vicinity of Lowestoft, the total length from mouth to barrier being approximately 117 miles. To a first approximation the speed of

propagation of a free wave can be taken as $(gh)^{\frac{1}{2}}$, i.e. $32\,\mathrm{ft\,s^{-1}}$ Thus for a disturbance to travel from Southend to the barrier, and back to the mouth where it is reflected by mis-matching, and arrive again at Southend, a total distance of 234 miles, would take some 11 hours. This interval of time is so long that mis-matching effects cannot materially influence the conclusions drawn from the computational results. A further safeguard in this respect is the decay experienced by any disturbance travelling seawards; an example of this effect is referred to in Section 12 and illustrated in Table 6 for a semidiurnal tide of period 12 hours.

Benefiting from the experience of Otter and Day, to ensure stability in the calculations the ratio ϵ/τ was kept above the greatest value of $\{g(h+\zeta)\}^{\frac{1}{2}}$ found in the channel, i.e. approximately $39\,\mathrm{ft\,s^{-1}}$. For

$$\tau = 600\,\mathrm{s}, \qquad 2a = 10^{-5}\,\mathrm{ft^{-1}}, \qquad N = 24 \quad \text{and} \quad k = 0{\cdot}002$$

this led to

$$\epsilon = 0{\cdot}2560 \times 10^{5}\,\mathrm{ft}, \quad k\tau = 1{\cdot}20\,\mathrm{s}, \quad \frac{g\tau}{\epsilon} = 0{\cdot}750\,\mathrm{s^{-1}},$$
$$\tfrac{1}{2}p = 0{\cdot}013320\,\mathrm{s\,ft.^{-1}},$$
$$\tfrac{1}{2}q = 0{\cdot}010311\,\mathrm{s\,ft.^{-1}}.$$

Southend corresponds to section $n = 12$ in the model, London Bridge to section 18 and Richmond Lock to section 24.

8. Calculations for the tide alone

Preliminary calculations by trial and error suggested an input at the mouth of $3\cos 30°m\tau$, which led to the results shown in Figure 3. These are in better agreement with observed neap tides in the Thames than might have been expected from the crudeness of the model. The general shapes of the curves closely resemble those found in nature. Table 3 lists the observed and model values of both range and mean tide level, and it will be seen that the largest differences occur near the barrier. The most likely explanation for these differences may be found in the fact that the bed of the Thames slopes upwards quite appreciably from the mouth, and Airy (1842, § 343) showed the importance of such a slope in raising upstream mean tide levels above that of the sea. By taking the x-axis parallel to the bed of the estuary, and hence introducing a small component of the force of gravity into the equation of motion, it would seem probable that a closer approximation to the tides in the Thames could be obtained in the model. For the purposes of the present investigation the amount of agreement obtained is all that could be desired.

Table 3

Comparison of observed and computed tides

Section	Range (ft)		Mean tide level (ft) referred to that at Southend	
	Computed	Observed at neaps	Computed	Observed at neaps
12 (Southend)	11·1	11·5	—	—
18 (London Bridge)	14·8	15·4	0·73	0·7
24 (Richmond Lock)	17·3	11·2	1·23	4·4

9. Comparison of computer results with those for the linear law of friction

Doodson (1956) showed the usefulness of the linear law of friction if it is required to study the propagation of a diurnal surge in the presence of a semidiurnal tide, when the shallow water distortions are not an object of interest. But his model was uniform in cross-section and rather deep (128 ft), and it is of considerable interest to learn whether the linear law is of practical value in much shallower water. In addition such an investigation, if successful, affords a welcome check upon the method of computation.

The linear law expresses the frictional term in the equation of motion as fu. Comparing this with the quadratic expression $ku|u|/h$ Proudman (1953, §151) showed that for a sinusoidal current

$$f = \frac{8}{3\pi}\frac{k}{h}U$$

approximately, where U is the amplitude of the current.

The theoretical solution for a semidiurnal tide in an exponential estuary of the dimensions used in this paper is given by equations (10, 11) in the appendix. Given the mean value of U along the channel all the necessary parameters, together with the constant R, can be evaluated. From the computer results (Table 4) an average value for the estuary is

$$U = 2{\cdot}20\ \text{ft s}^{-1}.$$

Other numerical values required are

$$\sigma = 30^\circ h^{-1} = 1{\cdot}4544\times10^{-4}\text{s}^{-1}, \quad a = 0{\cdot}5\times10^{-5}\text{ft}^{-1}, \quad h = 32\text{ft}$$

$$c^2 = 1{\cdot}024\times10^{-3}\text{ft}^2\text{s}^{-2} \qquad a^2 - \frac{\sigma^2}{c^2} = 0{\cdot}0434\times10^{-10}\text{ft}^{-2}$$

$$\mu = 0{\cdot}253\times10^{-5} \qquad \kappa = 0{\cdot}328\times10^{-5}$$

$$r = -0{\cdot}172\times10^{-5} \qquad s = 0{\cdot}828\times10^{-5}$$

$$\theta = 73^\circ{\cdot}0 \qquad \phi = -34^\circ{\cdot}2$$

Values of amplitude (H) and phase lag (g) of the semidiurnal constituent of elevation in the DEUCE results were obtained by harmonic analysis and are given in Table 4, together with U and γ for the semi-diurnal current. The origin of time is taken as high water at the mouth. Values of H', g', U' and γ' derived directly from linear theory are also given in this Table. To compare them with the DEUCE results the phase lags have to be increased by $15^\circ{\cdot}6$ to bring them to the same time origin, and the amplitudes have to be multiplied by the ratio

$$R = (U \text{ from DEUCE})/U', \quad \text{or} \quad 9{\cdot}87\times10^5.$$

The last columns in Table 4 contain these adjusted values, and the agreement between these and the DEUCE results is extremely good, proving the reliability of the linear law of friction for studying the propagation of the principal tidal constituent in a river resembling the Thames.

10. Calculations for the surge alone

Whichever of the non-linear terms are responsible for the interaction it is plain that the greatest effect will be experienced when the total depth of water is least.

Table 4

Comparison of DEUCE results with those from the linear theory for bottom friction

Section	DEUCE results						Theoretical results					
	H ft	g deg.	U ft s^{-1}	γ deg.	H'/R	g' deg.	U'/R	γ' deg.	H ft	g deg.	U ft s^{-1}	γ deg.
0 (Mouth)	3·00	0			0·301	−15·6			2·97	0		
1·5			1·72	110			0·173	90·6			1·71	106
4·5			1·97	120			0·199	106·4			1·96	122
6·0	4·01	19			0·399	6·6			3·94	22		
7·5			2·26	131			0·228	115·8			2·25	131
10·5			2·52	140			0·256	124·2			2·53	140
12·0	5·32	42			0·534	27·8			5·27	43		
13·5			2·77	148			0·280	131·2			2·76	147
16·5			2·82	155			0·285	136·6			2·81	152
18	7·04	63			0·709	44·6			7·00	60		
19·5			2·41	161			0·246	140·4			2·43	156
22·5			1·16	163			0·120	141·8			1·18	157
24	8·28	72			0·828	52·3			8·17	78		
			Mean = 2·20									

Negative surges were therefore the first to be investigated; if a negative surge at low water were to show no interaction effect, further researches along the proposed lines would be fruitless.

The form of surge chosen was that of a single sinusoidal oscillation given by

$$S = 2(\cos 15^\circ t - 1) \quad \text{for} \quad t = 0 \text{ to } 24,$$
$$S = 0 \quad \text{for} \quad t < 0 \text{ and } t > 24,$$

where t is in hours.

In a non-tidal estuary this surge is propagated as shown in Figure 4. The main points of interest are:

(a) the speed of propagation of the first fall in level is in agreement with the theoretical celerity of $32\,\text{ft}\,\text{s}^{-1}$;

(b) the small amplification as the surge progresses towards the barrier,

and (c) the extremely rapid transmission of the lowest level.

Calculations for this type of problem have been previously carried out by Reid (1957).

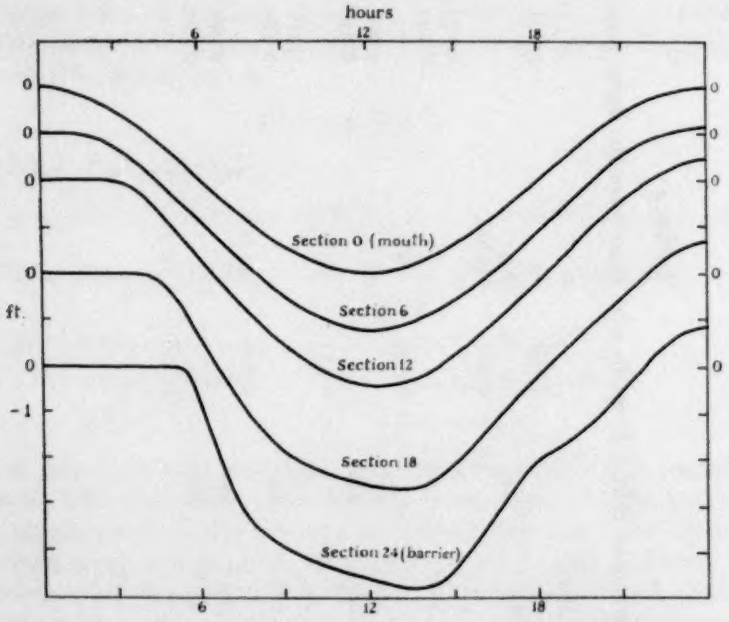

FIG. 4.—Computed surge elevations in a non-tidal exponential estuary. Prescribed input at the mouth is $2(\cos 15^\circ t - 1)$ for $t = 0$ to 24.

11. Calculations for tide plus surge

The first combination of tide and surge considered was a 4 ft negative surge, as defined in Section 10, phased so that its trough occurred at tidal low water at the mouth. Upon subtracting from the computed elevations the tide as computed in Section 8, the residues are found to differ appreciably (see Figure 5) from those of Section 10. In fact the computed surge exhibits precisely the interaction effect that is observed in nature in the Thames (see Figure 2). From Southend (Section 12) to the head of the estuary the surge troughs occur on the rising tide, but the

development of this tendency can be noted as near the mouth as Section 6. Moreover, it is remarkable that the trough of Figure 5 at $n = 12$ is 25 per cent lower than that of the surge alone (Figure 4), in accord with the observational result of Section 2.

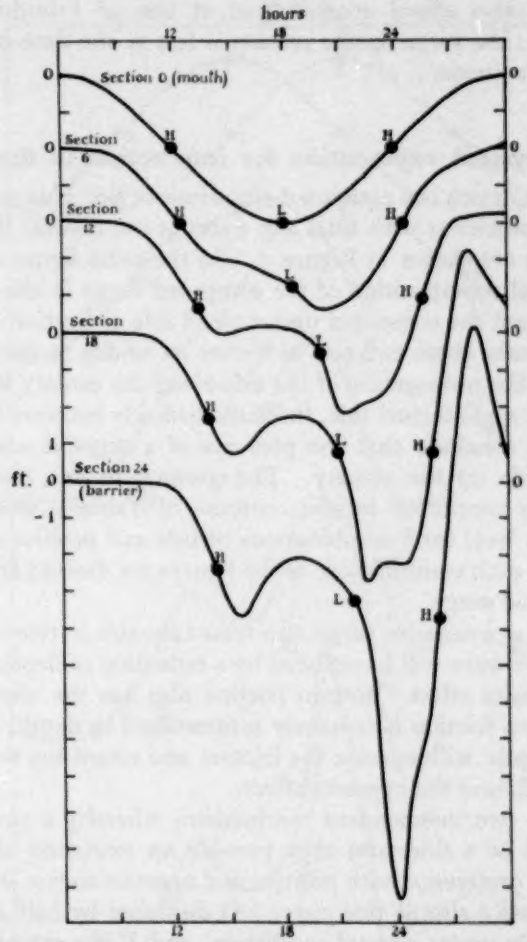

FIG. 5. Computed negative surge elevations for case of input trough coincident with tidal low water. H and L denote tidal high and low waters respectively.

To obtain complete confirmation that the model reproduces the observed interaction requires similar calculations to be made for other phase relations between tide and surge input, and the following cases have also been evaluated:

tidal amplitude (ft)	surge height (ft)	peak at	for residuals see Figure
3	+4	high water	6
		low water	6
		rising tide	7
		falling tide	7
	+6	as for +4 ft surge	—

Figures 6 and 7 exhibit the same phenomenon, viz., that in the estuary proper a surge is accentuated most on the rising tide. The computations for a 6ft surge have not been illustrated as they simply repeat, on a larger scale, the features mentioned.

The diagrams also afford confirmation of one of Proudman's conclusions (1955b), that " . . . the surge up the estuary is less at the time of high water than it is at the time of low water . . . ".

12. A simple physical explanation for interaction in the Thames

In Figure 8 are drawn the computed elevations of tide plus surge in the case of a negative surge coincident with tidal low water at the mouth; this is the case for which the residues are shown in Figure 5. In the same figure are shown the results of arithmetical superposition of the computed surge in the non-tidal estuary (see Section 10) upon the computed undisturbed tide of Section 8. If we consider the difference between these two sets of curves to be due to the influence exerted by the surge upon the propagation of the tide along the estuary it is apparent that, with respect to the undisturbed tide, the disturbed tide becomes increasingly later. We may therefore conclude that the presence of a negative surge causes the retardation of the tide up the estuary. The converse to this, that a positive surge hastens the tide, is supported by the contents of Table 5, which lists the time shifts of maximum level for 8 combinations of tide and positive surge. Two time shifts are given for each combination, as the figures are derived from computations covering one diurnal surge.

A fall in level, i.e. a negative surge, can retard the tide in two ways. The rate of progression of a free wave will be reduced by a reduction of depth; a positive surge will have the opposite effect. Bottom friction also has the effect of retarding a wave, and as bottom friction is inversely proportional to depth, a negative surge, by reducing the depth, will increase the friction and retard the wave even further; a positive surge will have the opposite effect.

Thus there are two independent mechanisms whereby a surge can influence the time of arrival of a tide, and they provide an extremely simple qualitative explanation for the preference both positive and negative surges show for the rising tide. Figure 9 shows a simple tide curve (A) displaced by half an hour (B). Let A represent the tide under normal conditions, and B the retarded tide due to a negative surge. It will be seen that the only state of tide which will contribute a further lowering of level is the rising tide. Now consider the case of a positive surge hastening the tide; this time B will represent the normal tide and A the hastened tide. Once again it will be seen that the only state of tide which will contribute a further appreciable rise in level is the rising tide.

One possible objection to the above explanation might be that the tides in the Thames are more nearly in the form of a standing oscillation than a progressive wave. This opinion has been very largely accepted in the past on the assumption that the estuary is uniform in cross-section. Otter & Day (1960) and Abbott (1960) have now shown that an exponential cross-section favours the progressive wave.

The theoretical solution for the principal semidiurnal tidal constituent, given in the appendix to this paper, clearly indicates two progressive waves for the chosen exponential channel. The incoming wave is given by the first expression in each of equations (10) and (11), and the reflected wave by the second expression. For

the incoming wave it is shown in Section 9 that the current leads the elevation by $\theta(= 73°)$ and that the amplitude of elevation increases from the mouth as $\exp(rX)$ with r negative and $X = 0$ at the barrier; in the reflected wave the current lags

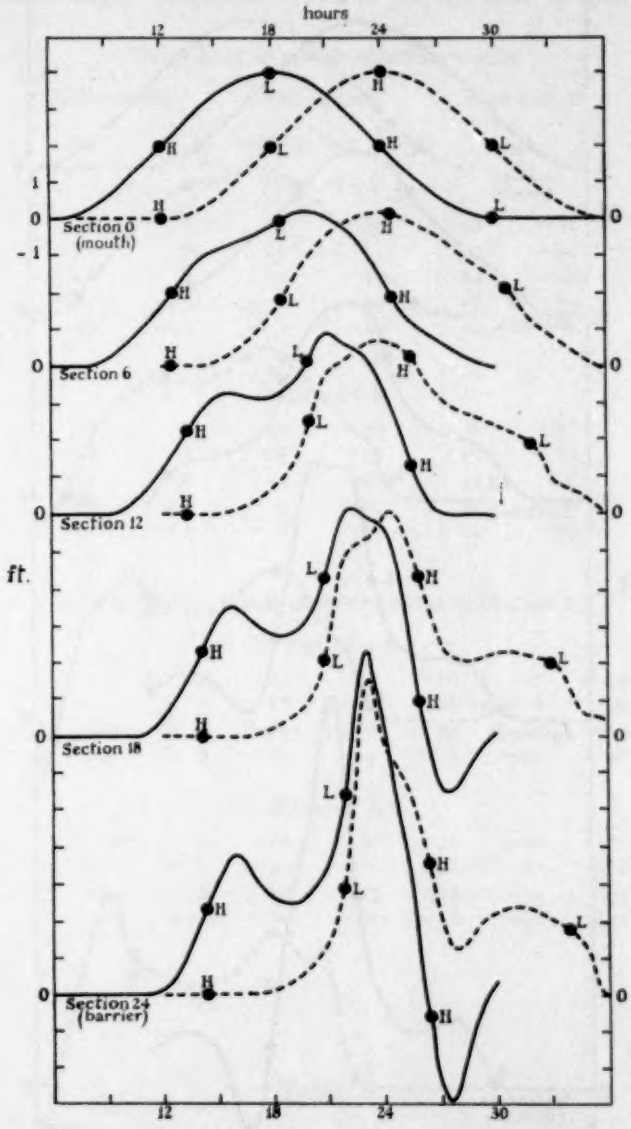

FIG. 6.—Computed positive surge elevations for cases of input peaks coincident with tidal high water (– – – – – –) and tidal low water (————). H and L denote tidal high and low waters respectively.

on the elevation by $\pi - \phi$ $(= 214°)$ and the amplitude of elevation decreases towards the mouth as $\exp(-sX)$ with s positive. Table 6 gives values of $\exp(rX)$ and $\exp(-sX)$ at points along the channel, and it is evident that the reflected wave is insignificant at the mouth, supporting the views of Otter & Day and of Abbott.

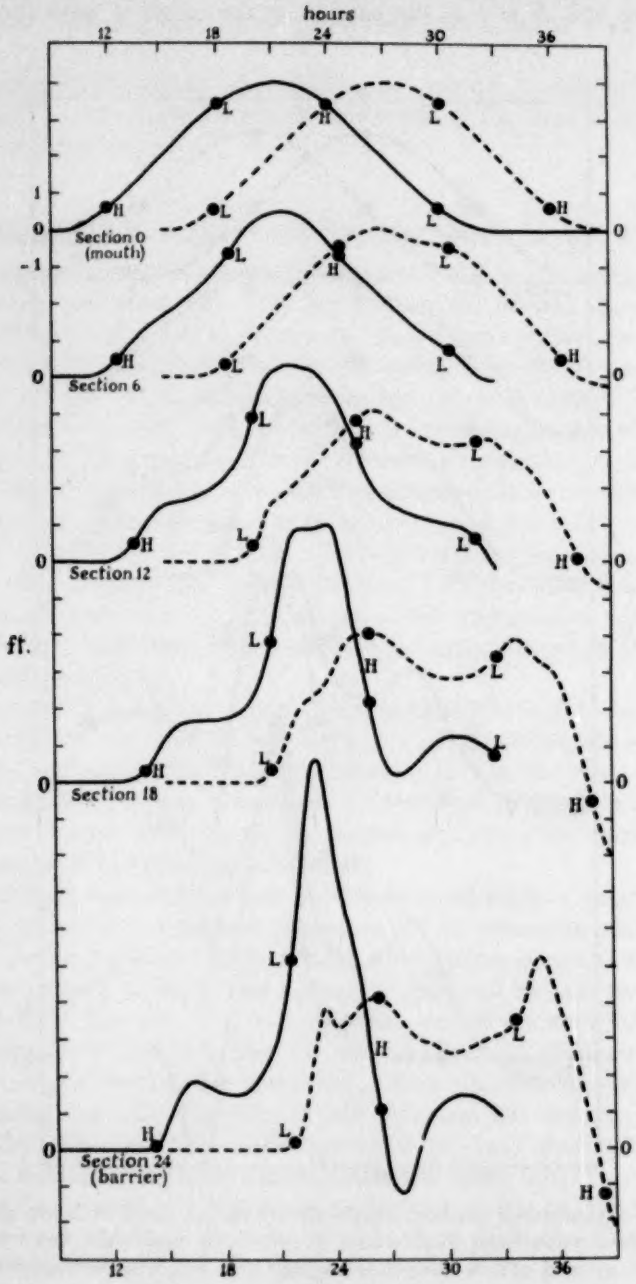

FIG. 7.—Computed positive surge elevations for cases of input peaks coincident with the rising tide (————) and the falling tide (– – – – –). H and L denote tidal high and low waters respectively.

Table 5

Time shifts of maximum level relative to the tide alone, for various combinations of tide and positive surge. Amplitude of tide is 3 ft, and units of time are minutes.

	Surge peak at mouth coincident with							
	High water		Falling tide		Low water		Rising tide	
	Lags on tide alone							
	Surge of 4 ft							
Section 0	0	− 5	30	−35	40	−40	40	−25
6	−10	0	15	?	30	−40	25	−30
12	−11	− 6	14	−41	24	−46	24	−36
18	−29	− 9	− 4	−44	16	−59	11	−54
24	−26	−11	− 1	−46	19	−66	14	−56
	Surge of 6 ft							
0	0	5	35	−50	60	−55	50	−35
6	−10	5	25	−50	40	−65	40	−45
12	−21	− 1	14	−51	34	−66	34	−46
18	−39	− 9	− 4	−59	26	−89	16	−79
24	−41	−11	− 1	−66	24	−96	19	−81
	Lags on tide alone relative to those at Section 0.							
	Surge of 4 ft							Mean
6	−10	5	−15	?	−10	0	−15	− 5	− 7
12	−11	− 1	−16	− 6	−16	− 6	−16	−11	−10
18	−29	− 4	−34	− 9	−24	−19	−29	−19	−20
24	−26	− 6	−31	−11	−21	−26	−26	−31	−22
	Surge of 6 ft							
6	−10	0	−10	0	−20	−10	−10	−10	− 9
12	−21	− 6	−21	− 1	−26	−11	−16	−11	−14
18	−39	−14	−39	− 9	−34	−34	−34	−44	−31
24	−41	−16	−36	−16	−36	−41	−31	−46	−33

Table 6

Relative amplitudes of incoming (e^{rX}) and reflected (e^{-sX}) waves for an exponential estuary resembling the Thames

$r = -0{\cdot}172 \times 10^{-5}$, $s = 0{\cdot}828 \times 10^{-5}$

Section	e^{rX}	e^{-sX}
0 (Mouth)	0·347	0·006
6	0·453	0·022
12	0·590	0·079
18	0·768	0·280
24 ($X = 0$)	1·000	1·000

Accepting the progressive wave regime of the tides in the Thames in personal correspondence, Proudman points out that formula (42) of his 1955a paper may be used to show that:

> "For equal sequences of meteorological conditions, the maxima of apparent surges are greater when they occur at a quarter tidal period before tidal high water than when they occur at a quarter tidal period after tidal high water".

This statement is in accord with the results of the present paper.

In passing, it is worth noting that Doodson's arguments of 1928 (see Section 2) are not so very different from those propounded here; he suggested a modification of tidal range by a surge whereas I suggest a time shift; he suggested wind stress as a potent factor whereas I suggest bottom friction.

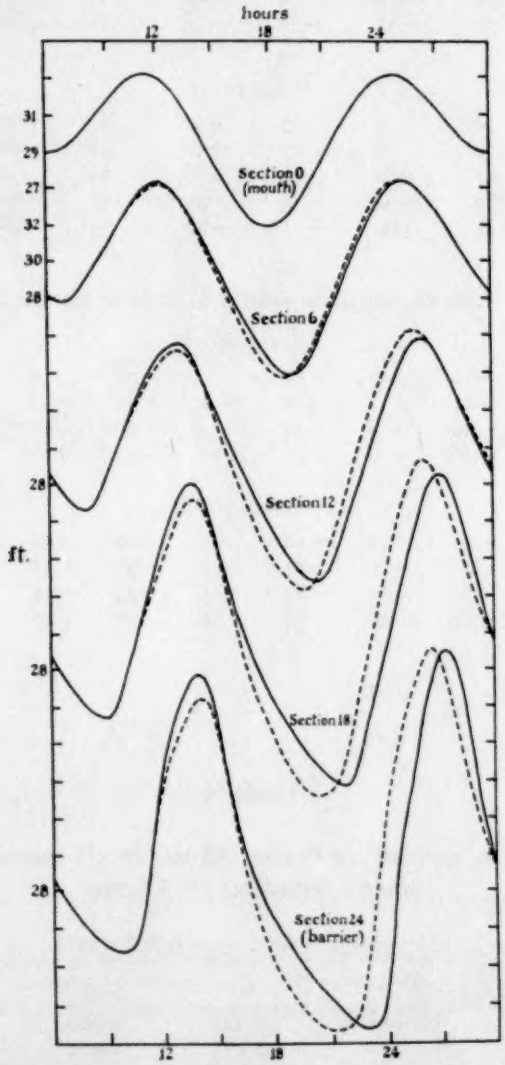

FIG. 8.—Comparison between computed elevations for an input of tide plus negative surge (————) and the superposition of computed elevations for tide alone and surge alone (– – – – –).

The above arguments relate to the time shift of a tide in the presence of a surge. Similar qualitative conclusions may be arrived at if the tide is considered as shifting the surge in time relative to the surge in non-tidal waters. To attempt a determination of the relative importance of these two aspects of the problem would appear to be profitless. What clearly emerges from the foregoing is that "surges" in the Thames, as defined by subtracting the undisturbed tide from the observed levels, cannot be forecast solely in terms of meteorological variables. Indeed, forecasting formulae for the Thames should be ideally designed to predict, not a surge which can be added to the predicted tide, but tide plus surge as a whole.

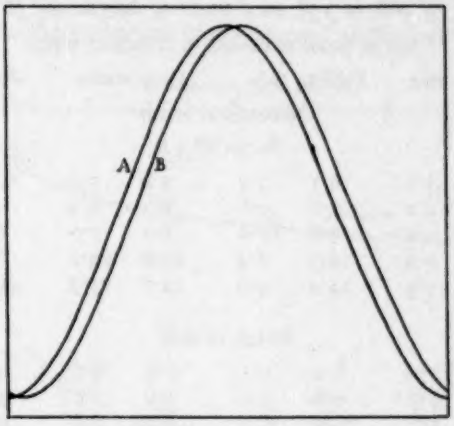

FIG. 9.—A semidiurnal oscillation (A) displaced half an hour (B).

The computer results, when viewed in the light of the physical mechanisms suggested, indicate that interaction is most likely when tide and surge have been travelling together for some distance in quite shallow water. This would explain why no interaction has been found at Tynemouth, Immingham and Lowestoft, the mean depth of water being too great. By the same token it would be expected that interaction should be found well up the River Humber, in the Wash and in the River Severn.

13. The propagation of maximum levels

It was stated in Section 1 that some practical results were required from the present investigation; in particular there is a need for a simple method of including the effect of interaction on the propagation of dangerously high levels into and along the Thames.

Table 7 lists the maximum levels reached at sections 0, 6, 12, 18 and 24 as obtained from the results of 8 combinations of positive surges with the same tide. Two heights are given for each combination as the figures are derived from computations covering one diurnal surge; the heights are referred to the undisturbed level of 32 ft. In the same table are given the amplifications of these levels, as they travel up the estuary, relative to the level at the mouth. They show that the amplification is a function of the level at the mouth, the nature of the function being illustrated in Figure 10. It is clear that there is a strong tendency for the higher, more dangerous levels to be amplified less than the lower levels. Another,

but less comprehensive way of putting this, is that dangerous "surge" peaks tend to avoid tidal high water.

Whilst of considerable practical importance, the amplifications given in Figure 10 cannot be applied directly to the Thames, as the mathematical model cannot be considered a sufficiently close approximation to nature; the results nevertheless indicate profitable lines for future research into both mathematical models and observational data.

Table 7

Maximum levels of tide plus surge referred to the undisturbed level of 32 ft. Amplitude of tide is 3 ft, and units of height are ft

	Surge peak at mouth coincident with:								
	High water		Falling tide		Low water		Rising tide		
	Maximum levels								
	Surge of 4 ft								Tide alone
Section 0	7·0	3·0	6·5	3·7	5·2	5·2	3·7	6·5	3·0
6	8·2	4·0	7·8	4·6	6·3	6·2	4·8	7·6	4·1
12	10·1	5·4	9·6	6·0	8·1	7·6	6·3	9·3	5·7
18	12·6	7·9	12·3	8·4	10·8	10·1	8·7	11·6	8·2
24	14·2	9·5	14·2	9·9	12·7	13·4	10·1	13·0	10·0
Surge of 6 ft									
0	9·0	3·0	8·2	4·1	6·4	6·4	4·1	8·2	
6	10·3	4·0	9·6	5·0	7·6	7·5	5·2	9·5	
12	12·2	5·2	11·5	6·3	9·4	8·8	6·7	11·1	
18	14·5	7·7	14·4	8·5	12·1	11·0	9·0	13·2	
24	16·2	9·4	16·5	10·0	14·2	12·3	10·3	14·3	
	Ratios of maximum levels to those at Section 0								
	Surge of 4 ft								
6	1·17	1·33	1·20	1·24	1·21	1·19	1·30	1·18	1·37
12	1·44	1·80	1·48	1·62	1·56	1·46	1·70	1·43	1·90
18	1·80	2·63	1·89	2·17	2·08	1·94	2·35	1·78	2·73
24	2·03	3·20	2·18	2·68	2·44	2·58	2·73	2·00	3·33
	Surge of 6 ft								
6	1·14	1·33	1·17	1·22	1·19	1·17	1·27	1·16	
12	1·36	1·71	1·40	1·54	1·47	1·38	1·63	1·35	
18	1·61	2·57	1·75	2·07	1·89	1·72	2·19	1·61	
24	1·80	3·13	2·01	2·46	2·22	1·92	2·51	1·74	

Appendix

Propagation of tides in a channel of constant depth and exponentially varying breadth under the influence of the linear law of friction.

We shall use the same notation as in Section 4 except that it is more convenient to take $X = L - x$ where L is the length of the channel, so that $X = 0$ at the barrier. Hence $b = b_0 \exp(2aX)$, and the positive direction of u is towards the sea. Also let $bu = V$. The equations of continuity and motion for first order terms only are

$$hV_X = -b\zeta_t, \; bg\zeta_X = -V_t - fV$$

where suffixes X, t represent partial differentiation with respect to these variables. For a single harmonic constituent of speed σ, V is given by the real part of $\exp(i\sigma t)F(x)$, and elimination of ζ from the above equations gives

$$V_{XX}-2aV_X+\frac{\sigma^2}{c^2}\left(1-i\frac{f}{\sigma}\right)V = 0.$$

The solutions of this homogeneous differential equation are derived from the roots of the auxiliary equation

$$p^2-2ap+\frac{\sigma^2}{c^2}\left(1-i\frac{f}{\sigma}\right) = 0 \tag{9}$$

and are given below for the condition of no current at the barrier ($u = 0$ at $X = 0$).

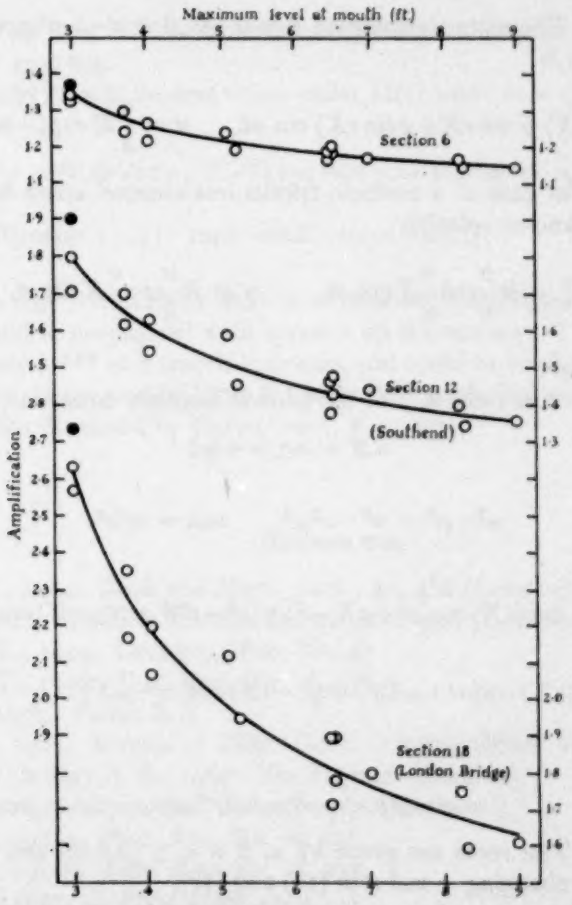

FIG. 10.—Amplification of maximum levels up an exponential estuary relative to those at the mouth, as a function of the maximum level at the mouth.

○ for tide + surge; ● for tide alone.

Case I. $f = 0$. Auxiliary equation: $p^2-2ap+\sigma^2/c^2 = 0$

(1) $a > \sigma/c$. The roots α and β are real and unequal,

$$\alpha = a+(a^2-\sigma^2/c^2)^{\frac{1}{2}}, \quad \beta = a-(a^2-\sigma^2/c^2)^{\frac{1}{2}}$$

and the solution is

$$\zeta = R[s\exp(rX) - r\exp(sx)]\cos\sigma t, \qquad u = -\frac{\sigma}{h}R[\exp(rX) - \exp(sX)]\sin\sigma t$$

where

$$r = \alpha - 2a, \qquad s = \beta - 2a, \text{ and } R \text{ is an arbitrary constant.}$$

(2) $a = \sigma/c$. The roots are real and equal, and the solution is

$$\zeta = R\exp(-aX)(1+aX)\cos\sigma t$$

$$u = \frac{\sigma}{h}R\exp(-aX)\,X\sin\sigma t.$$

(3) $a < \sigma/c$. The roots are complex, $\alpha = a+ir, \beta = a-ir$ where, $r^2 = \sigma^2/c^2 - a^2$, and the solution is

$$\zeta = R\exp(-aX)(r\cos rX + a\sin rX)\cos\sigma t, \qquad u = \frac{\sigma}{h}R\exp(-aX)\sin rX\sin\sigma t.$$

The particular case of a uniform frictionless channel arises here with $a = 0$, giving the well-known solution

$$\zeta = R\frac{\sigma}{c}\cos\frac{\sigma}{c}X\cos\sigma t, \qquad u = R\frac{\sigma}{h}\sin\frac{\sigma}{c}X\sin\sigma t.$$

Case II. $f \neq 0$.

(1) $a > \sigma/c$. The roots α, β of the general auxiliary equation (9) are complex:

$$\alpha,\beta = a \pm (\kappa + i\mu)$$

where

$$\kappa^2 - \mu^2 = a^2 - \sigma^2/c^2, \qquad 2\kappa\mu = \sigma f/c^2.$$

The solution is

$$\zeta = R\{(\mu^2+s^2)^{\frac{1}{4}}\exp(rX)\cos(\sigma t + \mu X - \theta) + (\mu^2+r^2)^{\frac{1}{4}}\exp(-sX)\cos(\sigma t - \mu X - \phi)\} \tag{10}$$

$$u = -\frac{\sigma}{h}R\{\exp(rX)\cos(\sigma t + \mu X) - \exp(-sX)\cos(\sigma t - \mu X)\} \tag{11}$$

where

$$r = \kappa - a, \qquad s = \kappa + a, \qquad \theta = \tan^{-1} s/\mu, \qquad \phi = \tan^{-1} r/\mu.$$

(2) $a < \sigma/c$. The roots are given by $\alpha, \beta = a \pm (\mu + i\kappa)$ and the solution is obtained by interchanging κ and u in (10) and (11).

The particular case of a uniform channel arises here with $a = 0$ and $\mu^2 - \kappa^2 = -\sigma^2/c^2$, for which the solution is

$$\zeta = R(\mu^2+\kappa^2)^{\frac{1}{4}}\{\exp(\mu X)\cos(\sigma t + \kappa X - \theta) + \exp(-\mu X)\cos(\sigma t - \kappa X - \theta)\}$$

$$u = -\frac{\sigma}{h}R\{\exp(\mu X)\cos(\sigma t + \kappa X) - \exp(-\mu X)\cos(\sigma t - \kappa X)\}$$

with

$$\theta = \tan^{-1}\mu/\kappa.$$

(3) $a = \sigma/c$. Here $\mu = \kappa = (\sigma f/2c^2)^{\frac{1}{2}}$, and the solution is the same as either of cases II(1) or (2).

Remarks on solutions

In the absence of friction and geostrophic effects (Case I) the incoming and reflected waves for all species of tide combine to give the well-known equations for standing oscillations. The introduction of friction (Case II) affects the waves so that in each of them the elevation and the current are not in phase, and standing oscillations cannot result from their superposition. In case II(1) the speed of propagation of both waves is σ/μ, in case II(2) it is σ/κ. With the dimensions chosen for the model,

$$ac = 1{\cdot}6 \times 10^{-4}\,\mathrm{s}^{-1}$$

and it follows that Case II(2) is applicable for all tidal constituents of period greater than $2\pi/ac$, or 10·9 hrs.

One particular case of interest arises under II(1) when $\kappa = a$. Then $\mu = \sigma/c$, $f = 2ac$ and

$$\zeta = R\{(\mu^2+4a^2)^{\frac{1}{2}}\cos(\sigma t+\mu X-\theta)+\mu\exp(-2aX)\cos(\sigma t-\mu X)\},$$

$$u = -\frac{\sigma}{h}R\{\cos(\sigma t+\mu X)-\exp(-2aX)\cos(\sigma t-\mu X)\}.$$

It will be seen that the incident wave is of constant amplitude, both in elevation and current, and is propagated with speed c up the estuary. The reflected wave decays at the rate e^{-2aX} as it travels seawards, and could be negligible at the mouth. This is the special case used by Otter & Day in their analytical work on the Thames barrage, and first discussed by Harris (1907, **5**, p. 295).

References

Abbott, M. R., 1960. *Dock and Harb. Auth.*, **41**, 482 (London).
Airy, G. B., 1842. Tides & Waves. *Encycl. Metropol.* (London).
Doodson, A. T., 1929. *Geophys. Mem.* No. 47.
Doodson, A. T., 1956. *Proc. Roy. Soc. A*, **237**.
Hansen, W., 1956. *Tellus*, **8**, 3.
Harris, R. A., 1907. *Manual of Tides* (Govt. Printing Office, Washington).
Otter, J. R. H. & Day A. S., 1960. *The Engineer* (London).
Proudman, J., 1953. *Dynamical Oceanography* (Methuen).
Proudman, J., 1955a. *Proc. Roy. Soc. A*, **231**.
Proudman, J., 1955b. *Proc. Roy. Soc. A*, **233**.
Proudman, J., 1957. *J. Fluid Mech.*, **2**, 4.
Proudman, J., 1958. *J. Fluid Mech.*, **3**, 4.
Reid, R. O., 1957. *A. & M. Coll. Texas, Tech. Report* 57-257.
Rossiter, J. R., 1954. *Phil. Trans. A*, **915**, 246.
Rossiter, J. R., 1959. *Quart. J.R. Met. Soc.*, **85**, 365.
Tomczak, G., 1952a. *Dtsch. Hydrogr. Z.*, **5**, 2/3.
Tomczak, G., 1952b. *Dtsch. Hydrogr. Z.*, **5**, 5/6.

Heat Flow in the Austrian Alps

Sydney P. Clark, Jr.

(Received 1961 March 21)

Summary

Data on underground temperature obtained during the construction of the Arlberg and Tauern tunnels in Austria have been combined with measurements of the thermal conductivity of 42 samples of rock from near the tunnels to calculate the terrestrial heat flow. The value in the Arlberg is found to be $(1{\cdot}9 \pm 0{\cdot}2) \times 10^{-6}$ cal/cm^2 s, and in the Tauern, $(1{\cdot}8 \pm 0{\cdot}2) \times 10^{-6}$ cal/cm^2 s. The new results are in good agreement with the value $1{\cdot}9 \times 10^{-6}$ cal/cm^2 s found earlier in the Loetschberg tunnel in Switzerland, and indicate that relatively high geothermal fluxes extend into the eastern Alps. The high flux can be attributed to radioactive heat generation in a thickened crust.

1. Introduction

Determinations of terrestrial heat flow in the Alps, based on the temperatures measured in the three longest Swiss railroad tunnels, were reported in a previous paper (Clark & Niblett 1956; hereafter referred to as I). In the summer of 1960 the writer had the opportunity to visit two of the great Austrian tunnels and collect samples for the measurement of thermal conductivity. The results, coupled with the temperatures observed during construction of the Arlberg and Tauern tunnels, yield two determinations of heat flow in the eastern Alps, which provide an interesting extension of the Swiss data.

The locations of the Arlberg and Tauern tunnels are shown in Figure 1. The Arlberg runs through gneisses and schists of the pre-Mesozoic basement beneath the Arlberg pass, which connects the Tyrol with the Vorarlberg. The tunnel was completed in 1884. The Tauern tunnel runs through granites and granite gneisses which out-crop in the so-called Hohe Tauern Window. It lies about 220 km to the east of the Arlberg, and it was completed in 1908.

2. Temperature measurements

Temperature profiles are shown in Figures 2 and 3. In the Arlberg the temperatures of the rock were measured with mercury thermometers in bore-holes 0·8 m deep in the walls of the tunnel. The measurements are described by Wagner (1884), from whose paper the data were taken. The temperature of the air of the tunnel was measured simultaneously; it was usually greater than the rock temperature, but the difference rarely exceeded 3 °C. Judging by the irregularities in the temperature profile of Figure 2, the measurements are uncertain by about 1 °C.

The temperatures in the Tauern tunnel were taken from handwritten reports of the construction company, which are preserved in the Verkehrsarchiv in Vienna. The technique and accuracy of the measurements are presumably roughly the same as in the Arlberg. The temperature measured at the point 4 km from the north portal appears to be definitely low in relation to the surrounding measurements, however, and a value interpolated from adjacent observations was used for this point (dashed line, Figure 3).

The Tauern tunnel encountered springs between 6 and 6·5 km from the north portal. These appear to have cooled the rock in their vicinity, and only the temperatures measured within 5·5 km of the north end of the tunnel were used to determine the heat flow.

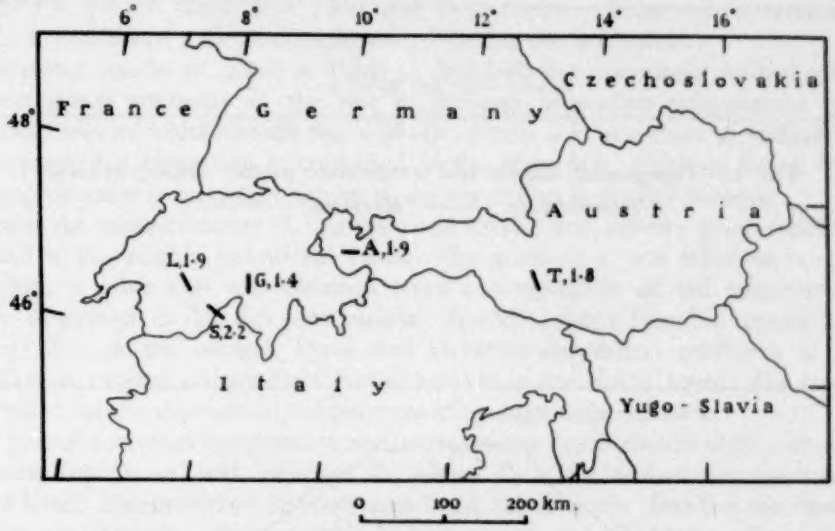

FIG. 1.—Location map. The Arlberg, Tauern, Gotthard, Loetschberg, and Simplon tunnels are shown as heavy dashes and are identified by the first letters of their names. The numbers following the letters are the heat flows in units of 10^{-6} cal/cm^2 s.

The temperatures at the portals of the tunnels were estimated by extrapolation of the temperatures within the tunnels. In the Arlberg a value of 6·3 °C was obtained in this way, which is reasonable for the elevation of the tunnel. A more complicated situation is encountered in the Tauern, since near the portal the tunnel runs in valley fill with only a few tens of metres of cover. About 0·5 km from the portal it passes under the steep cliffs which form the south wall of the Anlauftal; the temperature at this point, found by extrapolation to be 4·7 °C, is taken to be the same as the temperature at the portal. This temperature is unusually low for the elevation of the tunnel, probably because the point of observation lies at the foot of a steep cliff which faces northward.

Neither tunnel is level, and it is convenient to correct the temperatures in each to a common elevation. This was done using the uncorrected gradients given in Table 2, which were determined by expressing the observed temperatures as functions of vertical cover without correction for topographic irregularities. The Arlberg was corrected to an elevation of 1 300 m; the maximum correction

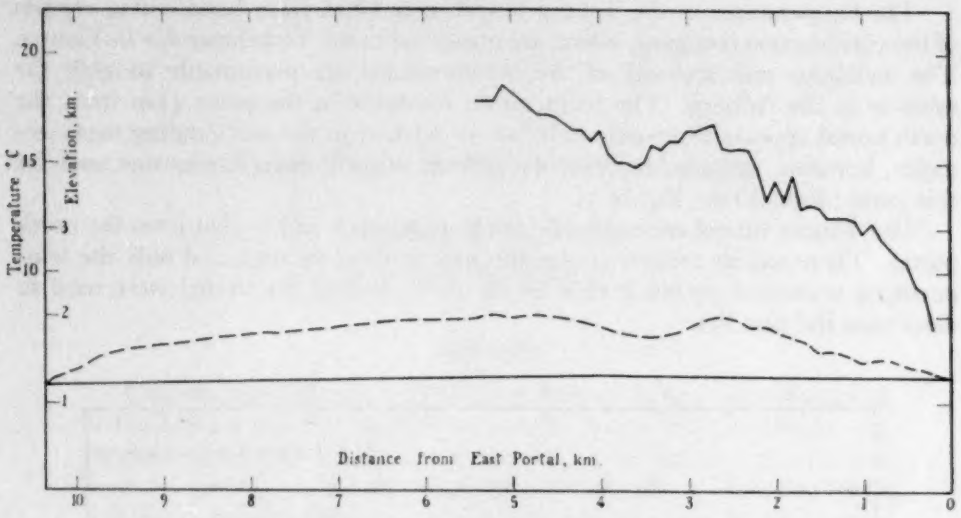

FIG. 2.—Topographic section and temperature profile, Arlberg tunnel, Temperature: ———; elevation: – – – – –.

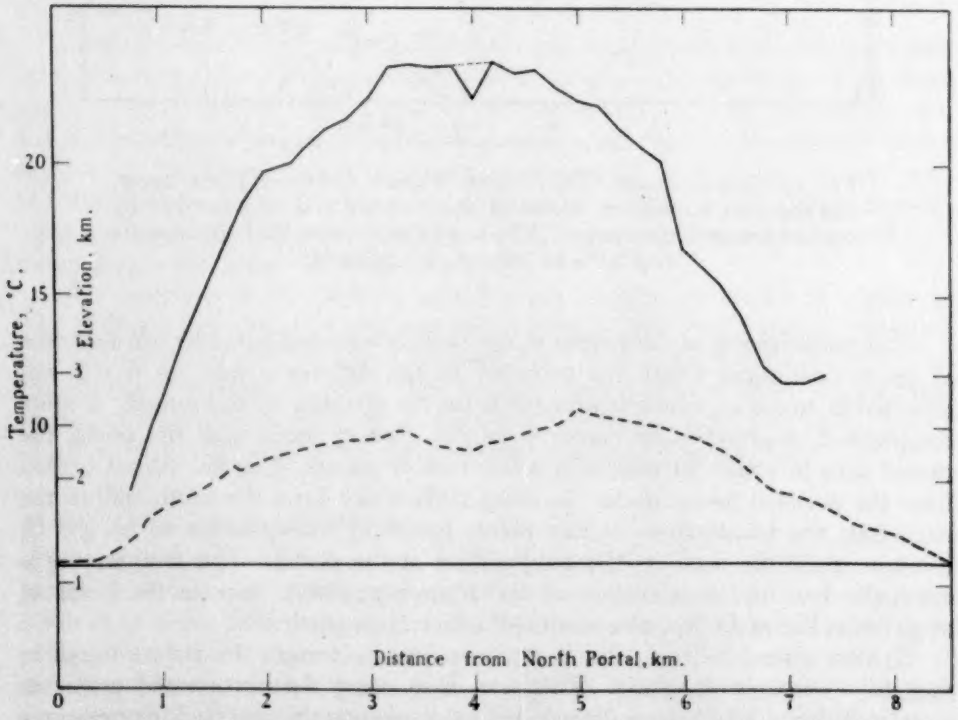

FIG. 3.—Topographic section and temperature profile, Tauern tunnel. Temperature: ———; elevation: – – – – –.

was 0·2°C. Temperatures in the Tauern were corrected by 0·5°C at most to bring them to an elevation of 1 200 m.

3. Geothermal gradients

Topographical corrections were made for stations at intervals of 0·5 km from the portals of both tunnels. The correction was the same as used in I (see also Clark 1957). Account was taken of the evolution of the topography by assuming that an initially plane surface was uplifted by an amount L in time t and simultaneously eroded to the present topography. The present (projected) position of the initial surface is a distance D above the tunnel, and the depth of a station is denoted by z. Calculations were made for $t = 25 \times 10^6$ years, $L = 4$ km, and $D = 3{\cdot}5$ km, and for $t = 4 \times 10^6$ years, $L = 3$ km, and $D = 2{\cdot}4$ km. These values were also used in I, and hence a direct comparison of the results is possible.

Corrected results are given in Table 1. Symbols not previously defined are α, the geothermal gradient; α', the rate of decrease of surface temperature with elevation; and a, which stands for $2/(\pi\kappa t)^{\frac{1}{2}}$, where κ is the thermal diffusivity. The topographic correction is contained in the term $\bar{h}(t)$, which is found from topographic maps in a manner similar to the correction in gravity surveys.

From the measurements of thermal conductivity and density given below, κ is found to be roughly 50 km^2/10^6 years. The gradient α' was taken to be 4·67 deg C/km, a value that was obtained from a compilation of soil temperatures briefly described in I. For comparison, Kerner (1905) found a gradient of 4·4 deg C/km in the central Tyrol and elevation-dependent gradients of 5·5 deg C/km at 1 250 m and 4·0 deg C/km at 2 000 m in the North Tyrol. His results were based on the decrease in temperature of springs with elevation.

A plot of corrected temperature against corrected depth should yield a straight line with slope $\alpha - \alpha'$ and intercept T_0, where T_0 is the surface temperature at tunnel level. Parameters of least-squares lines, fitted to the data for the various assumptions about the physiographic history, are given in Table 2 and two cases are shown in Figures 4 and 5. In the Arlberg tunnel the points representing the stations near the portal fall systematically above the line, and the temperature at the portal falls about 1°C below it. No point departs from the least-squares line by more than 1·1°C, however, and hence the results are within the uncertainties of the topographic correction and the measurements of temperature.

The temperatures at stations 1·0 and 1·5 in the Tauern tunnel fall as much as 3·6°C below the least-squares lines, and the intercepts of the lines are 1·5°C or more beneath the temperature at the portal. Three plausible explanations of the low temperatures can be given. The stations are close to the steep cliffs forming the south wall of the Anlauftal, and the topographic correction, which is approximate, may fail in cases of such rough topography. The cliffs face to the north, which may cause the temperatures at the surface, and consequently the temperatures at depth, to be abnormally low. Finally, the rocks in this vicinity are thermally anisotropic, conducting best in the plane of their foliation. The strike of the foliation is roughly perpendicular to the trend of the valley, so that there is a tendency for heat to be channelled towards the cliffs. This could also lead to low underground temperatures.

The data given in parts B and C of Table 2 were calculated by retaining or rejecting stations 1·0 and 1·5. The difference in gradient is 1·5 deg C/km at most, or about 7 per cent. Without the low points, the slope of the curve depends

Table 1

Topographic corrections

Station	Depth	Corrected temperature $T-\alpha' Laz$ (°C)			Corrected depth $z-\bar{h}(t)+az(D-z)$ (m)		
		$t=\infty$	$t=25\times10^6$ y, $L=4$ km	$t=4\times10^6$ y, $L=3$ km	$t=\infty$	$t=25\times10^6$ y, $D=3{\cdot}5$ km	$t=4\times10^6$ y, $D=2{\cdot}4$ km
			A. *Arlberg Tunnel*				
East Portal	0	6·3	6·3	6·3	0	0	0
0·5	130	10·4	10·3	10·3	165	180	185
1·0	175	11·9	11·8	11·7	250	270	280
1·5	300	13·1	12·9	12·8	380	410	425
2·0	510	14·3	14·0	13·7	515	570	595
2·5	660	15·7	15·3	15·0	565	635	670
3·0	555	16·6	16·3	16·0	605	660	690
3·5	480	15·1	14·8	14·6	595	645	670
4·0	575	16·7	16·4	16·1	635	695	725
4·5	680	17·2	16·8	16·4	660	735	765
5·0	680	18·3	17·9	17·5	690	765	795
5·4	675	17·7	17·3	16·9	690	765	795
			B. *Tauern Tunnel*				
North Portal	0	4·7	4·7	4·7	0	0	0
1·0	500	10·6	10·3	10·0	515	565	600
1·5	755	15·7	15·3	14·9	675	755	795
2·0	975	19·6	19·0	18·5	750	860	910
2·5	1 120	21·0	20·3	19·7	790	910	970
3·0	1 180	22·6	21·9	21·3	840	965	1 030
3·5	1 190	24·0	23·3	22·7	880	1 010	1 075
4·0	1 110	24·1	23·4	22·9	940	1 055	1 115
4·5	1 255	23·9	23·2	22·5	960	1 085	1 150
5·0	1 440	22·9	22·0	21·3	920	1 070	1 145
5·5	1 335	21·5	20·7	20·0	905	1 045	1 120

critically on the temperature at the portal since the remaining stations range over a corrected depth of only about 300 m and the shallowest of them is 750 m in depth. If the standard error of the slope is calculated in the usual way, no account is taken of the uncertainty of about 1 °C in the temperature at the portal. The standard deviations of the slopes given in part C of Table 2 were found by determining the variance of the slope as usual, and increasing this value by 1 (deg C/km)^2. This is very nearly equivalent to assuming that the temperature at the portal has a standard deviation of 1 °C which is independent of the scatter of the remaining points. The standard errors calculated in this way are close to those given in part B of Table 2. The differences between the 9-point and the 11-point solutions are much less than the differences between the extreme assumptions about the topographic history, and no serious additional uncertainty in the final results is introduced by the lack of an objective way of deciding which is superior.

Table 2

Parameters of least-squares lines

t 10^6 years	L m	D m	$\alpha - \alpha'$ deg C/km	Intercept °C	Standard deviation °C
			A. *Arlberg Tunnel*		
∞	...	...	15·01 ± 0·94	7·24	0·72
25	4 000	3 500	13·10 ± 0·74	7·26	0·62
4	3 000	2 400	12·03 ± 0·75	7·33	0·66
Uncorrected			14·02 ± 1·14	8·04	0·91
			B. *Tauern Tunnel, including stations* 1·0 *and* 1·5		
∞	...	...	21·75 ± 1·88	2·99	1·66
25	4 000	3 500	18·20 ± 1·47	3·14	1·50
4	3 000	2 400	16·47 ± 1·42	3·21	1·55
Uncorrected			13·97 ± 1·39	5·23	1·85
			C. *Tauern Tunnel, excluding stations* 1·0 *and* 1·5		
∞	...	...	20·20 ± 1·44	4·80	0·87
25	4 000	3 500	16·94 ± 1·40	4·77	0·96
4	3 000	2 400	15·31 ± 1·37	4·81	0·96

4. Thermal conductivity

Measurements of thermal conductivity were made on samples collected at the surface above the tunnels. Conductivity was determined in a modified divided bar apparatus, of the kind described by Birch (1950), at a mean temperature of 25 °C. The samples could be loaded with axial pressures up to 2 500 lb/in^2; the effect of this load was less than the experimental error, which is estimated to be about 2 per cent.

The rocks of the Arlberg presented a problem in sampling, because they are steeply dipping garnetiferous phyllites and micaceous gneisses. It was difficult to collect specimens from which disks, 1·5 inches in diameter, could be cut with the plane of the disk perpendicular to the plane of the foliation of the rock. Eight samples were collected from outcrops along the road which winds over the Arlberg pass. Despite efforts to make the sampling as representative as possible, it is undoubtedly biased in favour of the more resistant, less fissile units. These are

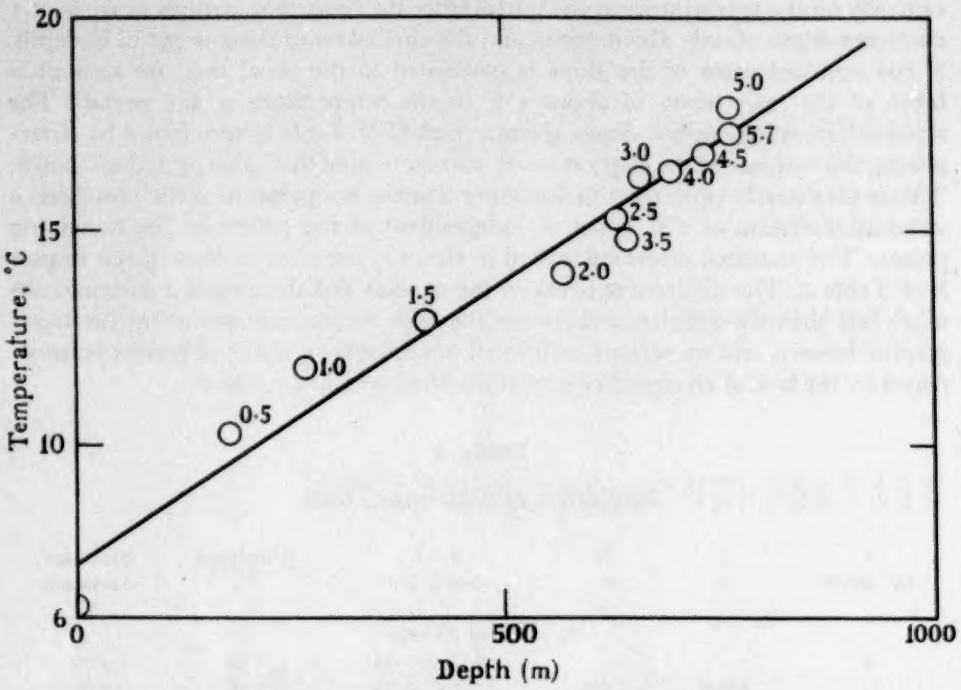

FIG. 4.—Corrected temperatures as function of corrected depth, Arlberg tunnel. The stations are numbered by their distances in kilometres from the east portal. $t = 25 \times 10^6$ years, $L = 4$ km, $D = 3{\cdot}5$ km.

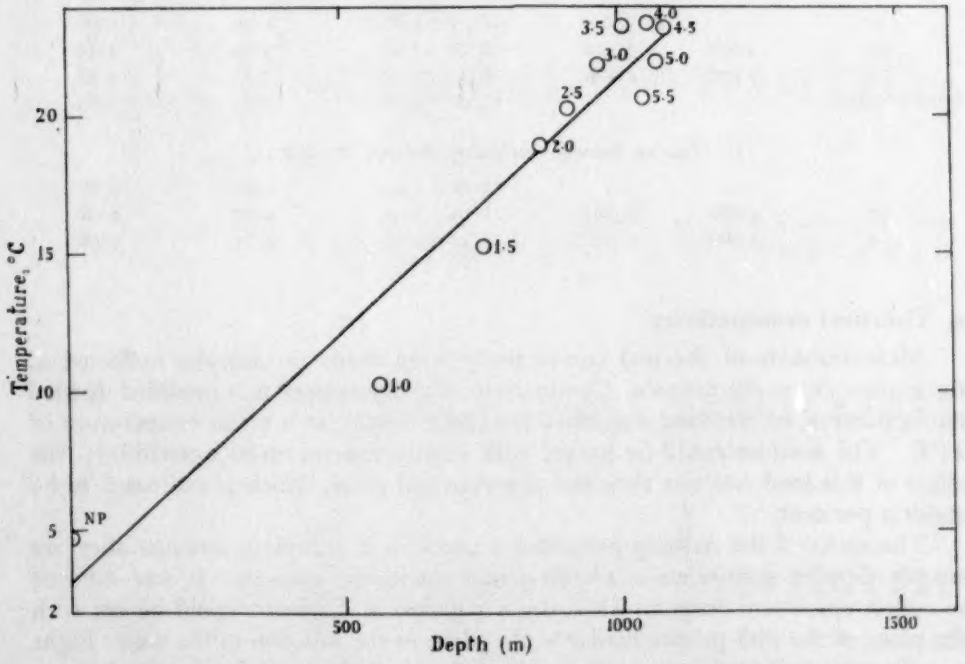

FIG. 5.—Corrected temperatures as function of corrected depth, Tauern tunnel. The stations are numbered by their distances in kilometres from the north portal. $t = 25 \times 10^6$ years, $L = 4$ km, $D = 3{\cdot}5$ km.

probably the best thermal conductors, but since the structure is such that they are arranged in parallel with the poorer conductors, these beds are the most important to sample.

Measurements of the conductivity in a direction parallel to the plane of the foliation were made on seven samples, and the conductivity normal to the foliation was measured for all eight specimens. Results are summarized in Table 3. Because of the steep dip of the foliation, the "parallel" specimens should be used to calculate the heat flow. These form a fairly homogeneous group with respect to conconductivity, despite considerable differences in appearance and mineralogical constitution. Lacking a far more elaborate sampling procedure, we can do no better than calculate the heat flow from the mean of the seven measurements.

Table 3

Thermal conductivity

No. of measurements	Orientation	Thermal conductivity, 10^{-3} cal/cm s deg C mean	range
	Arlberg Tunnel, gneiss and schist		
7	parallel	$10{\cdot}74 \pm 0{\cdot}37$	9·8–12·5
8	perpendicular	$7{\cdot}23 \pm 0{\cdot}36$	5·0–8·0
	Tauern Tunnel, granite and granitic gneiss		
			Tauern
13	parallel	$8{\cdot}87 \pm 0{\cdot}18$	8·1–10·4
9	perpendicular	$6{\cdot}85 \pm 0{\cdot}10$	6·5– 7·2
5	isotropic	$7{\cdot}50 \pm 0{\cdot}02$	7·46–7·54

Mean density, Arlberg, 7 specimens, $2{\cdot}686 \pm 0{\cdot}033$.
Mean density, Tauern, 19 specimens, $2{\cdot}610 \pm 0{\cdot}003$.

The rocks in the vicinity of the Tauern tunnel are rather uniform granites and granitic gneisses. Samples were collected from fresh talus slopes along the Mindener Weg, a footpath which crosses the mountains in a direction parallel to the tunnel and about 2 km to the east.

Most of the specimens showed clear-cut thermal anisotropy (Table 3). According to Exner's tectonic map of the region (Exner 1957, Plate VIII), the dip of the foliation ranges from slightly less than 30° to less than 60° in the vicinity of the tunnel. If the mean dip is $40° \pm 10°$, the vertical component of the conductivity of the anisotropic rocks is $(7{\cdot}68 \pm 0{\cdot}37) \times 10^{-3}$ cal/cm s deg C; most of the uncertainty in this figure arises from lack of quantitative information about the geologic structure between the tunnel and the surface. This number does not differ significantly from the mean conductivity of the few isotropic specimens.

The mean temperature of the rock between both tunnels and the surface is about 10°C to 12°C. The observed conductivity should be increased by about 2 per cent to take account of the difference between this temperature and the temperature of the measurements. We adopt the round figure $(11{\cdot}00 \pm 0{\cdot}37) \times 10^{-3}$ cal/cm s deg C for the conductivity of the rocks in the Arlberg tunnel, and $(7{\cdot}83 \pm 0{\cdot}37) \times 10^{-3}$ cal/cm s deg C for the conductivity in the Tauern.

5. Flow of heat

The flow of heat for the various assumptions about the topographic evolution are given in Table 4. Two versions of the results for the Tauern are included; they correspond to retention or rejection of stations 1·0 and 1·5. The results for the two tunnels are in good agreement with each other. At worst the difference only slightly exceeds the combined standard errors for the same assumption about the topographic history.

Table 4

Flow of heat

	Heat flow, 10^{-6} cal/cm^{2}s		
t 10^6 years	Arlberg	Tauern 11 points	Tauern 9 points
∞	2·16 ± 0·12	2·07 ± 0·18	1·95 ± 0·15
25	1·95 ± 0·10	1·79 ± 0·14	1·69 ± 0·14
4	1·84 ± 0·10	1·66 ± 0·14	1·56 ± 0·13
Adopted value	1·9 ± 0·2	1·8 ± 0·2	

The Austrian values are also in good agreement with results for the Loetschberg tunnel given in I. They are rather lower than the value $2{\cdot}2 \times 10^{-6}$ cal/cm^{2}s adopted in the Simplon and considerably higher than $1{\cdot}4 \times 10^{-6}$ (corrected to $1{\cdot}6 \times 10^{-6}$) cal/cm^{2}s, as found in the Gotthard tunnel. Estimates of the heat flow in the two Austrian tunnels were hazarded in I. They are in fair agreement with the present determination in the Arlberg, but in the case of the Tauern the estimate was too low. It was thought that the estimated fluxes were, if anything, too high, but this does not prove to be the case.

An estimate was also made in I of the heat flow in the Albula tunnel in eastern Switzerland. It was later discovered that the gradient in this tunnel was based on a single measurement of temperature made several months after construction was completed. Hence this estimate is wholly unreliable.

6. Discussion

On the basis of the estimates of the heat flow in Austria, it was concluded in I that the heat flow in much of the Alpine region was about $1{\cdot}5 \times 10^{-6}$ cal/cm^{2}s. The higher values in the Simplon and Loetschberg tunnels were considered to represent a more or less local anomaly. The previous discussion requires modification in the light of the present results, which show that high values of heat flow persist far to the east of the earlier determinations.

As in I, we shall assume a layered crust for purposes of discussion. The crust outside the mountains is assumed to consist of a layer of granitic rocks, 20 km thick, lying on 10 km of basaltic rock. In the mountains the granitic layer is thickened to 35 km and the thickness of the basaltic layer is unchanged. If 5×10^{-13} cal/cm^{3}s is produced by radioactivity in the granitic layer and 10^{-13} cal/cm^{3}s in the basalt, the heat flow in equilibrium with crustal radioactivity is $1{\cdot}85 \times 10^{-6}$ cal/cm^{2}s in the mountains and $1{\cdot}1 \times 10^{-6}$ cal/cm^{2}s elsewhere. This model leads to plausible heat flow in the lowlands and to nearly sufficient heat flow in the mountains; the remainder can be assumed to originate beneath the crust.

If the root of the Alps was formed relatively recently, the heat flow at the surface may not be in equilibrium with the radioactivity of the root, and account of this effect may be taken by the approximation used by Birch (1950, p. 618). If the root was formed 25×10^6 years ago, it is found by this method that the heat production in the granitic layer must be increased to 6×10^{-13} cal/cm^{3}s in order to obtain a heat flow of $1{\cdot}8 \times 10^{-6}$ cal/cm^{2}s from crustal radioactivity. The equilibrium heat flow outside the mountains is then $1{\cdot}3 \times 10^{-6}$ cal/cm^{2}s. Both this figure and the value of the radioactivity of the granitic layer are acceptable in view of present knowledge of these quantities. There appears to be no difficulty in accounting for the high heat flow in the Alps on the basis of radioactive decay in a thickened crust.

The relatively low heat flow in the Gotthard tunnel can be explained in an *ad hoc* fashion only. Heat production in the underlying crust may be unusually low in its vicinity. Values of 3×10^{-13} to 4×10^{-13} cal/cm^{3}s would be demanded, with the exact figure depending on the size and shape of the region of low heat production. Alternatively the vicinity of the Gotthard may have undergone less uplift in recent times than other parts of the Alps, despite the fact that this tunnel passes under the highest-standing part of Switzerland. At present there seems to be no way to decide between these explanations.

7. Acknowledgments

It is a pleasure to thank Dr Norbert Untersteiner of the Zentralanstalt für Meteorologie und Geodynamik, Vienna, for help in obtaining the information about temperatures in the tunnels. Without his generous assistance this study would have been impossible. Dr P. Mechtler, archivist at the Verkehrsarchiv, was also helpful in locating these data. Dr Eugene C. Robertson of the U.S. Geological Survey kindly made it possible for part of the work of shaping the specimens for the measurement of thermal conductivity to be done in the machine shop connected with his laboratory.

Geophysical Laboratory,
Carnegie Institution of Washington,
Washington, D.C., U.S.A.
1961 *March.*

References

Birch, F., 1950. *Bull. Geol. Soc. Amer.*, **61**, 567.
Clark, S. P., 1957. *Trans. Amer. Geophys. Un.*, **38**, 239.
Clark, S. P. and Niblett, E. R., 1956. *Mon. Not. R. Astr. Soc. Geophys. Suppl.*, **7**, 176.
Exner, C., 1957. *Erlänterungen zur Geologischen Karte der Umbegung von Gastein* (Geologische Bundesanstalt, Wien).
Kerner von Marilaun, F., 1905. *Meteor. Zeits.*, **22**, 159.
Wagner, J., 1884. *Jahrb. der K. K. Geolog. Reichanstalt*, **34**, 743.

The Deviation of the Vertical at Bidston in response to the Attraction of Ocean Tides

G. W. Lennon

(Received 1961 March 24)

Summary

The periodic deviation of the vertical in sympathy with the flux of tidal waters is of particular interest in the study of Earth tides and associated phenomena. In order to assist Earth tide studies at Bidston, the attraction exerted by the presence of tidal waters has been evaluated for this station. The major lunar semidiurnal constituent of the phenomenon, (M_2), has been obtained by direct computation from a knowledge of the tides in the vicinity, and a method has been devised for the inference of the principal solar semi-diurnal constituent, (S_2), and the larger lunar elliptic semi-diurnal constituent, (N_2), based upon regional values of the relationships between the phases and amplitudes of the appropriate constituents in the ocean tide.

The use of the horizontal pendulum for the measurement of variations in the tilt of the Earth's surface is particularly susceptible to the attractive effect of oceanic tides since deviations of the vertical occasioned thereby are recorded by the instrument as apparent tilts of the surface and consequently present confusing elements in the study of real crustal movement. The phenomenon is especially significant at Bidston which is sited on a peninsula between two tidal estuaries and only two miles distant from the shores of the Irish Sea in which are experienced tides up to 30 ft in range. Of the total recorded periodic tilt at Bidston, less than one tenth part can be attributed to the true earth tide and the remainder is due mainly to the effects of oceanic loading and oceanic attraction. In earlier work on crustal tilts at Bidston, the effects of loading and attraction have not been separated but have been considered as a unit having the same phase and azimuth. This assumption may well be justified within the limits of accuracy of the investigation, but it is felt that as the results of more detailed observation become available, allowing greater precision, then this assumption cannot be accepted without examination. It is possible for example that the loading effect may show a lag upon the loading tide whereas the attraction effect must necessarily be simultaneous with the tide. Furthermore, recent work suggests the fundamental influence of regional geological structure in determining the azimuth of crustal tilt so that, in this respect also, loading may be affected independently of attraction. Again, the range of influence of the two effects may be quite dissimilar in character thereby giving differences in both azimuth and phase. It is clear that in an attempt to understand the complex mechanism of periodic surface movement the evaluation of the part played by tidal attraction is a significant and essential step.

1. The source of tidal information

The primary requirement of an investigation of this type is a store of precise knowledge of ocean tides, which is not generally available, and it is fortunate that the waters adjacent to the British Isles have been the subject of careful investigation through the years, particularly at the Tidal Institute. As a result, the disposition of the principal lunar semidiurnal constituent, (M_2), in this area is known just sufficiently well for a direct computation of the M_2 constituent of tidal attraction to be attempted. In this respect the basis is the British Admiralty Co-tidal Chart of the M_2 constituent, which chart is itself founded upon work by Proudman and Doodson (1924) for the North Sea and by Doodson & Corkan (1932) for the English Channel and the Irish Sea.

Nevertheless the scope of the existing work was not immediately adequate for the study in hand and it was necessary first to extend the co-tidal chart westwards so as to include the eastern part of the Atlantic Ocean and also northwards to Iceland and the Faroes. In this task the coastal directions of the co-tidal and co-range lines were first computed, wherever possible, according to the theory developed by Proudman & Doodson (1924) and using the phase lags of the maximum tide and of the maximum flood stream. With the assistance of the azimuths so obtained it was then possible to fit co-tidal and co-range lines to the published tidal data derived from coastal observation at specific locations. Figure 1

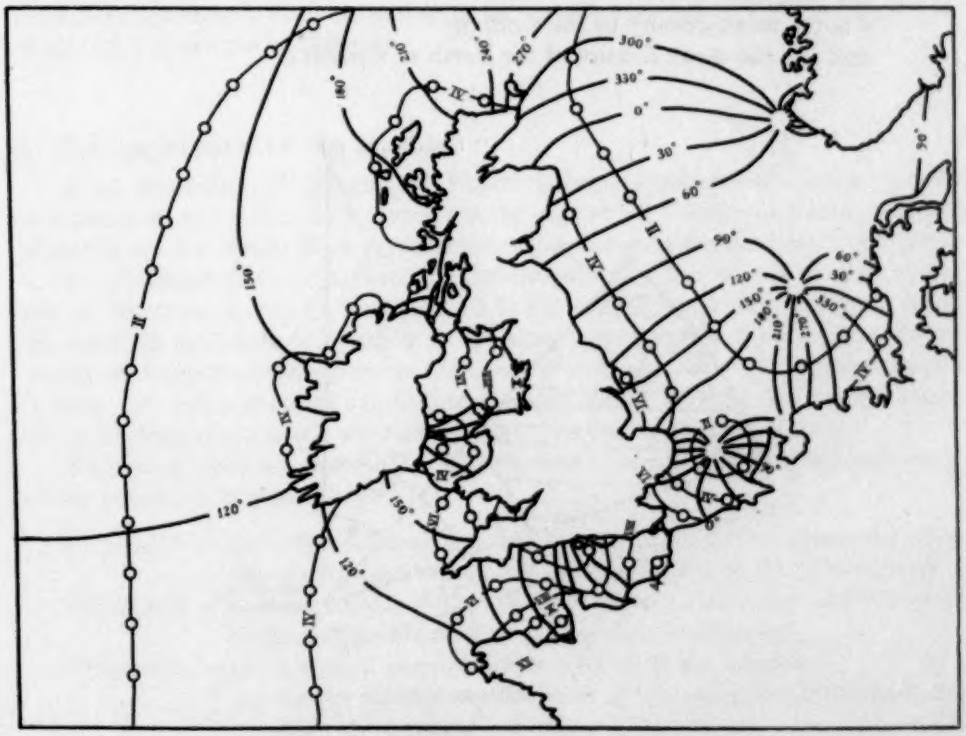

FIG. 1.—Co-tidal chart for the M_2 constituent.

——— co-tidal line showing the phase lag of M_2

——○—— co-range line showing the amplitude of M_2 in feet (Roman numerals)

illustrates the general framework of the resulting chart although it should be noted that the tidal basis actually utilized in the calculations was defined in considerable detail and with a fair degree of precision.

2. The computational method for the M_2 constituent of attraction

The problem of the deviation of the vertical has been the concern of geodesists for a considerable period since the effect of local geology and relief upon the techniques of precise surveying has had to be considered. As a result methods of determination of the magnitude of the effect from the physical phenomena are well known and the selection of a technique is mainly a question of convenience. In this case the choice has fallen upon a classical formula developed by A. R. Clarke in his work of 1880 and used extensively in a modified form by J. F. Hayford (1909) in geodetic adjustment some thirty years later.

Referring to Figure 2, the formula defines the meridian component of the deflection at the station, produced by a mass of the surface material of the Earth, in the form:

$$D = 12''{\cdot}44 \times (\delta/\rho) \times h \times (\sin\theta_2 - \sin\theta_1) \times \log_e R_2/R_1$$

where D is the deflexion caused by a stratum h statute miles thick lying within a four-sided compartment of the form shown as a hatched area in the diagram.
δ is the mean density of the stratum
and ρ is the mean density of the Earth as a whole.

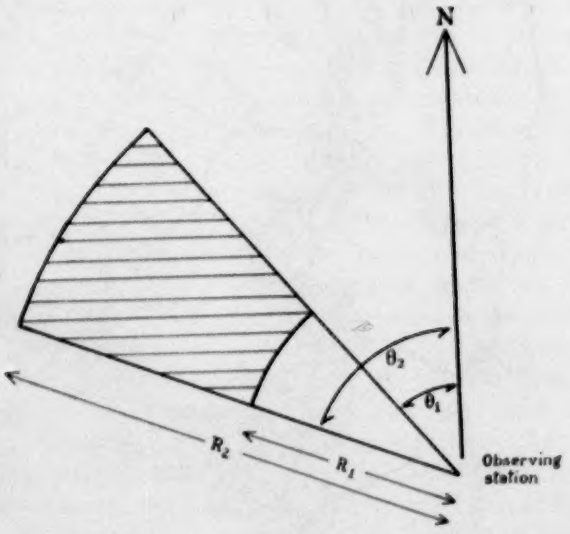

FIG. 2.

The value of ρ in the computations which follow is taken to be 5·515 g/cm^3 and for δ, which in this case must represent the mean density of sea water proper to the region, a value of 1·026 g/cm^3 has been used.

Clarke's formula has been modified slightly in replacing θ by α, where α is measured from south through west so that $\alpha_1 = 180° - \theta_2$ and $\alpha_2 = 180° - \theta_1$. It is possible then to define tidal attraction as follows:

Component of deviation to the south

$$1{\cdot}438 \times C \times \log_e R_2/R_1 \times (\sin \alpha_2 - \sin \alpha_1) \times 10^{-2} \text{ milliseconds}$$

Component of deviation to the east

$$1{\cdot}438 \times C \times \log_e R_2/R_1 \times (\cos \alpha_2 - \cos \alpha_1) \times 10^{-2} \text{ milliseconds}$$

where C is the amplitude, in centimetres, of the appropriate constituent of the tide representative of the compartment.

By applying these formulae to a network of compartments radiating outwards from the station over the adjacent tidal waters up to a range so distant that the computed effect becomes of negligible magnitude, it is possible to calculate the total component of deflection in the two directions. It is important to note however that the phenomenon is periodic and consequently changing in time. The time element is introduced, in accordance with normal tidal practice, as a phase angle representing the lag of the tidal effect upon the appropriate constituent of the equilibrium tide. The phase has a spatial distribution and therefore must receive detailed geographical attention. It is necessary to allocate a mean value of the phase lag to represent each compartment and to sum the effects given by several compartments in a vectorial sense so that the phase as well as the amplitude of the total deflection is obtained.

3. The application of the method

As an illustration of the method, Figure 3 shows a network of compartments, numbered 16 to 33, selected to represent the area of St. George's Channel, Bristol Channel and the South West Approaches, after due consideration has been given to the delineation of the coastline and the disposition of the M_2 constituent of the tide in the area. It can be seen that while the compartments are designed to fit the coastline as closely as possible, at the same time consideration is given to the variations in the tidal constants. In the north of the area where the variation in M_2 is large, the compartments are correspondingly small while in the south, where the tidal changes are small, the compartments in contrast are much larger.

The calculations are given in Table 1, Section C where the following definitions of the column headings apply:

Column A = the value, allocated to the compartment, of the phase lag upon the equilibrium tide of the M_2 constituent in the tidal waters.

Column B = the amplitude of the M_2 constituent in the tidal waters proper to the compartment and measured in centimetres.

Column C = the quantity entered under column B but adjusted
(a) for the inadequacy of the fit of the compartment boundaries upon the coastline, or
(b) for the drying areas within the compartment.

R_1, R_2, α_1 and α_2 as defined earlier in Figure 2 and in associated comments.

S = component of deviation to the South in milliseconds.

E = component of deviation to the East in milliseconds as previously defined.

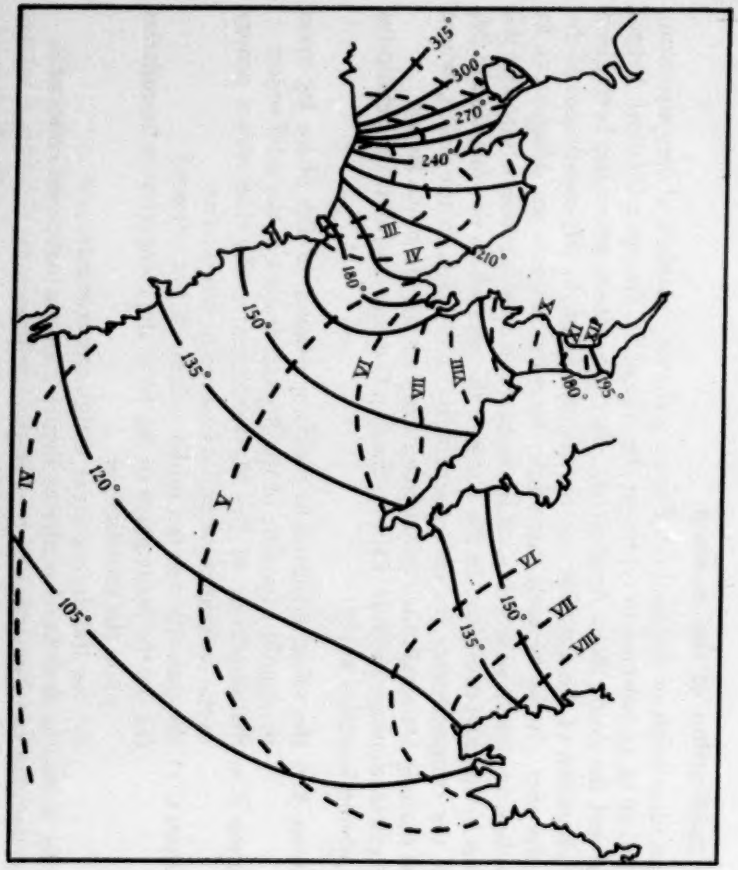

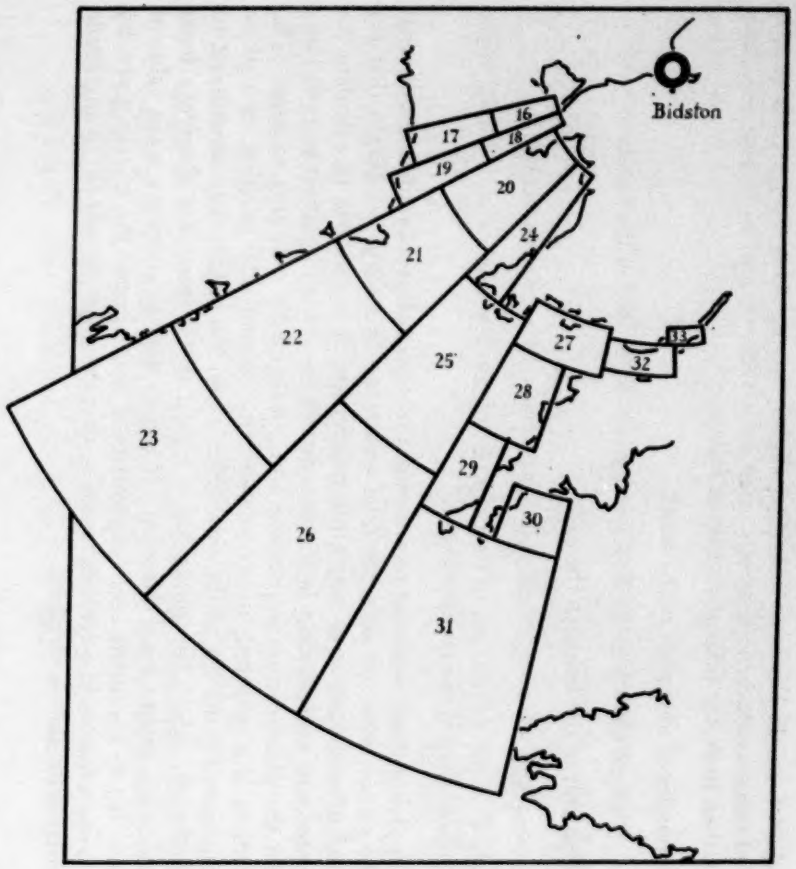

FIG. 3.—Left diagram: Co-tidal chart for the M_2 constituent
———— co-tidal line showing the phase lag of M_2 (15° interval)

Right diagram: Network of compartments
— — — co-range line showing the amplitude of M_2 in feet (1 foot interval)

Table 1

Calculations for the M_2 constituent of tidal attraction.

Section A. The Mersey Estuary, the Dee Estuary and Liverpool Bay.

(See Figure 4)

Compartment	A	B	C	R_2/R_1	α_2	α_1	S	E
1	13	—	107	1·062	294·5	285·5	0·0049	0·0137
2	7	—	88	1·074	301·0	294·5	0·0048	0·0091
3	2	—	70	1·209	310·0	294·5	0·0275	0·0435
4	345	—	201	1·463	315·5	297·5	0·2046	0·2768
5	336	—	305	1·275	310·5	291·5	0·1812	0·3013
6	333	—	329	1·679	307·0	291·5	0·3231	0·5767
7	330	—	329	1·357	291·5	266·0	0·0971	0·6300
8	325	—	326	1·306	266·0	235·5	−0·2171	0·6214
9	322	—	320	1·459	235·5	209·5	−0·5766	0·5286
10	319	—	250	1·875	209·5	180·0	−1·1128	0·2928
11	316	—	262	2·424	180·0	165·0	−0·8633	−0·1137
12	317	—	271	1·592	186·0	165·0	−0·6582	−0·0518
13	315	—	192	1·429	175·5	165·0	−0·1778	−0·0305
14	315	—	262	1·531	183·0	165·0	−0·4991	−0·0524
15	315	—	280	2·697	165·0	130·5	−2·0037	−1·2642
16	313	—	290	2·046	165·0	130·5	−1·4976	−0·9448
17	314	—	286	1·703	165·0	130·5	−1·0982	−0·6930
18	315	—	286	2·202	130·5	105·0	−0·6672	−1·2681
19	309	—	293	2·046	130·5	105·0	−0·6200	−1·1782
20	308	—	290	1·703	130·5	105·0	−0·4562	−0·8671
21	318	—	60	1·500	105·0	90·0	−0·0119	−0·0905
22	318	—	15	1·171	90·0	80·0	0·0005	−0·0059
23	316	—	281	2·046	105·0	73·0	0·0278	−1·5947
24	310	—	290	1·703	105·0	73·0	0·0212	−1·2238
25	320	—	210	1·991	73·0	51·0	0·3725	−0·7006
26	330	—	150	1·809	51·0	27·0	0·4131	−0·3346
27	345	—	140	1·741	27·0	0·5	0·4971	−0·1217
28	0	—	24	1·259	0·5	351·0	0·0131	0·0010

Vectorial Totals: $S\cos A = -5{\cdot}463$, $S\sin A = +6{\cdot}430$, $E\cos A = -4{\cdot}504$, $E\sin A = +5{\cdot}872$.
Deviation to South: Amplitude 8·438 millisecs; Phase Lag 130°·5.
Deviation to East: Amplitude 7·400 millisecs; Phase Lag 127°·5.

Table 1

Section B. Irish Sea.

(See Figure 5)

Compartment	A	B	C	R_1/R_2	α_2	α_1	S	E
1	305	255	170	3·000	90·0	77·5	0·0637	−0·5812
2	311	255	255	3·000	120·0	90·0	−0·5398	−2·0145
3	317	275	275	3·000	150·0	120·0	−1·5903	−1·5903
4	320	307	307	3·000	188·5	150·0	−3·1421	−0·5965
5	295	160	120	1·667	90·0	77·5	0·0209	−0·1908
6	310	190	190	1·667	120·0	90·0	−0·1872	−0·6981
7	320	235	200	1·667	150·0	120·0	−0·5378	−0·5378
8	325	260	255	1·667	168·0	150·0	−0·5472	−0·2101
9	315	125	120	1·444	90·0	77·5	0·0150	−0·1372
10	318	160	163	1·444	120·0	90·0	−0·1154	−0·4306
11	325	180	155	1·444	150·0	120·0	−0·2998	−0·2998
12	332	245	240	1·250	168·0	150·0	−0·2249	−0·0864
13	340	255	255	1·078	180·0	168·0	−0·0574	−0·0061
14	320	105	105	1·240	140·5	131·0	−0·0385	−0·0375
15	330	95	93	1·119	150·5	140·5	−0·0205	−0·0142

Vectorial Totals: $S \cos A = -5{\cdot}480$, $S \sin A = +4{\cdot}642$, $E \cos A = -5{\cdot}174$, $E \sin A = +5{\cdot}269$.
Deviation to South: Amplitude 7·182 millisecs; Phase Lag 139°·6.
Deviation to East: Amplitude 7·385 millisecs; Phase Lag 134°·5.

Table 1

Section C. St. George's Channel, Bristol Channel and South West Approaches.

(See Figure 5)

Compartment	A	B	C	R_2/R_1	α_2	α_1	S	E
16	275	137	137	1·534	77·5	69·5	0·0334	−0·1128
17	270	80	80	1·470	77·5	69·5	0·0175	−0·0593
18	255	126	126	1·687	69·5	63·0	0·0433	−0·0984
19	235	55	55	1·473	69·5	63·0	0·0140	−0·0318
20	230	115	115	1·944	63·0	45·0	0·2022	−0·2782
21	190	120	114	1·449	63·0	45·0	0·1118	−0·1539
22	143	140	143	1·500	63·0	45·0	0·1533	−0·2111
23	120	128	150	1·333	63·0	45·0	0·1064	−0·1464
24	215	135	135	2·183	45·0	36·0	0·1808	−0·1544
25	157	190	190	1·613	45·0	30·0	0·2706	−0·2075
26	125	157	157	1·600	45·0	30·0	0·2198	−0·1686
27	170	285	285	1·190	30·0	12·5	0·2024	−0·0787
28	155	240	240	1·290	30·0	19·5	0·1459	−0·0672
29	143	205	205	1·234	30·0	23·5	0·0627	−0·0318
30	145	165	165	1·130	20·5	12·5	0·0388	−0·0116
31	125	160	168	1·487	30·0	12·5	0·2718	−0·1057
32	190	360	360	1·115	12·5	359·0	0·1318	−0·0133
33	198	415	415	1·065	0·5	352·5	0·0523	+0·0033

Vectorial Totals: $S \cos A = -1{\cdot}704$, $S \sin A = +0{\cdot}428$, $E \cos A = +1{\cdot}264$, $E \sin A = -0{\cdot}005$.
Deviation to South: Amplitude 1·757 millisecs; Phase Lag 165°·8.
Deviation to East: Amplitude 1·264 millisecs; Phase Lag 359°·8.

Table 1

Section D. English Channel.

(See Figure 5)

Compartment	A	B	C	R_2/R_1	α_2	α_1	S	E
34	160	180	180	1·271	12·5	6·0	0·0695	−0·0113
35	140	223	226	1·187	12·5	6·0	0·0624	−0·0102
36	175	173	175	1·442	6·0	358·0	0·1284	−0·0046
37	165	260	260	1·143	6·0	358·0	0·0697	−0·0023
38	193	125	125	1·250	358·0	348·5	0·0660	0·0079
39	188	250	240	1·231	358·0	348·5	0·1181	0·0139
40	180	370	375	1·106	358·0	348·5	0·0892	0·0105
41	230	90	93	1·184	348·5	343·5	0·0191	0·0047
42	232	155	155	1·131	348·5	343·5	0·0232	0·0057
43	310	125	120	1·215	343·5	330·0	0·0726	0·0312
44	275	190	180	1·258	343·5	330·0	0·1283	0·0551
45	322	233	233	1·374	330·0	324·5	0·0860	0·0552
46	322	290	290	1·270	324·5	316·0	0·1137	0·0945
47	330	250	250	1·135	316·0	306·0	0·0520	0·0598

Vectorial Totals: $S \cos A = -0{\cdot}345$, $S \sin A = -0{\cdot}303$, $E \cos A = +0{\cdot}181$, $E \sin A = -0{\cdot}224$.
Deviation to South: Amplitude 0·460 millisecs; Phase Lag 221°·3.
Deviation to East: Amplitude 0·288 millisecs; Phase Lag 309°·1.

Table 1

Section E. North Sea.

(See Figure 6)

Compartment	A	B	C	R_2/R_1	α_2	α_1	S	E
1	345	160	170	1·412	306·0	294·0	0·0881	0·1527
2	315	71	71	1·246	294·0	282·0	0·0145	0·0447
3	35	71	71	1·261	294·0	282·0	0·0153	0·0471
4	172	167	160	1·606	282·0	267·5	0·0227	0·2741
5	180	60	70	1·579	282·0	267·5	0·0096	0·1156
6	150	150	155	1·606	267·5	243·5	−0·1099	0·4252
7	175	75	75	1·579	267·5	243·5	−0·0513	0·1984
8	250	60	65	1·233	267·5	255·0	−0·0065	0·0421
9	320	90	90	1·243	267·5	255·0	−0·0094	0·0606
10	200	20	20	1·233	255·0	243·5	−0·0043	0·0113
11	15	35	35	1·243	255·0	243·5	−0·0078	0·0205
12	105	137	145	1·606	243·5	210·5	−0·3827	0·4104
13	112	70	70	1·579	243·5	225·0	−0·0864	0·1200
14	85	10	13	1·644	243·5	225·0	−0·0174	0·0242
15	82	75	75	1·579	225·0	210·5	−0·0983	0·0761
16	40	20	23	1·644	225·0	210·5	−0·0328	0·0254
17	82	165	165	1·413	210·5	199·0	−0·1492	0·0688
18	55	130	140	1·698	210·5	186·0	−0·4295	0·1417
19	17	70	70	1·217	210·5	186·0	−0·0797	0·0262
20	335	50	50	1·174	210·5	180·0	−0·0586	0·0160
21	300	45	42	1·152	210·5	180·0	−0·0434	0·0118
22	345	120	120	1·236	186·0	176·0	−0·0637	0·0011

Vectorial Totals: $S\cos A = -0{\cdot}175$, $S\sin A = -1{\cdot}099$, $E\cos A = -0{\cdot}676$, $E\sin A = +0{\cdot}945$.
Deviation to South: Amplitude 1·112 millisecs; Phase Lag 260°·8.
Deviation to East: Amplitude 1·162 millisecs; Phase Lag 125°·6.

Table 1

Section F. Eastern Atlantic.

Compartment	A	B	C	R_2/R_1	α_2	α_1	S	E	(See Figure 6)
23	97	135	135	1·695	12·5	354·0	0·3287	−0·0186	
24	100	112	112	1·898	63·0	12·5	0·6962	−0·5391	
25	118	100	105	1·264	74·5	63·0	0·0257	−0·0660	
26	125	63	63	1·700	103·5	63·0	0·0391	−0·3304	
27	135	112	137	1·392	103·5	74·5	0·0058	−0·3261	
28	158	105	115	1·594	133·5	103·5	−0·1904	−0·3508	
29	140	65	65	1·700	133·5	103·5	−0·1225	−0·2257	
30	175	120	110	1·594	157·5	133·5	−0·2527	−0·1737	
31	170	85	85	1·286	148·0	133·5	−0·0601	−0·0490	
32	140	55	55	1·322	148·0	133·5	−0·0432	−0·0352	
33	190	105	102	1·286	161·0	148·0	−0·0754	−0·0360	
34	165	55	55	1·322	161·0	148·0	−0·0451	−0·0215	
35	200	140	120	1·111	166·5	157·5	−0·0271	−0·0088	
36	217	106	104	1·286	170·5	161·0	−0·0604	−0·0154	
37	220	60	60	1·322	170·5	161·0	−0·0386	−0·0098	
38	243	100	95	1·286	180·0	170·5	−0·0567	−0·0048	
39	250	60	60	1·322	180·0	170·5	−0·0397	−0·0033	
40	335	91	90	1·174	157·5	142·0	−0·0484	−0·0283	
41	165	80	65	1·278	152·0	126·0	−0·0778	−0·0677	
42	270	45	45	1·174	142·0	133·5	−0·0114	−0·0104	

Vectorial Totals: $S \cos A = +0{\cdot}695$, $S \sin A = +1{\cdot}044$, $E \cos A = +1{\cdot}418$, $E \sin A = -1{\cdot}397$.
Deviation to South: Amplitude 1·254 millisecs; Phase Lag 56°·3.
Deviation to East: Amplitude 1·990 millisecs; Phase Lag 315°·4.

Table 1

Section G. The summation of the contributions from all regions to give total M_2 effect.

Vectorial Totals: $S \cos A = -12{\cdot}472$, $S \sin A = +11{\cdot}142$, $E \cos A = -7{\cdot}491$, $E \sin A = +10{\cdot}460$.
Deviation to South: Amplitude 16·725 millisecs; Phase Lag 138°·1.
Deviation to East: Amplitude 12·865 millisecs; Phase Lag 125°·6.

In this manner the Irish Sea, the English Channel, the North Sea and the Eastern Atlantic up to a range of approximately 800 miles from Bidston were treated as separate regions and both directional components of the respective contributions of these areas to the total attraction of the mean lunar tide were computed. It was not considered necessary to proceed beyond this range since the contributions from the distant compartments were becoming quite small and were further reduced by the introduction of a factor equal to the cosine of the angle of depression below the horizon. In any case, in an amphidromic system, such as is known to exist to the west in the Atlantic and also to the north near the Faroes, contributions from oceanic areas in the middle distance can be regarded as largely counterbalanced by the effect of larger tides, in opposite phase, at even greater distance. An Atlantic and Arctic limit was selected in this way, partly by experiment and partly by judgement based upon theoretical argument.

4. The treatment of local tides

Clearly the proximity of a large tidal range in the immediate vicinity of the station called for special treatment in the computations for the estuaries of the Mersey, the Dee and for Liverpool Bay within a range of twenty miles. Unfortunately it is in this very range that the most serious difficulties are met. On the one hand it is necessary to cope with large drying areas in the estuaries where the attracting tide appears as a discontinuous feature. On the other hand the phase and amplitude of M_2 were known precisely only at a small number of locations, in fact three in all, and although the three locations provide a good cover in a geographical sense, they do not adequately represent the variations in tidal characteristics which must be significant in the assessment of attraction. The difficulties were eventually surmounted by a detailed investigation of whatever tidal information was available. In the first place differences between high and low water times at several localities were converted to M_2 phase differences. Secondly, although harmonic tidal constituents were not generally available, characteristic mean tidal curves were known for certain locations and interpolation provided an adequate cover of these characteristic curves. It was found possible to introduce sample drying heights into the curves which were then analysed to determine the mean lunar tide. This process indicated an effective amplitude and an appropriate phase value for M_2 under the varying conditions.

An example of the stages of calculations for a compartment in this troublesome region is given below:

Amplitude of M_2 in the compartment	10·0ft.
Drying area as a proportion of the total area of the compartment, obtained by planimeter	0·38
Mean drying height (above datum)	12·0ft.
On the basis of a 12ft. drying height introduced into the characteristic tide curve, itself interpolated to represent the compartment, analysis gives the effective mean amplitude in the drying area as	7·2ft.
The overall effective amplitude of M_2 for the compartment is therefore $(0{\cdot}38\times 7{\cdot}2)+(0{\cdot}62\times 10{\cdot}0)$	8·9ft.

On this basis it was possible to proceed according to the techniques described earlier so that satisfactory calculations of the attractive effects for these areas were obtained. That this local region should eventually be shown to provide approximately half the total effect is justification for the intensive treatment given.

5. The effect of the curvature of the Earth's surface

The depression, below the horizon of the station, of the contributing compartments was earlier cited as a factor reducing the significance of distant areas. The need for a cosine reduction factor in the calculations on this account was a matter which required investigation, particularly since the observing station at Bidston stands at a height of 178 feet above mean sea level. Fortunately, for tidal waters in proximity to the station which have been seen to provide the most important contributions to the phenomenon under investigation, the reduction effect was found to be quite negligible and only on reaching the extreme limits of the area studied did these considerations amount to a change of 0·5 per cent in the computed values. In view of the relatively small significance of contributions at this range to the total effect and in view also of the relative uncertainty in the basic data in these remote offshore areas, the reduction factor due to depression below the horizon was finally disregarded.

6. The calculations for the M_2 constituent

The calculations have been performed upon a regional basis in Table 1, Sections A to F, and the networks of compartments used in the calculations are shown in Figure 4 for Section A, Figure 5 for Sections B, C and D, and Figure 6 for Sections E and F. For each section the vectorial totals are determined so that the regional values of both the magnitude and phase of the deviation can be provided. A final vectorial sum of the regional contributions gives the definition of the total vectors of the M_2 constituent of tidal attraction in Section G. An examination of the results shows that the effect of the ocean tide upon the direction of the vertical in any region is to introduce a periodic elliptical motion, the delineation of which depends upon a number of complex inter-related factors including the azimuth and range of the body of water from the observing station, the amplitude of the tide and the phase lag of the appropriate constituent in the tide. The axes of the total vector ellipses which for Bidston represent the regional contributions to the M_2 effect are shown in Figure 7 and provide a visual assessment of the attraction in a geographical sense.

7. The inference of the principal solar and larger lunar elliptic semi-diurnal constituents, S_2 and N_2

Although the disposition of M_2 is known with considerable accuracy in the waters adjacent to the British Isles, the same cannot be said for any other tidal constituent. This is partly due to the fact that whereas it is a relatively simple matter to calculate M_2 from non-harmonic data, in so far as it represents the average tide, it is a much more difficult matter to determine from similar sources S_2 and N_2, which represent variations upon the average tide. For the latter constituents one is therefore restricted to a much smaller store of data in the form of harmonic constants and even here it is found that the smaller constituents are

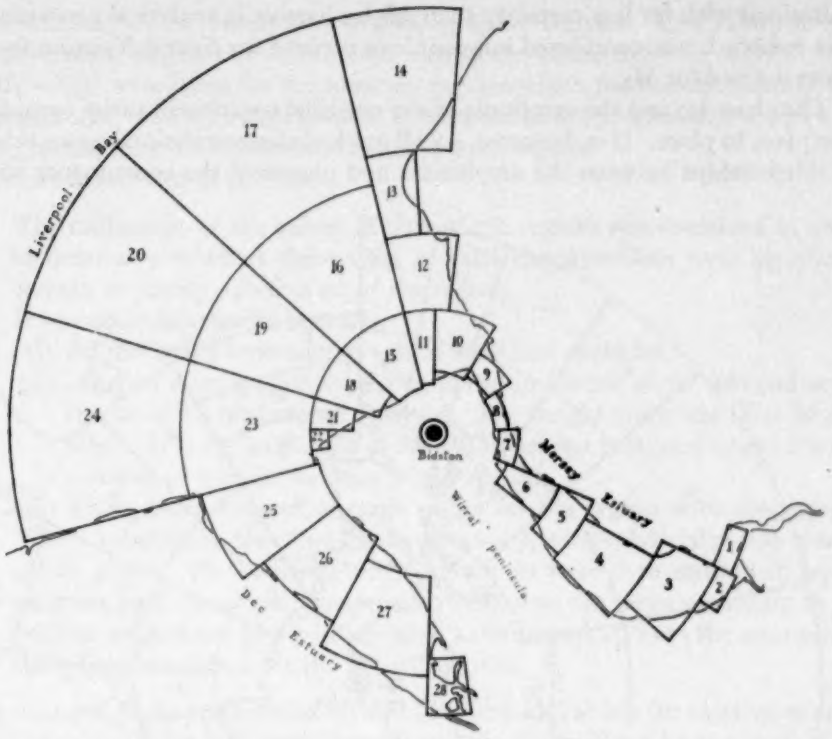
Liverpool Bay
Bidston
Mersey Estuary
Wirral peninsula
Dee Estuary

FIG. 4.

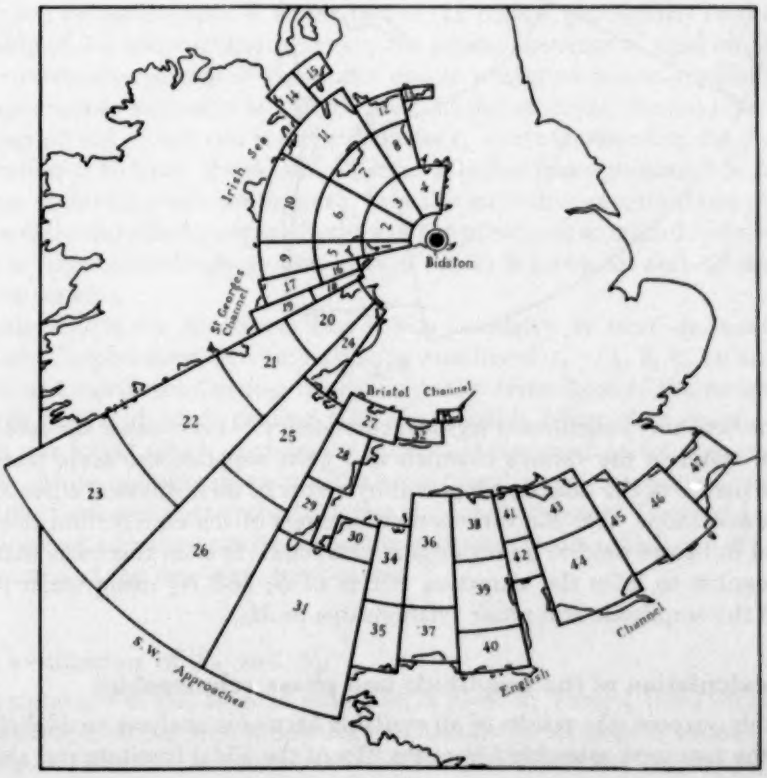
Irish Sea
St Georges Channel
Bidston
Bristol Channel
S.W. Approaches
English Channel

FIG. 5.

determined with far less certainty than M_2 by harmonic analytical processes. For these reasons it was considered impossible to proceed for S_2 and N_2 using the techniques devised for M_2.

The phase lag and the amplitude of any one tidal constituent varies considerably from place to place. It is, however, a well marked characteristic of ocean tides that the relationships between the amplitudes and phases of the constituents within a

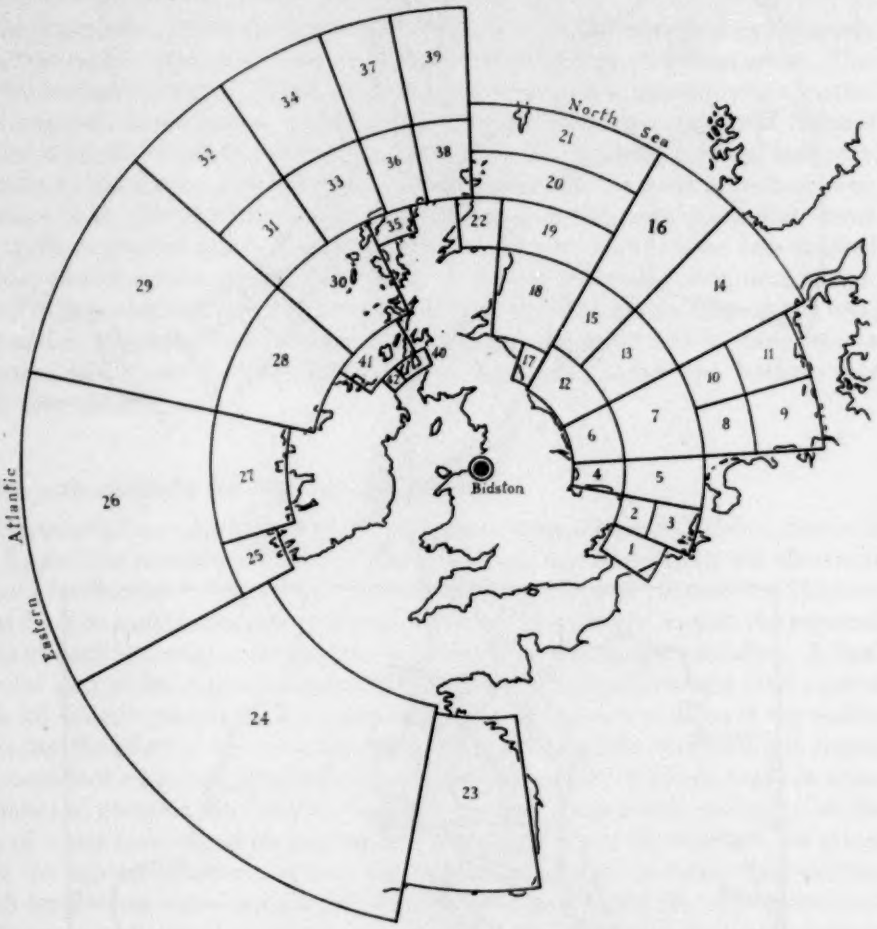

FIG. 6.

single species show a significant regional consistency. It is because the rather large bodies of water in the various channels and gulfs superimpose some restrictions upon the nature of the tidal development by virtue of their physical characteristics of depth and shape, that the various modifications of the equilibrium tide which are found in nature tend to be regional in character. It is on this basis that it was found possible to infer the attraction effects of S_2 and N_2 using mean regional values of the amplitude and phase relationships to M_2.

8. The calculation of the amplitude and phase relationships

For this purpose, the results of all available harmonic analyses of tidal observations in the area were assembled from the files of the Tidal Institute and also from

the publications of the International Hydrographic Bureau. The values of the amplitude ratios, M_2/S_2 and M_2/N_2 and also of the phase differences $(S_2-M_2)°$ and $(M_2-N_2)°$ were listed for the same six regions which formed the bases of the M_2 calculations. The task then became an exercise in the systematic reduction of data to give the most reliable mean values for each region.

The procedure was as follows:

A. The uniformity of the values in each of the regions was examined in order to determine whether differences in tidal characteristics were significant enough to justify subdivision of the region.

B. If no subdivision was to be made:
   (i) All obviously inconsistent values were first excluded.
   (ii) Weights were applied according to the amplitude of the tide and to the length of the tidal record analysed. The weight given was $W = M \times P$, where M is the amplitude of M_2 to the nearest foot, and where P is the number of months duration of the record.
   (iii) Using these weights, average values for the region were determined.

C. Where subdivision was found to be necessary, each subdivision was treated as (*B*) above. The values of the subdivisions were then combined, separately for each directional component, weighting the mean according to the relative importance of the subdivision in its contribution to the appropriate directional component in the M_2 calculations.

An example of the calculations involved is given in Table 2 for the area covered by St. George's Channel, Bristol Channel and the South West Approaches. Here it is clear that the Bristol Channel area, taken as subdivision 2, gives characteristically different values from those of the rest of the region, particularly in the phase relationship of M_2 and S_2. Furthermore, the greater coverage of tidal information in such a relatively small area would give undue weight to this anomalous feature if the region was to be treated as a single unit. In this example, the reduction of the data is carried out in full and is self explanatory. Since in assessing the deviation of the vertical at Bidston, the Bristol Channel area has less significance in an east–west sense than in a north–south sense, then the respective contributions made by the two subdivisions to the regional values of the phase and amplitude relationships is made to differ accordingly so that a set of values is given for each of the directional components.

In calculations for the North Sea it was necessary to treat the continental coastal areas, represented by compartments numbered 1, 3, 5, 8, 9, 10 and 11 of Figure 6, as a subdivision giving values distinctive from those of the remainder of the North Sea, and when dealing with the English Channel, a more complex situation was found which necessitated individual treatment of four separate subdivisions. More uniform characteristics were found in the other three regions so that for the Eastern Atlantic, the Irish Sea and for the Mersey, Dee and Liverpool Bay, a single set of values can be applied in each case in the calculation of both the north–south and the east–west components.

9. The evaluation of S_2 and N_2

The summary of this stage of reduction is given in Table 3 from which it is a simple matter to derive appropriate regional results for S_2 and N_2 based upon the M_2 values of Table 1. The interpretation of the data in this way is given in Table 4

Table 2

Example of calculation of amplitude and phase relationships

St. George's Channel, Bristol Channel and South West Approaches

Port	P	$(S_2-M_2)°$	$(M_2-N_2)°$	M_2/S_2	M_2/N_2	M	W	Subdivision
Penzance	6	44	22	3·010	5·272	6	36	1
Devonport	12	53	19	2·729	5·437	5	60	1
Milford Haven	12	44	19	2·698	5·342	7	84	1
Pembroke	1	44	16	2·705	5·259	8	8	1
Tenby	1	44	20	2·753	5·541	9	9	1
Bury Pt.	1	45	21	2·705	5·181	9	9	2
Porthcawl	½	55	20	2·537	4·952	10	5	2
Barry Dock	1	52	21	2·675	6·421	13	13	2
Cardiff	½	48	36	2·880	9·255	13	6	2
Newport	1	56	26	2·708	6·736	14	14	2
Beachley	1	68	18	2·747	5·162	14	14	2
Avonmouth	12	59	13	2·859	5·763	14	168	2
Ilfracombe	½	41	3	2·913	10·019	11	6	2
Appledore	1	46	18	2·762	5·278	8	8	2
*Weston-super-Mare	½	50	−50	3·094	8·308	15	8	2
Watchet	½	57	10	2·339	4·394	13	6	2
Cobh	12	45	21	3·192	5·412	5	60	1
Brest	12	40	19	2·737	4·872	7	84	1

P = length of tidal record analysed, in months.
M = amplitude of M_2 to nearest foot.
W = final weighting = $P \times M$.
*N_2 values for Weston-super-Mare neglected as inconsistent.

	$(S_2-M_2)°$	$(M_2-N_2)°$	M_2/S_2	M_2/N_2
Subdivision 1. Weighted Means	44·8	19·6	2·835	5·251
Subdivision 2. Weighted Means	57·0	15·3	2·818	5·919

Now Subdivision 2, the Bristol Channel, comprises Compartments 27, 28, 32 and 33 in the calculations for M_2.
The ratio of the M_2 effect in Subdivision 1 to Subdivision 2
is ·764/·236 for the North/South Component (See Table 1, Section C)
and ·916/·084 for the East/West Component.
The above means for Subdivisions 1 and 2 are combined on this basis to give

	$(S_2-M_2)°$	$(M_2-N_2)°$	M_2/S_2	M_2/N_2
North/South Component	47·7	18·6	2·831	5·409
East/West Component	45·8	19·2	2·834	5·307

Table 3

Regional relationships of amplitude and phase

		N	$(S_2-M_2)°$	$(M_2-N_2)°$	M_2/S_2	M_2/N_2
Mersey, Dee and Liverpool Bay	N/S component E/W component	—	44·0	22·5	3·134	5·282
Irish Sea	N/S component E/W component	13	41·5	23·9	3·299	5·249
St. George's Channel, Bristol Channel and South West Approaches	N/S component E/W component	18	47·7 45·8	18·6 19·2	2·831 2·834	5·409 5·307
English Channel	N/S component E/W component	24	48·8 48·8	18·9 20·9	2·779 3·025	5·120 5·179
North Sea	N/S component E/W component	86	43·7 45·8	23·8 23·7	3·047 3·143	5·247 5·355
Eastern Atlantic	N/S component E/W component	35	35·9	20·6	2·784	5·010

N = Number of ports used as a basis for the determination of the relationships.

where the regional values have also been summed vectorially to determine the total S_2 and N_2 constituents of deviation experienced at Bidston. Just as the axes of the total vector ellipses were produced in Figure 7 for the regional contributions to the M_2 effect, so Figure 8 reproduces the axes of the total vector ellipses for the total S_2 and N_2 effects and compares them with the corresponding ellipse for M_2. Finally in Table 5, the fundamental dimensions of all the ellipses determined in this study are tabulated.

Table 4

Tidal attraction at Bidston

Mean solar tide S_2

Area	To South		To East	
	Amplitude millisecs	Phase lag g°	Amplitude millisecs	Phase lag g°
Mersey, Dee, Liverpool Bay	2·692	174·5	2·361	171·5
Irish Sea	2·177	181·1	2·239	176·0
St. George's Channel, Bristol Channel and S.W. Approaches	0·621	213·5	0·446	45·6
English Channel	0·166	270·1	0·095	357·9
North Sea	0·365	304·5	0·370	171·4
Eastern Atlantic	0·450	92·2	0·715	351·3
Total effect	5·186	181·6	3·897	168·7

Major lunar elliptic constituent N_2

Area	To South		To East	
	Amplitude millisecs	Phase lag g°	Amplitude millisecs	Phase lag g°
Mersey, Dee, Liverpool Bay	1·598	108·0	1·401	105·0
Irish Sea	1·368	115·7	1·407	110·6
St. George's Channel, Bristol Channel and S.W. Approaches	0·325	147·2	0·238	340·6
English Channel	0·090	202·4	0·056	288·2
North Sea	0·212	237·0	0·217	101·9
Eastern Atlantic	0·250	35·7	0·397	294·8
Total effect	3·167	115·4	2·440	101·7

Table 5

Dimensions of total vector ellipses

Mean lunar tide, M_2	Major semi-axis millisecs	Minor semi-axis millisecs	Direction of major axis (from North)
Mersey, Dee, Liverpool Bay	11·219	0·292	41°·2 West
Irish Sea	10·286	0·458	45°·8 West
St. George's Channel, Bristol Channel and S.W. Approaches	2·150	0·249	35°·3 East
English Channel	0·460	0·290	2°·3 West
North Sea	1·485	0·611	46°·8 East
Eastern Atlantic	2·012	1·214	79°·3 East
Total effect M_2	20·984	2·219	37°·4 West
Total effect S_2	6·449	0·700	36°·7 West
Total effect N_2	3·971	0·461	37°·4 West

10. An assessment of the results

The deviation of the vertical has now been defined as a very small periodic tilt, but in order to establish the significance of this phenomenon it is valuable to view the results in the light of their implications within the study of earth tides at the Bidston station.

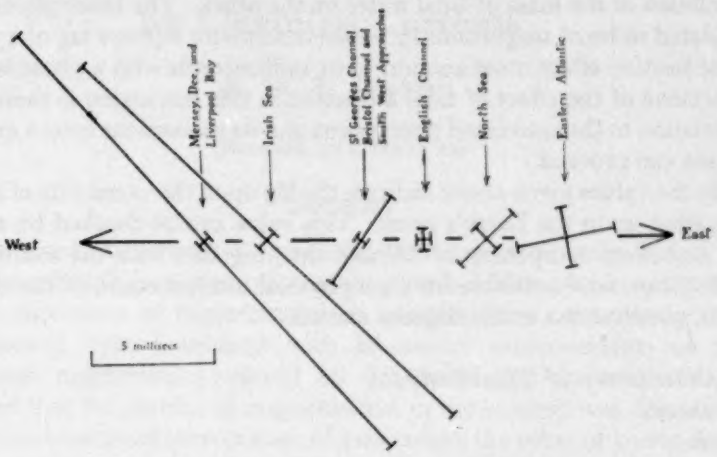

FIG. 7.—Total vector ellipses of the regional contributions to M_2.

An example can be taken by examining the north–south component of tilt of the M_2 constituent. Observations of tilt recorded by a modified Milne-Shaw Seismograph were made at Bidston throughout the International Geophysical Year, 1957–8. The harmonic analysis of 19 consecutive sets of 29 day periods of

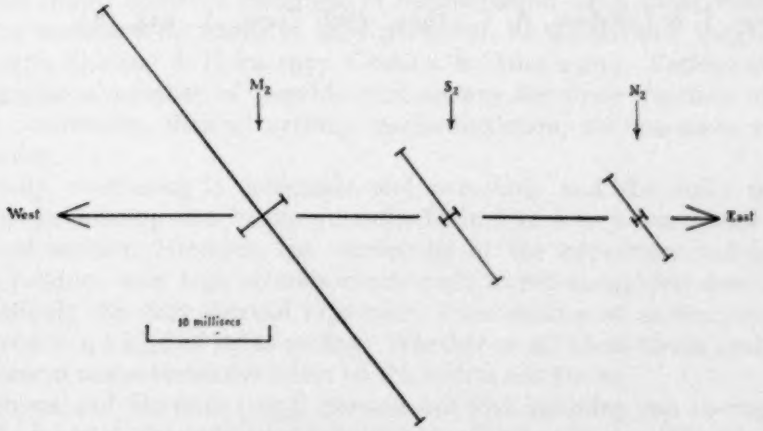

FIG. 8.—Total vector ellipses for M_2, S_2 and N_2.

observation gave an observed amplitude of 73 milliseconds for M_2 with a phase lag of 141°, in the convention that tilts down to the south are positive. This quantity is known to contain the body tide of the Earth in addition to those influences introduced by the oceanic tide. Assuming certain well-established values for the Love numbers, it is possible to attribute 5 milliseconds to the body tide at this station

with a phase lag approximating to 0° and if the body tide is removed from the observed quantity there remains a measure of the oceanic influences amounting to 77 milliseconds in magnitude and 143° in phase lag. Proceeding with this analysis, it is known that the oceanic influences must themselves be subdivided into real surface tilts due to the loading of the ocean tide in the vicinity of the station on the one hand, and apparent tilts caused by periodic deviation of the vertical as a result of the attraction of the mass of tidal water on the other. The latter phenomenon is here calculated to be of magnitude 17 milliseconds with a phase lag of 138° so that the oceanic loading effect must amount to 61 milliseconds with a phase lag of 145°. The importance of the effect of tidal attraction in this connexion is thereby established in relation to the associated phenomena and its assessment from a geophysical point of view can proceed.

Already the values given above indicate the lag upon the ocean tide of its loading effect operating upon the Earth's crust. This value can be checked by arguments using the east–west component of M_2 and this, together with the solutions given for S_2 and N_2 are now available for a geophysical interpretation of the continuing series of tilt observations at the Bidston station.

Liverpool Observatory & Tidal Institute,
Birkenhead.
1961 *March.*

References

Clarke, A. R., 1880. *Geodesy*, Oxford 294.
Doodson, A. T. & Corkan, R. H., 1932. *Phil. Trans. A.*, **231**, 29.
Hayford, J. F., 1909. *The figure of the earth and isostasy.* Washington Govt. Printing Office.
Proudman, J. & Doodson, A. T., 1924. *Phil. Trans. A.*, **224**, 185.

The Re-magnetization of a Surface Outcrop by Lightning Currents

K. W. T. Graham

(Received 1961 March 30)

Summary

Scattered directions of magnetization are commonly found in samples taken from surface outcrops in South Africa. An investigation of the directions of magnetization in samples from one outcrop of a Pilanesberg dyke combined with laboratory measurements of the remanent magnetism produced by d.c. fields and spark discharges showed that the pattern of magnetization in the outcrop was due to two horizontal electrical currents one of 5 000 amps, the other of 50 000 amps. These currents are almost certainly associated with lightning discharges. The effect of a.c. demagnetization in removing the magnetization produced by lightning is discussed.

1. Introduction

Almost invariably magnetically stable samples from surface outcrops in South Africa have shown scattered directions of magnetization while those from deep quarries or underground workings have proved to be consistently magnetized. (Gough 1956, Graham & Hales 1957, Graham & Hales 1961). Various workers have suggested a number of possible explanations for these "surface effects" including weathering, thermal cycling, magnetostriction, thermo-stress cycling and lightning.

Generally, weathering is detectable and avoidable and the daily thermal cycling of an outcrop can be shown to be limited to a very few inches below the exposed surface. However, the weathering of the uppermost half-inch of rock can produce very high stresses which might be felt several feet down in the rock. Similarly the daily thermal expansion of the surface of an outcrop could possibly result in a kind of stress cycling. Whether or not these forces could have any permanent magnetostrictive effect on the rock is not known.

Hallimond and Herroun (1933) pointed out that lightning can re-magnetize rocks and advised that samples used in laboratory experiments should be taken from depths of about 50 ft. If lightning were responsible for the remagnetization of rocks, one might expect to find the remanent magnetic directions forming a pattern of concentric rings round the point at which the current reached the ground. Random sampling over a wide area would be expected to yield samples magnetized almost horizontally but with random declinations. The directions of magnetization of the numerous samples collected by the author are not concentrated in the horizontal plane. It was thought before this investigation was undertaken that it

followed that lightning was not of major importance in the remagnetization of surface samples.

2. Work on an outcrop of the Robinson dyke

The Robinson dyke is a member of the family of Pilanesberg (or Pilansberg) dykes. Gough (1956) had shown that this dyke, as well as five others, was randomly magnetized at the surface but consistently magnetized at depth. Gough's figures for the basic part of this dyke exposed underground are:

No. of samples: 42
Direction of mean N-seeking pole: Azimuth 14°·1,
Inclination: 71°·8,
Radius of cone of 99 per cent confidence (α) = 4°·9.

One of the outcrops of the Robinson dyke sampled by Gough was chosen for a study of the "surface effects". The exposure is about 50 ft square, fairly flat and weathered to not more than half an inch below the surface.

By means of a special drill rig (Grahan & Keiller 1961) a total of 20 oriented cores were drilled from this outcrop. Some of the cores were 3 ft long and others 6 ft long. All were drilled vertically. The cores, one inch in diameter, were cut into specimens one inch long, the specimens being numbered from the top of the core downwards. Generally 10 specimens could be cut from 12 inches of core. The direction and intensity of magnetization of each of the 784 specimens were measured by means of a spinner-type magnetometer.

3. Laboratory experiments

The measurements of the direction of magnetization described in Section 5 showed qualitatively that the pattern of magnetization could be accounted for in terms of horizontal currents near the surface of the rock, and laboratory experiments on the magnetization of specimens were carried out in order to estimate the magnitude of the currents involved. It is convenient to discuss the laboratory experiments before describing the results of the field work.

(*a*) *Magnetization experiments*

Six specimens from the deepest bore cores were selected for experiments using a d.c. magnetic field. The specimens had intensities close to $2{\cdot}8 \times 10^{-3}$ gauss. This value was calculated from Gough's (1956) figures as the mean intensity of underground samples from the basic part of this dyke.

The direction and intensity of magnetization of each specimen were measured before and after each experiment.

In the d.c. magnetization experiments the specimen was placed in a solenoid, the current in which was slowly increased to a predetermined value at which it was held constant for a given time and then slowly decreased to zero. The orientation of the specimen relative to the axis of the solenoid was in general such that the original direction of magnetization was at right angles to the axis of the solenoid.

The direction and magnitude of the remanent magnetic vector produced by the applied field was calculated by vector subtraction from the measured vectors of magnetization before and after the application of the field. The known direction of the applied field was not used in the calculation. The angle between the direction

of applied field and the direction of the calculated remanent vector of magnetization produced by it is a measure of the validity of the method. It was found that in all cases this angle was within the limits of the experimental error, never exceeding 5°.

This vector of remanent magnetism has been plotted on the vertical axis in Figures 1 and 2. It will be seen that the curve starts to depart from the horizontal axis at about 8 oe and that 12 oe is sufficient to produce a small but significant magnetic vector. The curve shows no signs of approaching saturation at 380 oe. It would appear as though the best curve through the points has a slight "kink" at about 210 oe.

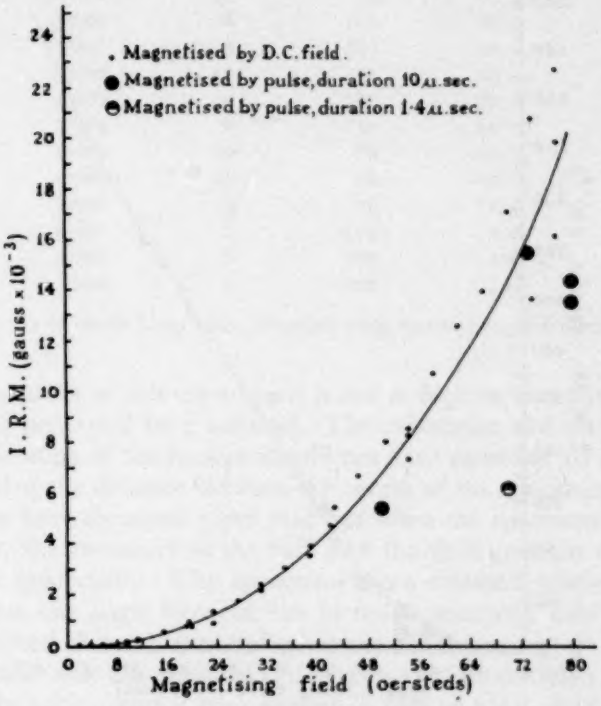

FIG. 1.

No magnetic anisotropy was observed in these experiments.

During the experiments the time of application of the d.c. field was varied from 15 seconds to 28 hours. Within experimental error, the remanent vector was not affected by the time of application of the d.c. field. The random storage of specimens in the Earth's field for periods of several months showed no significant effect.

In spite of the fact that for this rock the remanent magnetism is independent of the duration of the applied d.c. field for periods ranging from 15 seconds upwards, it could not be said that the field due to a lightning discharge would behave similarly. A lightning flash consists of one or more consecutive strokes, usually four in South Africa (Schonland 1956). Each stroke consists essentially of a "leader" (stepped or otherwise) carrying a fairly low current, followed by the main flash. It should be noted that although the electrical breakdown for the leader proceeds from cloud to ground while that for the main flash is from ground

to cloud, nevertheless, the actual current or flow of electrons is in the same direction throughout any particular discharge. (Generally the cloud is negatively charged and electrons move from cloud to ground.) There can therefore be no alternating field as suggested by Rimbert (1958). Instead the field is made up of a number of d.c. pulses, all of the same sign.

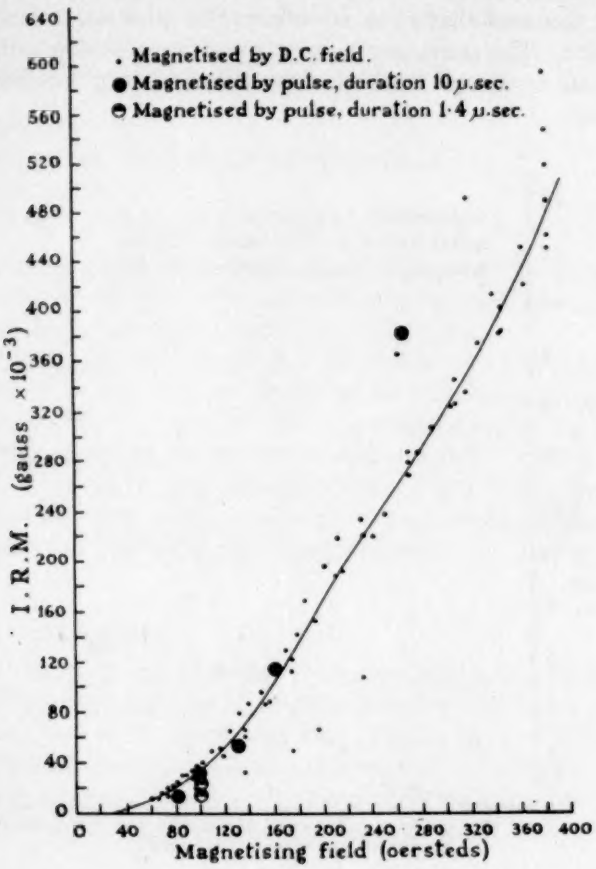

FIG. 2.

The current in the main stroke varies from 10 000 amps to more than 160 000 amps. In 50 per cent of the discharges recorded in Rhodesia, the current exceeded 40 000 amps (Anderson & Jenner 1954). The time taken for this current to reach its peak varies from 1 to 19 μs, with an average of 6 μs, while the time taken for the current to fall from its peak value to half its peak value varies from 7 to 115 μs with an average of 24 μs (Chalmers 1957, p. 252).

With the co-operation of Mr J. Kritzinger of the Department of Electrical Engineering of the University of the Witwatersrand it was possible to evaluate the effect of very short pulse fields on the magnetic remanence of specimens from the Robinson dyke. The rock specimens were placed at known distances from a long straight conductor connected via a spark gap to a high voltage impulse generator and were subjected to the pulse fields resulting from high current discharges along the conductor. Photographs of the trace of a calibrated oscillograph were taken so that estimates of the current, pulse shape and duration of

discharge could be made. (See Kritzinger 1961 for further information on circuits.) The direction and intensity of magnetization was measured before and after each experiment and the vector produced by the field was estimated in the manner described above. The results of these experiments are presented in Table 1 and the magnetic vector is plotted against the field as large circles in Figures 1 and 2.

Table 1

Specimen No.	Peak current amps	Distance cm	Field oe	Duration* μs	No. of shots	Magnetic vector gauss $\times 10^{-3}$
6/48	4 000	16	50	10	1	5·4
6/48	4 000	8	100	10	1	29
6/48	4 000	3	267	10	1	386
6/49	4 000	11	73	10	1	15·7
6/49	4 000	5	160	10	1	114
11/48	3 900	6	130	10	1	53
11/51	4 000	10	80	10	1	14·5
11/50	4 000	10	80	10	5	13·7
11/47	3 200	9	70	1·4	1	6·3
11/46	3 000	6	100	1·4	1	15·8
6/47	3 000	6	100	1·4	1	27·5
6/46	3 000	6	100	1·4	5	33·5

* Duration of spark from start, through peak current to half-current.

The accuracy of this experiment is not as high as that obtainable when using a d.c. field generated by a solenoid. The calibration and reading errors involved in the estimation of the current should not have exceeded 10 per cent. The error in measuring the distance between the centre of the specimen and the conductor should not have exceeded 5 per cent but when the specimen is very close to the conductor, the curvature of the field and the field gradient across the specimen would be appreciable. The specimens were oriented relative to the conductor by eye, but the angle between the intended magnetic field and the calculated vector reached 9° in one case and otherwise did not exceed 5°.

It is clear that the effect of d.c. pulses of 9 μs. duration from start, through the peak to half current is very similar to that of a d.c. field applied for a much longer time. The effect of the shorter pulses of 1·4 μs. duration may be a little lower but it is not known whether these differences are significant or not. As shown in Table 1, the effect of several pulses of the same size is not significantly different from that of a single pulse. It is, therefore, very probable that the magnetic effect on this rock of one or more main strokes of a lightning discharge will follow the curves shown as Figures 1 and 2, and these curves will be used to estimate the field and thence the current responsible for the remagnetization of part of this outcrop.

(*b*) *Demagnetization by alternating current*

Alternating current demagnetization experiments were performed on specimens from this outcrop, primarily in order to determine to what extent, if any, it is possible to remove the secondary magnetization without affecting the original T.R.M. By this means it might be possible to make an estimate of the direction and intensity of the T.R.M. of a rock, in spite of the fact that the original magnetization had been swamped by magnetizations acquired subsequently.

The apparatus used is similar in principle to that described by Creer (1959) in which the specimen is simultaneously rotated about a horizontal and a vertical axis by means of a pair of bevel gears. The alternating magnetic field is slowly and smoothly increased to any desired level and then similarly reduced to zero. In our apparatus, the lower bevel gear is also rotated but at a speed different from that of the main cradle. This ensures a more random motion of the specimen which presents every possible direction in it to the a.c. field. The peak field at the centre of the coil is set to the desired level by means of a Variac. The coil, mounted on a trolley, is then slowly pulled up to and over the spinning specimen by means of a winch. After any desired length of time the field at the specimen may be reduced very nearly to zero by reversing the winch and removing the trolley to about five feet from the specimen. The increase and decrease of the field is, of course, not linear with time but it can be made to vary very slowly and smoothly over a wide range. It was found empirically that better results were obtained using 500 c.p.s. alternating current from a generator than by using 50 cycles from the "mains". A large pair of Helmholtz coils was arranged so as to cancel the d.c. field of the Earth at the specimen. It was found experimentally that cancellation of the Earth's field or doubling the field made no difference to the a.c. washing experiments and the use of the Helmholtz coils has been discontinued.

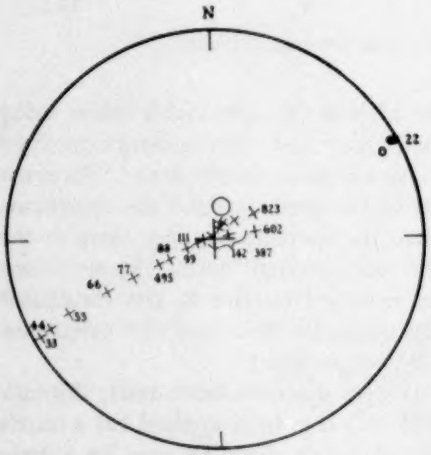

FIG. 3.

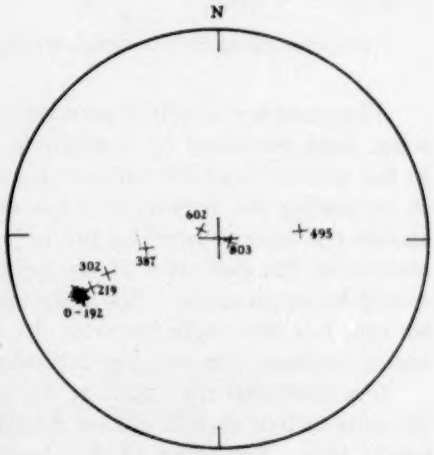

FIG. 4.

Lower hemisphere stereographic projections of the directions of remanent magnetization of specimens 1/26 and 12/13 after each stage of a.c. demagnetization. × = North pole downwards. • = South pole downwards. ○ = Cone of 99 per cent confidence for mean direction of magnetization (Gough 1956). Figures denote peak a.c. field in oersteds.

The direction and intensity of magnetization of the specimen is measured after each of the successively larger applications of d.c. field. Figure 3, a lower hemisphere stereographic plot, shows the way in which the direction of remanent magnetization of specimen 1/26 changes with increasing a.c. field. After being subjected to a peak field of 160 oe its direction of magnetization is very close to that determined by Gough (1956) for the basic part of this dyke in Robinson Deep Gold Mine. Further increases in the field do not alter the direction appreciably until the intensity of magnetization is less than about one tenth of Gough's

mean intensity of magnetization for this dyke of $2{\cdot}8 \times 10^{-3}$ gauss. For larger demagnetizing fields, the directions of magnetization start to scatter.

The initial intensity of magnetization of specimen 1/26 was $17{\cdot}9 \times 10^{-3}$ gauss (see also Figure 5) i.e. about six times more strongly magnetized than unaffected rock at depth. Similar results are obtainable from specimens with initial magnetizations up to about 30×10^{-3}, i.e. about ten times the intensity of the original T.R.M. In each case the direction of magnetization moves towards and finally pauses at a point very close to Gough's mean direction. Some scatter may occur with fields exceeding about 600 oe.

In specimens whose secondary magnetization is more than about 10 times stronger than the T.R.M., a.c. washing does not effectively restore the original direction of magnetization. Figure 4 shows the progress towards the original direction of magnetization of specimen 12/13 whose initial intensity was $2{\cdot}1 \times 10^{-1}$ gauss. No clear "end point" is reached. After treatment in the a.c. field of 387 oe, the intensity of magnetization was down to $1{\cdot}1 \times 10^{-4}$ gauss and it is clear that the effective coercive force of such strong magnetization is very close to that of the T.R.M.

Rimbert (1958) drew attention to the difference in the intensity vs a.c. demagnetizing field curve for magnetization probably due to lightning and that due to a d.c. field. Figure 5 confirms this observation. The demagnetization curves for the specimens probably magnetized by natural lightning begin with a gentle slope which increases to a point where the curve becomes nearly linear.

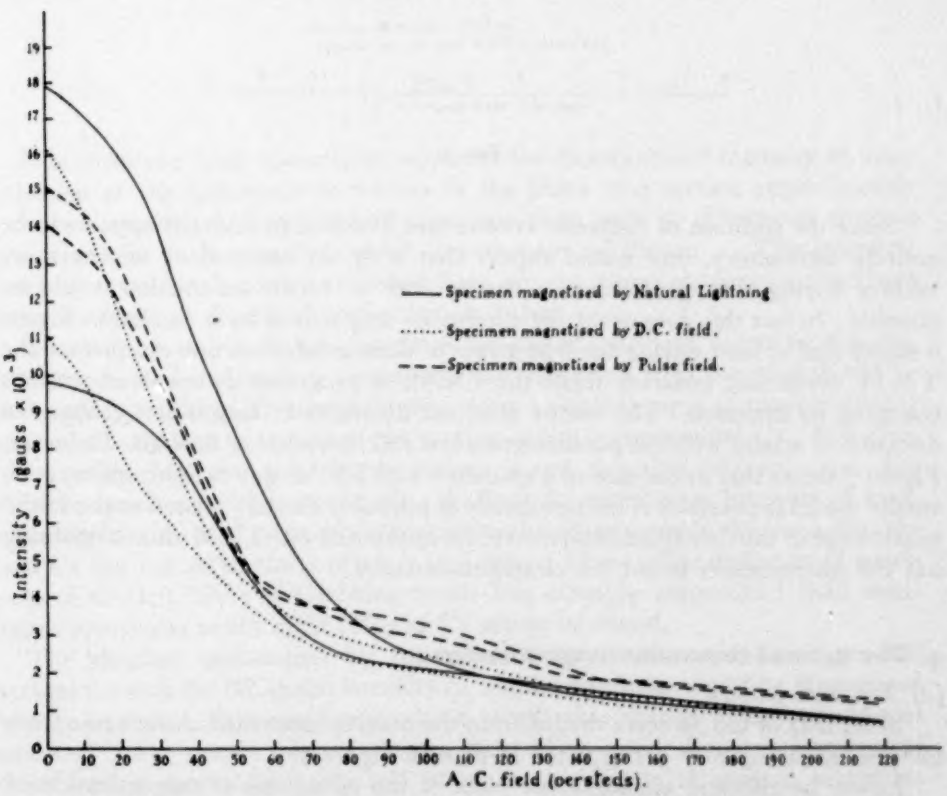
Specimen magnetised by Natural Lightning
Specimen magnetised by D.C. field.
Specimen magnetised by Pulse field.
Intensity (Gauss × 10⁻³)
A.C. field (oersteds).

FIG. 5.

The curves for the specimens magnetized by a d.c. field do not show this initial gentle slope. Specimens 11/50 and 11/51 were magnetized by the field due to an artificial spark discharge (see Section 3a), specimen 11/50 was subjected to one such discharge while 11/51 was magnetized by five equal discharges at short intervals. The demagnetization curves for these two specimens do not appear to be significantly different from each other and they resemble the curves for the specimens magnetized by natural lightning more closely than they do those magnetized by a d.c. field.

The slight plateau formed by each demagnetization curve at intensities ranging from 2 to 4×10^{-3} gauss probably represents the stage at which the I.R.M. becomes comparable with the T.R.M. This supports the assumption that the average T.R.M. of this outcrop of the Robinson dyke has much the same intensity of magnetization as the underground exposures studied by Gough (1956). The mean for the underground exposures (calculated from Gough's figures) of $2{\cdot}8 \times 10^{-3}$ gauss is consistent with these and other demagnetization curves

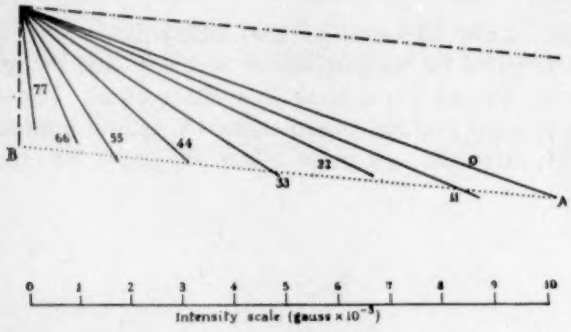

FIG. 6.

Since the addition of magnetic vectors (see Sections 3a and 4b) appears to be entirely satisfactory, one would expect that with the removal of one or more vectors during demagnetization a similar sort of vector subtraction would be possible. In fact this does occur for specimens magnetized by a d.c. field. Figure 6 shows that at least during the first stages of demagnetization one can picture the T.R.M. remaining constant while the I.R.M. is progressively removed without changing its direction. The vector resultant decreases in length and changes in direction in accord with the parallelogram law and moves along line AB. However, Figure 7 shows that in the case of a specimen with I.R.M. due to lightning no such simple model is possible. This peculiarity is probably directly related to the initial gentle slope of the demagnetization curve for specimens with I.R.M. due to lightning but the phenomenon is not yet clearly understood.

4. The natural remanent magnetization

(*a*) *The main pattern*

Seventeen of the 20 cores drilled from the outcrop described above came from the area about 14 ft by 5 ft depicted in plan as Figure 8.

Lower hemisphere stereographic plots of the directions of magnetization of the specimens from each of cores 1, 4, 12, 14, 20 and 8 are shown as Figures 10

to 15 respectively. On the whole the specimens from these cores as well as those from most of the other cores, are magnetized in directions which fall on nearly vertical, approximately NE–SW great circles. The "strike" of each of these planes of magnetization is shown as the line through each of the "bore holes" in Figure 8. As will be seen from the plan, these vertical NE–SW planes nearly coincide with the approximate plane from which the specimens of cores Nos. 8, 16, 1, 4, 12, 13, 9, 14 and 20 were drilled.

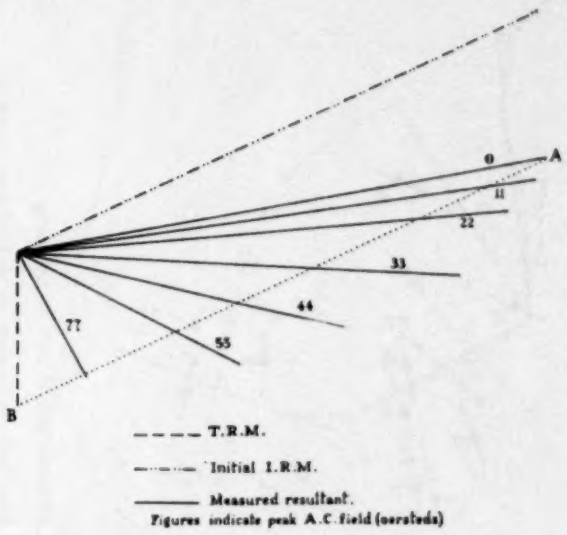

FIG. 7.

It is therefore fairly accurate to represent the direction and intensity of magnetization of the specimens as vectors in the plane of a section approximately through these cores. Every fourth specimen from each of the above cores is represented in such a section which is presented as Figure 9. The magnetic vectors for core No. 8, shown as dashed lines, are not direct observations but have been calculated as described in Section 4b below.

Except for core No. 8, the pattern of the direct remanent magnetic observations represented in Figure 9 is qualitiatively consistent with one that would be produced by an electrical current flowing along a single straight conductor passing perpendicularly into the plane of the section at the point marked C1. However, it is equally clear that this simple picture is not quantitatively accurate. For example, specimen 16/9 is about 2 ft 4 in. from C1 and has an intensity of magnetization of $2{\cdot}2 \times 10^{-2}$ gauss while specimen 9/17 is very nearly the same distance from C1 but has an intensity of $1{\cdot}9 \times 10^{-1}$ gauss. Many other examples of specimens to the left (SW) of C1 being much less strongly magnetized than equidistant specimens to the right (NE) of C1 are to be found.

The simplest explanation for this phenomenon is that there is a gradual increase towards the NE in the intensity to which a specimen could be magnetized by a given field. This could occur by a progressive change in the quantity or nature of the magnetic minerals in the rock. This possibility was investigated by subjecting specimens 14/29 and 16/30 to d.c. fields of various strengths. Within the limits of experimental error the two specimens behaved identically

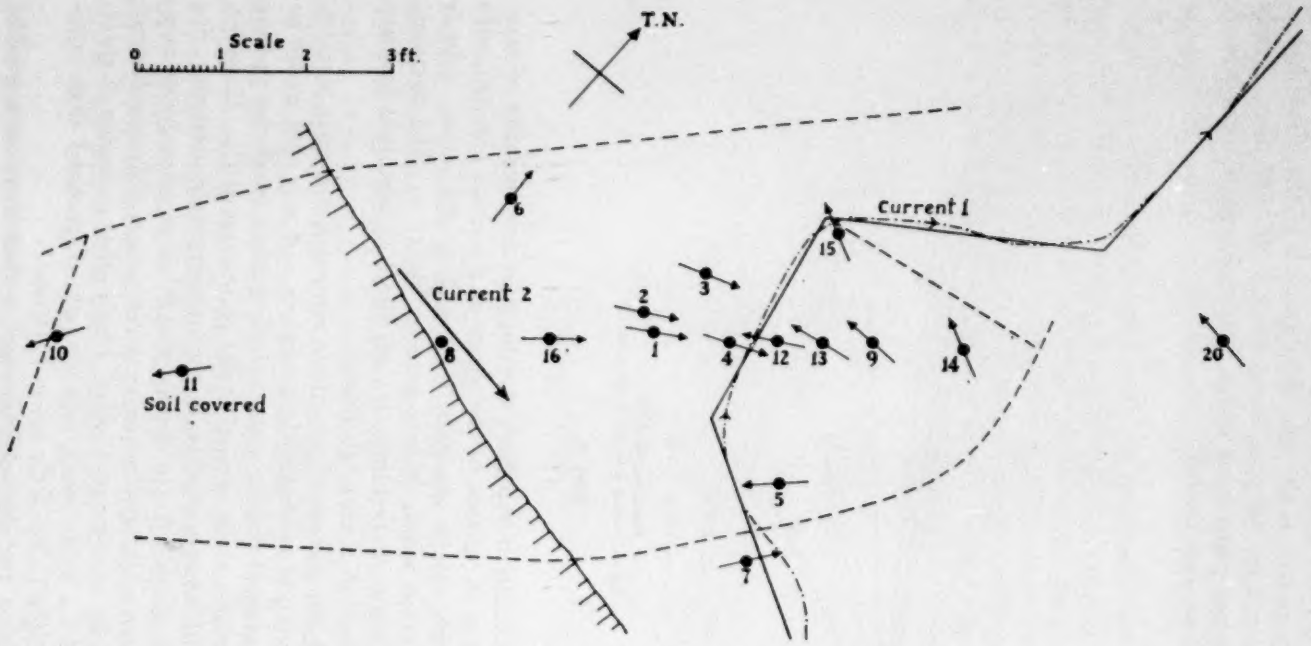

Key

- Bore hole.
- Joints.
- Limit of soil cover.
- Hypothetical path of lightning.
- Probable actual path of lightning.
- Bore hole, with plane of vertical great circle on which observed magnetic vectors lie. A straight current, in the direction indicated by the arrow, would flow perpendicularly to this plane.

FIG. 8.

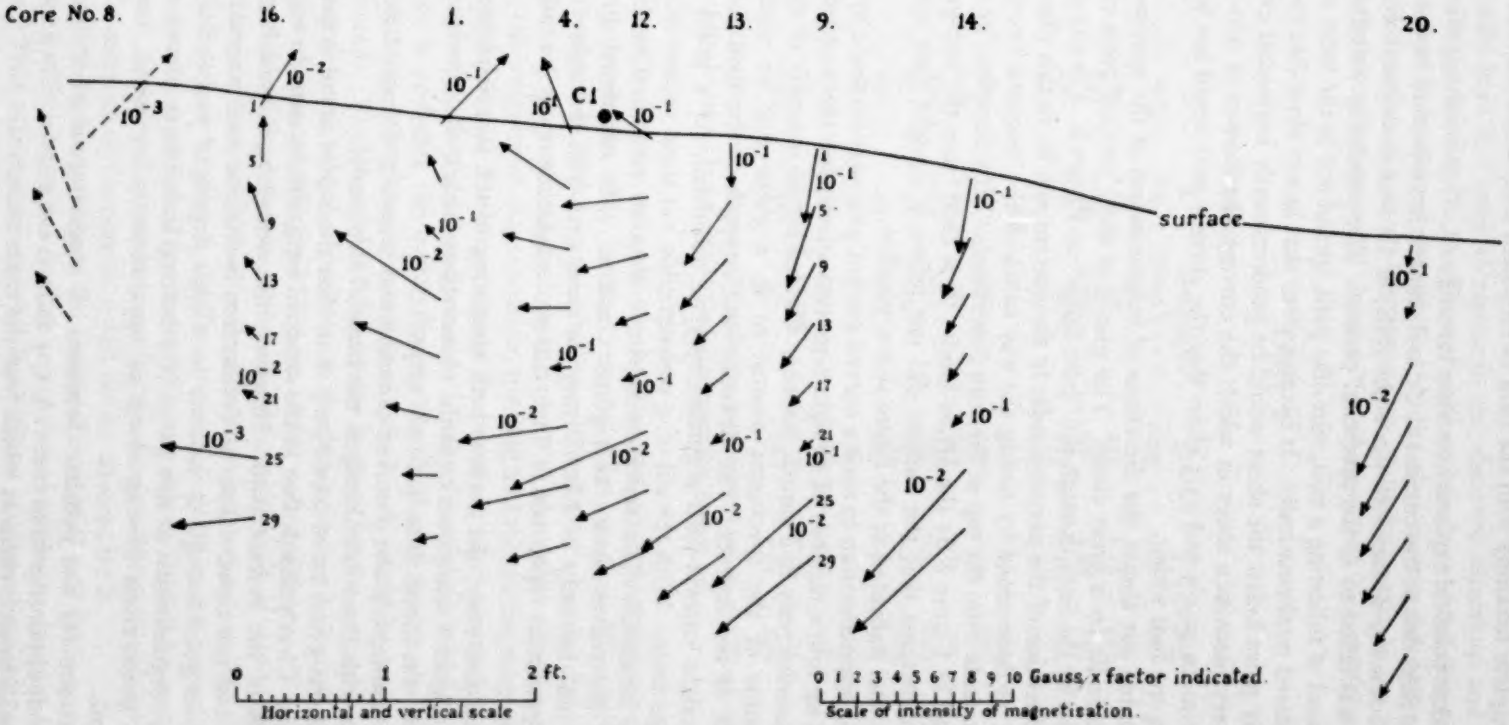

FIG. 9.—A section through part of the outcrop showing the variations in the direction and intensity of magnetization. The north-seeking poles have been plotted.

and in complete harmony with the field *vs* remanent magnetism curves described earlier.

Two other possible explanations were investigated. One involving the vectorial sum of the field due to the current at C1 and another large current in the opposite direction but some distance to the right (NE) of C1 was abandoned when a test core (No. 20) failed to fit the predicted pattern. The possibility that the current at C1, instead of following a thin, wire-like path, spread out in the form of a sheet was considered mathematically. It became clear that in any sheet-like model, the field at any point below the sheet would be predominantly horizontal even if the point is very close to a sheet in which the current distribution is non-uniform. Such specimens as 4/5 and 13/5 show that the current path could not have been more than one foot wide.

As pointed out above, the directions of magnetization of the specimens from any one core lie on a great circle. The planes of these vertical great circles are represented by the lines through the "bore holes" on Figure 8. For any particular core the direction of the perpendicular to the current will lie in this plane and its sense can be determined by noting the way in which the magnetic vectors rotate as one proceeds from the top of the core downwards. This direction for each core is indicated in Figure 8 by the arrow heads. It is clear from the non-parallelism of these directions that the current did not follow a straight path and a path similar to that indicated in the figure seems possible.

A good approximation to such a curved current path may be made by dividing the curve up into a number of straight segments whereupon the problem may be tackled quantitatively in a simple manner. Guided by the intensity of magnetization of some of the specimens nearest to it, a guess may be made at the magnitude of the current. The direction and strength of the field due to each of the straight current-path segments may be calculated for a point occupied by any specimen. With the aid of a stereographic net these vectors in 3 dimensions may be added. The resultant field can then be converted to I.R.M. by means of the curves shown as Figures 1 and 2. The calculated direction of the field and intensity of I.R.M. may be compared with the values observed for the particular specimen. The current magnitude may be adjusted if necessary.

By trial and error, the current path consisting of the four straight segments shown in Figure 8 was found to fit the observations fairly well. The best value of the current was found to be $5{\cdot}0 \times 10^4$ amps.

Table 2 compares the observed direction and intensity of magnetization of 14 specimens with those calculated on the basis of this model.

Specimens 5 and 25 of core No. 7 show that the model is not accurate at its extremities. Clearly this is due to the assumed semi-infinite straight segments at either end of the current path. However, the overall agreement between the observed and calculated values of declination, inclination and intensity of magnetization is good enough to indicate to a high degree of probability that the pattern of magnetization of this part of the outcrop is due to an electrical current of about 50 000 amps flowing along an approximately horizontal, narrow but curved path.

The reason for the peculiar directions of magnetization of the uppermost three or four specimens from cores 16, 1, 4 and 2 is not known. They may be due to very small branch currents which feed the main current.

(*b*) *Core No.* 8

The solid lines in Figure 16 represent the observed directions and intensities of magnetization of core No. 8. These directions are also plotted stereographically in Figure 15. Note the way in which the direction rotates through nearly 360° between the surface and about 3 ft and also the initial decrease in the intensity of magnetization to a minimum at about 1 ft 9 in. (specimen No. 17) followed by an increase.

Table 2

	Observed			Calculated			
Specimen No.	*D* deg.	*I* deg.	Intensity gauss × 10^{-3}	*D* deg.	*I* deg.	Field oe.	Intensity gauss × 10^{-3}
1/21	243	+12	29	245	+18	103	37
2/9	244	+55	99	250	+45	137	72
3/25	256	−5	23·6	261	+10	106	39
4/13	244	−1	270	253	−1	224	210
5/13	224	−36	280	223	−32	261	260
7/5	215	+1	480	210	+19	662	> 500
7/25	226	−18	34	224	−7	124	56
9/13	265	−54	310	275	−52	260	260
12/17	251	−20	146	257	−21	195	160
13/9	256	−48	380	263	−60	377	470
14/17	282	−50	116	282	−41	166	110
15/17	286	−9	135	283	−7	178	130
16/13	233	+55	15·2	235	+56	81	21
20/21	288	−56	41	280	−51	120	53

Note: *D* (declination) is measured clockwise from true North to the North-seeking pole. *I* (inclination) is positive if the North-seeking pole is up.

If perpendiculars are drawn from the observed directions of magnetization of the first 3 specimens, they intersect at the point marked "Current 2". The remanent magnetism of these 3 specimens could be due to a long straight horizontal current flowing perpendicularly into the plane of the paper through this point. Knowing the intensity of magnetization, the field and thence the magnitude of the current may be found. Specimen 1 gives a value of $4{\cdot}3 \times 10^3$ amps while specimens 2 and 3 give $5{\cdot}0 \times 10^3$ amps. Specimen 1 may be slightly weathered so that 5 000 amps is probably the better figure. The field and thence the intensity to which each of the remaining specimens of core No. 8 would be magnetized may now be found. The direction of this vector is given by the perpendicular to the line joining the centre of the specimen to the point marked "Current 2" and the Vector C is shown accordingly in Figure 16 for each specimen.

On the basis of the demagnetization experiments described above, the thermo-remanent magnetization of this core is assumed to be the same as that determined by Gough (1956) underground, viz. $D = 14°{\cdot}1$ $I = 71°{\cdot}8$, mean intensity $= 2{\cdot}8 \times 10^{-3}$ gauss and is represented by vector D in the figure. It will be noted that for specimens 1, 2 and 3 this vector is negligible compared with the observed vector so that the estimate of the current 2 will not be affected by it.

For any particular specimen, the vectorial sum of C and D does not produce the observed vector M, and a further vector A is required to account for the observations. This vector, drawn as the dashed lines in Figure 16, may be found by completing the parallelogram as shown for specimen No. 8.

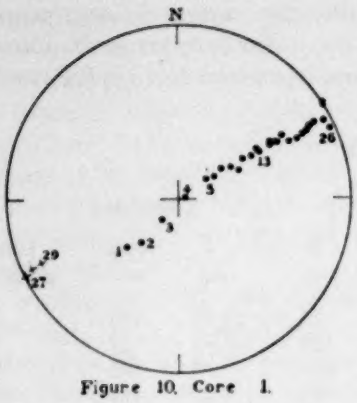

Figure 10. Core 1.

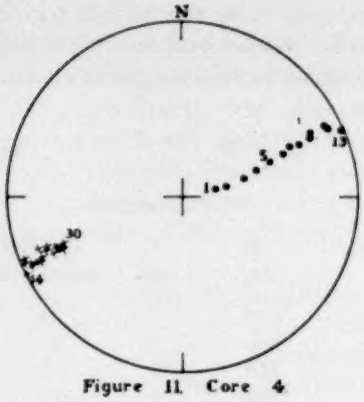

Figure 11. Core 4.

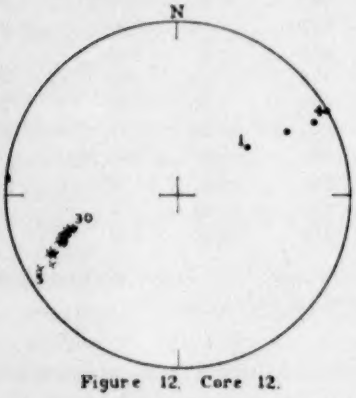

Figure 12. Core 12.

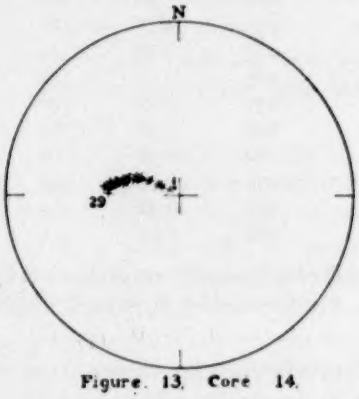

Figure 13. Core 14.

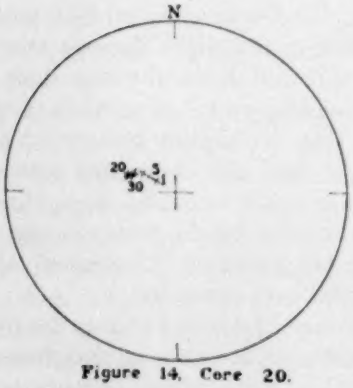

Figure 14. Core 20.

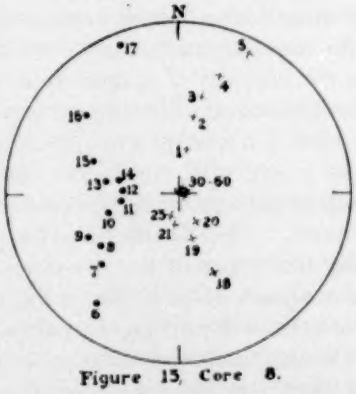

Figure 15. Core 8.

× = North pole downwards. ● = South pole downwards. The specimens are numbered from the top to the bottom of each core.

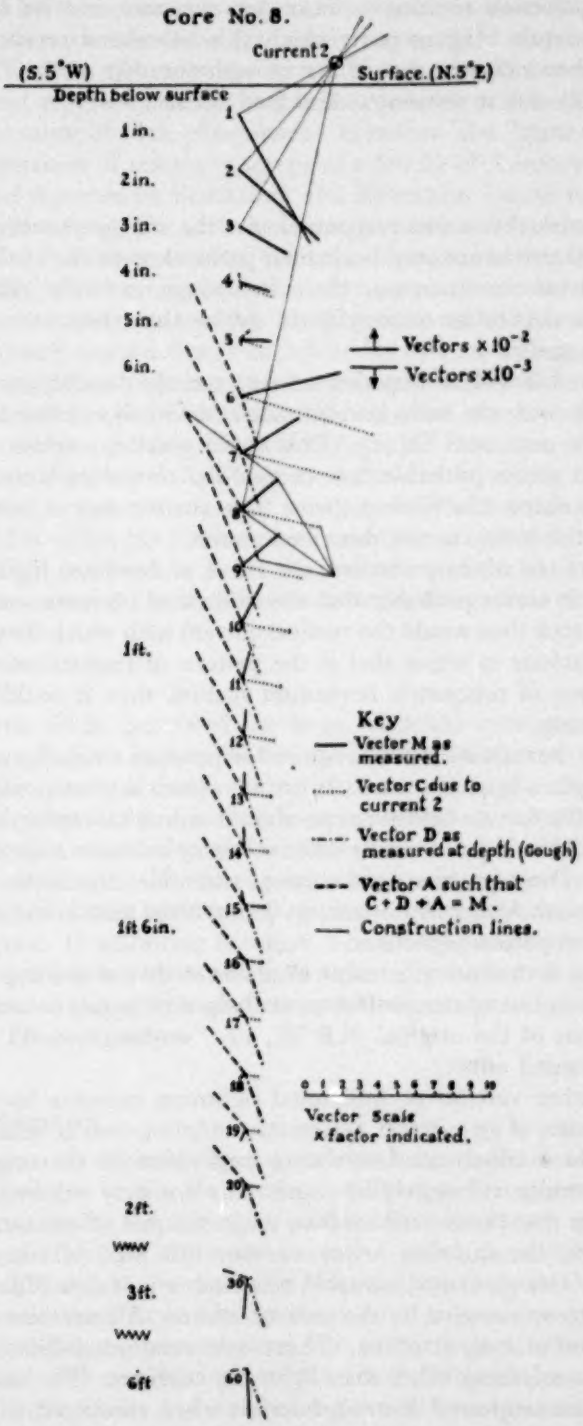
Core No. 8.
Current 2
(S.5°W)
Surface. (N.5°E)
Depth below surface
1 in.
2 in.
3 in.
4 in.
5 in.
6 in.
1 ft.
1 ft 6 in.
2 ft.
3 ft.
6 ft
Vectors x 10⁻²
Vectors x 10⁻³
Key
Vector M as measured.
Vector C due to current 2
Vector D as measured at depth (Gough)
Vector A such that C + D + A = M.
Construction lines.
0 1 2 3 4 5 6 7 8 9 10
Vector Scale
x factor indicated.

FIG. 16.

The behaviour of vector A is rather more systematic than that of the observed vector M. Its direction remains more or less constant and its intensity falls off smoothly with depth. Figure 9, in which this calculated vector A is shown by dashed lines, shows clearly that it fits in with the rest of the "Main Pattern". It is undoubtedly due to current 1 described above.

5. Discussion

Both the electrical currents responsible for the remagnetization of part of this outcrop followed predominantly horizontal paths close to the surface of the rock. The magnitude of the currents, their behaviour and the characteristic a.c. demagnetization curves leave very little doubt that they are associated with lightning discharges.

From Figure 8 it will be seen that current 2 could possibly curve towards the North to join up with the main current. Another small current may have joined the main current near core No. 15. This could possibly explain the magnetism of core No. 6. It seems probable that cores Nos. 10 and 11 were magnetized by another large current to the West of them. This current may or may not have been associated with the main current described above.

In the area of the outcrop studied, the effect of a vertical lightning current is not seen at all. It seems probable that the horizontal currents could remagnetize a greater area of rock than would the vertical current with which they are associated. It is clearly fallacious to argue that if the pattern of magnetization of a surface outcrop is not one of concentric horizontal vectors, then it could not have been caused by lightning.

For this rock the minimum field required to produce a significant change in the remanent magnetism is about 12 oe. It can be shown arithmetically that to avoid entirely such fields due to lightning one should not use samples from a depth of less than 50 ft. Securing accurately oriented samples from a depth of 50 ft is a formidable task. Deep quarries, road cuttings and mines should be used wherever possible but in South Africa such workings do not often exist in the rock formations of most interest to palaeomagnetism.

The next best technique at present available is that of drilling to 3 or 6 feet. Although the directions of magnetization at these depths can be very significantly different from that of the original N.R.M., a.c. "washing" would, in most cases, remove the unwanted effect.

Clearly, if either vertical or horizontal lightning currents have affected the remanent magnetism of an outcrop, systematic sampling over an area of say 50 ft by 50 ft cannot yield a consistent, but wrong impression of the original magnetic direction. The results will merely be negative in that they will be scattered.

Having shown that the overall random magnetization of one outcrop is due to lightning currents, the question arises whether this kind of remagnetization is common or not. Gough (1956) sampled ten outcrops of five Pilanesberg dykes, including the outcrop sampled by the present author. All ten were found to have scattered directions of magnetization. There is no reason to believe that the cause of the scatter was anything other than lightning currents. The marked decrease in scatter of the underground Karroo dolerites when compared with the surface samples (Graham & Hales 1957) has already been mentioned. Similarly samples of the lower "Shales" of the Table Mountain Series taken from a deep road cutting were found to be consistently magnetized whereas those from the mountain side

were inconsistently magnetized (Graham & Hales 1961). In both these cases it is thought that lightning currents may have been the cause of the scattering.

Workers in other countries have frequently encountered surface outcrops with scattered magnetization. These negative results are generally mentioned only in passing, or are not reported at all so that it is impossible to form an opinion as to the frequency or cause of such phenomena. However, the "minor deviations" in the magnetic directions of certain outcrops of a family of Tertiary tholeitic dykes of North England reported by Bruckshaw and Robertson (1949) may be attributable to lightning currents. The patterns of magnetization of some outcrops studied by Bruckshaw and Robertson are very similar in character to that described above.

The possibility of the remagnetization of many surface outcrops by lightning currents makes it necessary to use the "conglomerate stability test" with caution. J. W. Graham (1949) argued that if each boulder or rock slab in a conglomerate is consistently magnetized but the remanent magnetic directions for the various boulders is different to the point of randomness, then the rock from which the boulders are derived is probably magnetically stable. However, it is obvious that, particularly where horizontal lightning currents are involved, the direction of magnetization of a surface outcrop may vary rapidly over a small area. Thus, this test is only valid if either (a) the samples came from a considerable depth below the surface or (b) it can be shown that the separation of the specimens from each boulder is of the same order as the distance between the various boulders sampled.

6. Conclusions

The magnetic fields generated by large electrical currents associated with lightning discharges have re-magnetized the portion of the outcrop studied and may be the cause of many of the "scattered" directions of magnetization encountered in the palaeomagnetic study of surface samples. The only completely satisfactory way of avoiding this hazard is to restrict oneself to samples collected from depths of greater than about 50 ft. However, systematic sampling over even a fairly small area cannot yield consistent but "wrong" directions of magnetization resulting from lightning currents. If scattering is found, a.c. washing may prove useful, particularly if the specimens have come from moderate depths such as 3 to 6 feet.

J. W. Graham's (1949) "conglomerate test" for magnetic stability should be used only with extreme caution.

7. Acknowledgments

It is a pleasure to acknowledge my indebtedness to Professor G. R. Bozzoli and Mr J. Kritzinger of the Department of Electrical Engineering, University of the Witwatersrand. But for their enthusiastic assistance the experimental magnetization of rock specimens by means of pulse currents would not have been possible. Thanks are also due to Dr Hewitt, Director of the National Institute for Telecommunications Research, for the loan of a 500 c.p.s. generator used in the a.c. demagnetizing experiments, and also to Mr J. A. Keiller who built most of the apparatus. We are indebted to the South African Council for Scientific and Industrial Research for a grant covering the salary of an assistant. Above all, I would like gratefully to acknowledge the extremely enthusiastic support and constructive criticism of Dr A. L. Hales, Director of the Bernard Price Institute of Geophysical Research.

Note added in proof.—A recent paper by A. Cox (*U.S. Geol. Survey Bull. No.* 1083E, 1961) further demonstrates that the re-magnetization of surface outcrops by lightning currents is very common.

Bernard Price Institute of Geophysical Research,
University of the Witwatersrand,
Johannesburg,
South Africa.
1961 *March.*

References

Anderson, R. B. & Jenner, R. D., 1954. *Trans. S.A. Inst. Elec. Eng.*, **45**, 215.
Bruckshaw, J. McG. and Robertson, E. I., 1949. *Mon. Not. R. Astr. Soc. Geophys. Suppl.*, **5**, 308.
Chalmers, J. A., 1957. *Atmospheric Electricity* (Pergamon Press) p. 252.
Creer, K. M., 1959. *Geophys. J.*, **2**, 261.
Gough, D. I., 1956. *Mon. Not. R. Astr. Soc. Geophys. Suppl.*, **7**, 196.
Graham, J. W., 1949. *J. Geophys. Res.*, **54**, 131.
Graham, K. W. T. & Hales, A. L., 1957. *Phil. Mag. Suppl., Advances in Physics*, **6**, 149.
Graham, K. W. T. & Hales, A. L., 1961. *Geophys. J.*, **5**, 318.
Graham, K. W. T. & Keiller, J. A., 1961 (in press).
Hallimond, A. F. & Herroun, E. F., 1933. *Proc. Roy. Soc.*, **141**, 302.
Kritzinger, J. J., 1961. *Trans. S.A. Inst. Elec. Eng.* (in press).
Rimbert, F., 1958. D.Sc. thesis, Faculty of Science, University of Paris.
Schonland, B. F. J., 1956. *Handbuch der Physik*, **22**, (Berlin: Springer).

On Solar Wind Generation of Polar Geomagnetic Disturbance

K. D. Cole

(Received 1961 March 24)

Summary

Solar wind generation of polar geomagnetic storms is examined on a model suggested by Piddington. His theory is criticized and inferences are drawn which may be tested against observation. A comparison of solar wind and atmospheric dynamo generation of magnetic disturbance (and auroras) is made. It is suggested that a combination of these two processes may be necessary to explain the total phenomena.

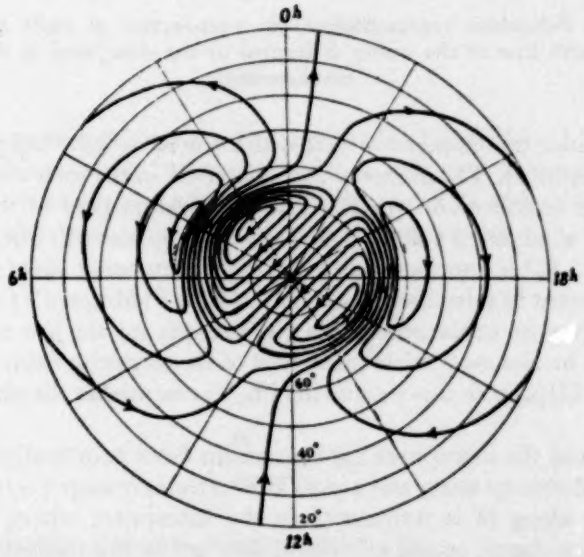

FIG. 1. (Taken from Fukushima & Oguti 1952.) Current-system of the S_D-field for the equinoctial season. (Electric current of $1{\cdot}5 \times 10^5$ amp flows between adjacent stream lines.)

1. Introduction

Piddington (1960) uses the hypothesis of a "solar wind" blowing outwards from the Sun in his explanation of the longitude dependent geomagnetic disturbance *Ds* (cf. Figure 1). (A related suggestion comes from Johnson (1960)). It is the purpose of this paper to re-analyse his model with the view to criticizing his analysis and to drawing inferences from the theory which may be tested by observation. It

will be assumed that the reader is familiar with Piddington's (1960) version of analysis of the model.

2. General description of physical processes

It is assumed that the "solar wind" does not invade a cavity (whose surface is S) about the Earth. The wind blows with a velocity $\mathbf{w}$, through the geomagnetic field $\mathbf{H}$. On Piddington's (1960) theory one would expect S to be elongated away from the Sun and dome-shaped on the day side. Figure 2 illustrates a cross-section of S by a plane normal to the Sun–Earth line through the centre of the Earth. Such a cross-section may be about 5 Earth radii in radius.

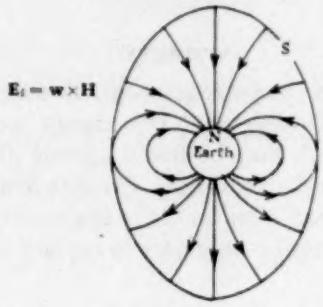

FIG. 2. Schematic representation of cross-section at right angles to Sun–Earth line of the cavity S formed by the solar wind in the Earth environment.

Let us consider the instant $t = 0$ at which the solar wind has just commenced blowing (see Figure 2). The motional induction field in the solar wind $\mathbf{E}_i (= \mathbf{w} \wedge \mathbf{H})$ causes a charge distribution over S. The polarization field of this charge has a value $\mathbf{E}_p$ in the wind and a value $\mathbf{E}_p'$ inside S. $\mathbf{E}_p$ opposes $\mathbf{E}_i$ but does not necessarily balance it. $\mathbf{E}_p'$ is unopposed and, having a component along the geomagnetic field, causes current to flow along it. This explains Piddington's (1960) equation 8 for which he gives no explanation; this gives reason for the $\mathbf{j}(= 0, 0, \mathbf{j}_z(r))$ of his section 6 which he assumed exists (as a twist of the magnetic field). It will be seen later in Section III(a) how this electric field $\mathbf{E}_p'$ is essential to the phase propagation of such a twist.

Between S and the ionosphere (I) the current flows principally along $\mathbf{H}$ for the ratio of the conductivity along and across $\mathbf{H}$ is extremely large ($\sim 10^4$ or 10^5). The flow of current along $\mathbf{H}$ is terminated in the ionosphere where the consequent build-up of space charge causes current to flow across the magnetic field. (In the whole of the region inside S the best conducting path across the magnetic field is in the dynamo region of the upper atmosphere ~ 100 km height above the Earth's surface.) The magnetic field lines between S and the ionosphere are then virtually electrostatic equipotential lines.

In the initial stages of establishing a steady electrostatic field system in the ionosphere the phase speed of current flow along $\mathbf{H}$ inside S is the Alfvén speed as demonstrated by Piddington (cf. Section 3(a)). In the steady state it is the electrostatic field system established within the ionosphere which drives current there responsible for geomagnetic variations as observed at the ground (cf. Section 3(b)).

3. Theory

(*a*) *Current flow between S and I*

The current density (**j**) in a fully ionized gas in which the gradient of pressure of electrons can be neglected is given by (Cowling 1957)

$$\sigma_0 \mathbf{E}' = \mathbf{j} + \omega\tau H^{-1}\mathbf{j} \wedge \mathbf{H}, \tag{1}$$

where $\mathbf{E}' = \mathbf{E}_p' + \mathbf{v} \wedge \mathbf{H}$

$\mathbf{E}_p'$ = electrostatic field

$\mathbf{v}$ = momentum per unit mass produced inside S.

ω = gyro frequency of electrons

τ = time between collisions of electrons with ions

$\sigma_0 = ne^2\tau/m_e$

e, m_e = charge, mass of an electron

n = electron density

$\mathbf{H}$ = magnetic field.

From (1)

$$\mathbf{j} = \sigma_0 \mathbf{E}_{\parallel}' + \sigma_1 \mathbf{E}_{\perp}' + \sigma_2 \frac{\mathbf{H} \wedge \mathbf{E}_{\perp}'}{H}, \tag{2}$$

where

$$\sigma_1 = \sigma_0/(1 + \omega^2\tau^2),$$

$$\sigma_2 = \sigma_1\omega\tau,$$

and $\parallel$, $\perp$ represent components parallel, perpendicular to H.

In the Earth's exosphere between S and I, ω may vary between 10^7 (at I) and 10^4 (at S) whilst τ may vary between 10^{-3} (just above I) and 1 (at S). Thus between S and I, $\omega\tau > 10^3$, thus $\sigma_0 \gg \sigma_2 \gg \sigma_1$. Hence equation (2) is well approximated by

$$\mathbf{j} = \sigma_0 \mathbf{E}_{\parallel}' + \sigma_2 \frac{\mathbf{H} \wedge \mathbf{E}_{\perp}'}{H}, \tag{3}$$

and the equation of motion

$$\rho \frac{d\mathbf{v}}{dt} = \mathbf{j} \wedge \mathbf{H}, \tag{4}$$

where ρ is the density, becomes, using equation (3),

$$\rho \frac{d\mathbf{v}}{dt} = \sigma_2 H \mathbf{E}_{\perp}'. \tag{5}$$

Now consider the following model. In a system of cylindrical coordinates (r, θ, z) a magnetic field $\mathbf{H} = (0, 0, H_z)$ exists prior to the application of an electric field $\mathbf{E}_p = (0, 0, \mathbf{E}_z)$. The field is assumed to contain a uniform distribution of fully ionized gas. As a result of $\mathbf{E}_p$ currents will flow causing additional magnetic field and motion. At this subsequent time let $\mathbf{v} = (v_r, v_\theta, v_z)$ and $\mathbf{H} = (h_r, h_\theta, H_z)$.

Then equation (5) yields

$$\frac{dv_r}{dt} = -\sigma_2 h_r E_z + \sigma_2 H_z(v_\theta H_z - v_z h_\theta),$$

$$\frac{dv_\theta}{dt} = -\sigma_2 h_\theta E_z + \sigma_2 H_z(v_z h_r - v_r H_z), \tag{6}$$

$$\frac{dv_z}{dt} = -\sigma_2 H_z(v_r h_\theta - v_\theta h_r).$$

To the writer's knowledge the equations (6), so fundamental to present-day research in controlled nuclear fusion, have never been solved completely. It may be possible to get an inkling of the morphology of the processes they describe in certain particular cases with the assistance of physical intuition rather than mathematical deduction.

In the idealized twist propagation examined by Piddington a tacit assumption has been made that $v_r = h_r = 0$, *viz.*, there is no pinch effect. In this case the equations (6) yield

$$v_\theta/h_\theta = v_z/H_z, \tag{7}$$

and

$$\rho \frac{dv_\theta}{dt} = -\sigma_2 h_\theta E_z. \tag{8}$$

In equation (7) v_z appears to be arbitrary. However, it represents the relative velocity of matter and magnetic field and therefore is the phase speed (i.e. Alfvén speed) of the (v_θ, h_θ) disturbance along H_z. It is clear that the $\mathbf{j}\,(=0, 0, j_z(r))$ of Piddington's section 6 is due to the component of electric field along H_z (cf. equation 3) so that $j_z(r) = \sigma_0 E_z$. Piddington offers no explanation of this current. Moreover it is seen from equation (8) that the current (providing a $\mathbf{j} \wedge \mathbf{H}$ force) which changes v_θ is the Hall (σ_2) current generated by E_z acting across h_θ; this explains Piddington's J_r. Piddington's explanation of his J_r is confusing, first because he invokes isotropic conductivity and secondly because his equation (15) is inconsistent with his equation (13) and the statement to which it is connected. Piddington's twist corresponds to a special case of equations (7) and (8) above in which v_θ takes a stepwise change across the wave front (a phase surface).

Piddington suggests that independent "twist cylinders" develop in the dawn and dusk longitudes and "grow" (at the Alfvén speed) towards the Earth along the geomagnetic field lines. The above analysis shows that a more reasonable suggestion is as follows: surfaces (S_{ph}) of particular phase (in disturbance) slough from S and shrink towards the Earth at the Alfvén speed along the geomagnetic field lines. This means that the Hall current suggested by equation (8) and likewise Piddington's J_r current find continuity on these surfaces (S_{ph}). This dispenses with the necessity of having a return current back along the surface of the twist cylinders suggested by Piddington. It also nullifies his explanation of the preliminary reverse impulse *Ds*(*PR*) which he attributes to a polarization field (his E_p) due to partial inhibition of J_r. For, since J_r is continuous over an S_{ph}, this E_p no longer exists. A more likely explanation of *Ds*(*PR*) (which is inevitable on Piddington's theory) is that the sign of E_p' initially established in the ionosphere may be sometimes opposite to that of the finally established field. This would

depend on the distribution of ionization inside S at $t = 0$. This would explain also its generally small size.

(*b*) *Electrostatic field in the ionosphere*

From $t = 0$ onwards current will flow in the ionosphere due to E_p'. The steady state will be reached only after a time equal to the transit time of a hydromagnetic wave from S to I. However, since the instant $t = 0$ is indefinite to the extent of the time it takes the "solar wind" to traverse the system, there can be little point here in distinguishing these events except in so far as it bears on the theory of *Ds*(*PR*). It is the opinion of the writer that the propagation of phase discussed in Section III(a) above is substantially irrelevant to enlightenment on the direct cause of the main features of that *Ds* current system which results from the model considered here. This will now be discussed.

In the steady state the geomagnetic field lines from S to I will be virtually electrostatic equipotential lines. Current will flow orthogonal to the magnetic field lines but in greatest concentration in the lower ionosphere (cf. Baker & Martyn 1953). Thus current generated at S will flow down the geomagnetic field lines in the dawn hemisphere (under the influence of a very small electrostatic field), across the ionosphere principally in polar regions then up the geomagnetic field lines in the dusk hemisphere. There may also be some ionosphere current at lower latitudes with continuity either in the same or opposite hemispheres.

In order to determine approximately the morphology of the electrostatic field established in the ionosphere we first assume that the space inside S is an insulator. This enables the charge distribution on S to be readily determined in a steady state. Allowance is then made for the fact that the space inside S is a good conductor. Thus the charge distribution that would have formed on S diffuses along the geomagnetic field lines under the influence of an external electrostatic field. The sources and sinks of electrostatic field in the ionosphere may then be found approximately.

The current flowing in the solar wind is

$$\mathbf{j} = \sigma_0 \mathbf{E}_\parallel + \sigma_1 \mathbf{E}_\perp + \sigma_2 \frac{\mathbf{H} \wedge \mathbf{E}_\perp}{H}, \tag{9}$$

where $\mathbf{E} = \mathbf{E}_p + \mathbf{w} \wedge \mathbf{H}$ and $\mathbf{E}_p$ is the polarization field in the wind. In the steady state ($\partial/\partial t = 0$) no current would flow at the surface S in the direction of the unit normal ($\mathbf{n}$) to S and $\mathbf{E}_p$ would be entirely normal to S, viz. $\mathbf{j} \cdot \mathbf{n} = 0$. Thus on the assumption that S is an insulator we find using equation (9) that at S

$$E_p = \frac{-\sigma_2 \mathbf{H} \wedge \mathbf{w} \wedge \mathbf{H} \cdot \mathbf{n}/H + \sigma_1 \mathbf{w} \wedge \mathbf{H} \cdot \mathbf{n}}{\sigma_0 (\mathbf{H} \cdot \mathbf{n})^2/H^2 + \sigma_1 (1 - (\mathbf{H} \cdot \mathbf{n})^2/H^2)}. \tag{10}$$

Since $\sigma_0 \gg \sigma_1$ here, we can discuss equations (10) for two kinds of regions:

(i) $\mathbf{H} \cdot \mathbf{n} \approx 0$,

$$E_p = \frac{-\sigma_2 \mathbf{H} \wedge \mathbf{w} \wedge \mathbf{H} \cdot \mathbf{n}/H + \sigma_1 \mathbf{w} \wedge \mathbf{H} \cdot \mathbf{n}}{\sigma_1}, \tag{11}$$

(ii) $\mathbf{H} \cdot \mathbf{n} \neq 0$,

$$E_p = \frac{-\sigma_2 \mathbf{H} \wedge \mathbf{w} \wedge \mathbf{H} \cdot \mathbf{n}/H + \sigma_1 \mathbf{w} \wedge \mathbf{H} \cdot \mathbf{n}}{\sigma_0 (\mathbf{H} \cdot \mathbf{n})^2/H^2}. \tag{12}$$

It follows from equations (11) and (12) that since $\sigma_0 \gg \sigma_1$ the most dense accumulation of space-charge on S occurs around points such that $\mathbf{H} \cdot \mathbf{n} = 0$, i.e. where a line of force is tangential to S. With the shape for S suggested above we should find two lines along which $\mathbf{H} \cdot \mathbf{n} = 0$: One line in the dawn hemisphere would possess positive charge, and the other line in the dusk hemisphere would carry negative charge.

Now the space inside S is not an insulator but consists of a system of highly conducting electrodes (the geomagnetic field lines). As a first approximation one would expect the electrostatic field created in the ionosphere (in the steady state) to be that obtained by projecting the charge distribution on S along the magnetic field lines to the ionosphere. Hence there will be a source of positive charge at a line in the dawn ionosphere such that the geomagnetic field lines through it are tangential to S. Likewise there will be a sink of charge in the dusk ionosphere. Thus instead of just two relatively small areas in each polar ionosphere for the precipitation of opposite space charge (Piddington 1960) there would be two areas elongated in longitude and thin in latitude extent.

(*c*) *Current flow in a uniform, horizontally stratified ionosphere.*

The electrostatic field patterns in the polar ionosphere may be obtained approximately by regarding this region as plane with an homogeneous orthogonal (vertical) magnetic field. The electrostatic field lines will be coplanar with the ionosphere. In the quiet ionosphere the ratio (η) of the height integrated Hall and Pedersen conductivities, viz. $\int \sigma_2 \, dh$: $\int \sigma_1 \, dh$ is about 2 (c.f. Piddington 1960). Thus by equation (2) the current direction makes an angle of $\tan^{-1}\eta$ with the electric field direction.

Piddington suggests that the current from a radial electric field would flow in closed loops (c.f. the paragraph containing his equation 2). Rather the current flow due to a radial electric field would be along centred equiangular spirals $r = a \exp(\theta/\eta)$. Now from the known structure of the ionosphere Hall current predominates over Pedersen current around 100 km height but Pedersen current predominates above about 130 km (cf. Baker & Martyn 1953). To express the magnetic effects at the ground in terms of an equivalent current system (at a specified height) we must weight the Pedersen current by a factor on account of its greater height. For the quiet ionosphere assumed by Piddington an underestimate of the factor would be $\frac{1}{2}$. Hence the equation of the spirals of the consequent equivalent current system would be $r = a \exp(\theta/4)$. Such spirals increase their radius vectors by a factor of $\exp(2\pi/4)$, i.e. ≈ 4 in one turn. Such curves are vastly different from the closed loops Piddington attempts to explain. Additional assumptions about the structure of the ionosphere would have to be made to make the spirals approximate loops, for instance, that the ratio of total ionization below 150 km to that in the *F* region is very large. An idea of a lower limit to the ratio η in the equivalent current system can be got as follows. There are approximately 30 stations spread over an area of 3 000 km by 3 000 km to determine the structure of the *Ds* current loops. This gives an average of about 500 km between stations. One would therefore expect a resolution of 500/3 000 = 0·17 in determining the dimensions of loops. So that to approximate loops spirals would be allowable with an opening factor of 1·17. Thus a lower limit of $\eta = 2\pi/\ln 1{\cdot}17 \approx 40$ is established. This is an order of magnitude greater than in the quiet ionosphere assumed by Piddington.

It has been observed above (Section 3(b)) that the source and sink of charge in the ionosphere will be elongated in longitude and thin in latitude extent. However, their precise elongation depends not only on the shape of S but also on the distribution of $\mathbf{v}$. There appears little hope at present of finding either of these two things. Hence to a first approximation the source and sink of charge are considered as points on the dawn and dusk longitudes respectively.

Considering the polar regions to be flat with a vertical magnetic field we may approximate the electrostatic field by that of a dipole $\eta \approx \frac{1}{2}$ for the equivalent current system in a quiet ionosphere (assumed by Piddington). Figure 3 shows the two systems of interlocking spirals of current that result from a dipole electric field. These are vastly different from the closed loops that Piddington wished to explain.

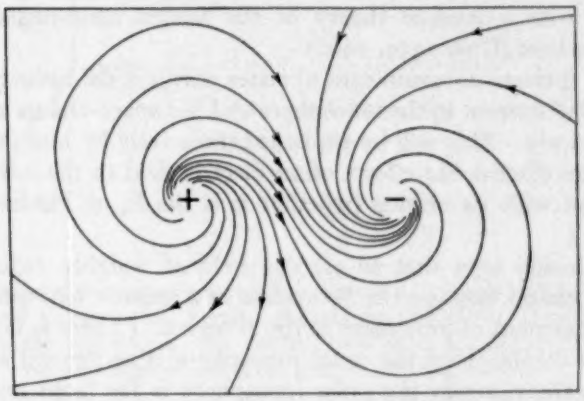

FIG. 3. Flow lines of current system that would be produced by a dipole electric field caused by a solar wind. (Magnetic field into plane of paper.)

It may be that in fact the *Ds* current system is an interlocking pair of systems of spirals (cf. Figure 3) and that the present network of observing stations is not good enough to resolve them. It may be of significance that spiral forms of the aurora do occur. The above theory suggests that such spiral auroras should open clockwise in the southern hemisphere (as seen from the ground) and anti-clockwise in the northern. This should be checked against observations.

4. Comparison of solar wind generation theory and dynamo theory of aurora and magnetic disturbance

On the basis of observations then available Cole (1959, 1960) suggested that auroras constitute luminous segments of lines of the *Ds* current system (cf. Figure 1). Observations reported since (Davis 1960; Denholm & Bond 1960) support this view. In the following discussion no distinction in plan position will be made between aurora and disturbance current; they will be treated as aspects of the one phenomenon. A simple model of the pattern of auroral orientation and movement that is not inconsistent with the reported observations is as follows: closed loops of the *Ds* system contract about a morning "cell" and expand about an evening "cell". (Since the observations of Davis & Kimball 1960, were taken from near the latitude of the centres of the cells they may be explained by fluctuations in latitude

of the cells' centres.) This approach gives primacy in physical importance to the current system. Luminosity (in the form of auroras) may be brought about in at least two ways. Firstly, a small variation in the *Ds* current (brought about by a change in conductivity or electric fields in the ionosphere) may cause a hydromagnetic wave to propagate upwards into the region of geomagnetically trapped radiation and scatter protons downward (cf. Welch & Whittaker 1960) thus producing luminosity and further magnetic variation and so on till there is depletion of "available" trapped radiation. Secondly, the *Ds* system may act simply as a large magnetic anomaly comparable in size to the South Atlantic anomaly, causing the lowering of mirror points of trapped charged particles into the atmosphere with similar consequences. On this physical basis the auroral isochasms and the diurnal variation of auroras may be explained (cf. Cole & Jacka 1961).

It is of interest to compare the above electrostatic field theory and Piddington's (1960) theory with a dynamo theory of the aurora and magnetic disturbance developed elsewhere (Cole 1959, 1960).

Piddington (private communication) states that it is the induction field (his $\mathbf{E}_i$) which drives Hall current in the ionosphere and not space-charge accumulations as he stated previously. This will be explained more fully by him in a sequel paper. However we can discuss the effects of an electric field in the ionosphere without being concerned with its origins (whether it is the $\mathbf{E}_i$ of Piddington or the $\mathbf{E}_p'$ deduced above).

We have already seen that an electric field of roughly radial configuration cannot explain closed loops of the *Ds* system in a *uniform* ionosphere unless there is a great enhancement of ionization in the *E* region. (There is no conclusive evidence that this condition of the polar ionosphere is as general as magnetic disturbance.) On the contrary the polar ionosphere is far from uniform as postulated in Section 3(c) above and by Piddington. The evidence is strong that some auroras contain abnormally high current density compared to their surroundings (cf. Heppner 1954). Auroras frequently appear as striations on ionograms. Radar observations of some auroras is common. Rocket investigations of the polar ionosphere show large gradients of electron density in the vicinity of auroras. These things support the assertion that the *Ds* aurora system has considerable filamentary structure in the form of numerous concentric and successively larger loops of high line density of ionization (cf. the lines of Figure 1) superimposed on a background of diffuse ionization. The current created in such structures by electric fields is vastly different from that in a uniform ionosphere.

Let us consider then an auroral form (say a homogeneous arc) as an infinite plane slab of highly ionized air immersed in the ionosphere parallel to the (vertical) geomagnetic field. An electric field is applied perpendicular to $\mathbf{H}$ (Figure 4). It has been shown elsewhere (Cole 1960) that the component of velocity ($\mathbf{V}$) of the slab in the direction of the unit normal ($\mathbf{n}$) to the slab is given by

$$\mathbf{V} \cdot \mathbf{n} \approx E^0 \sin \alpha / (1 + \nu_e \nu_i / \omega_e \omega_i), \tag{13}$$

where $\omega_{e,i}$ are the gyro-frequencies of electrons, ions and $\nu_{e,i}$ their collision frequencies with neutral particles. The current (j_p') flowing along the model aurora is given by equation 8(b) of Cole (1960). In the steady state and when the electron density in the aurora is very much greater than that outside it this equation yields

$$j_p' \approx -\sigma_3 E^0 \sin \alpha \tag{14}$$

in the direction of $\mathbf{n} \wedge \mathbf{H}$, where $\sigma_3 = \sigma_1 + \sigma_2^2/\sigma_1$.

Figure 5 shows plots of the factors $1/(1+\nu_e\nu_i/\omega_e\omega_i)$ and σ_3 as a function of ω_e/ν_e and height assuming with Baker & Martyn (1953) that $(\omega_e/\nu_e)(\omega_i/\nu_i) = 1\,650$. Equation (14) demonstrates that an aurora moves normal to itself (i.e. laterally)

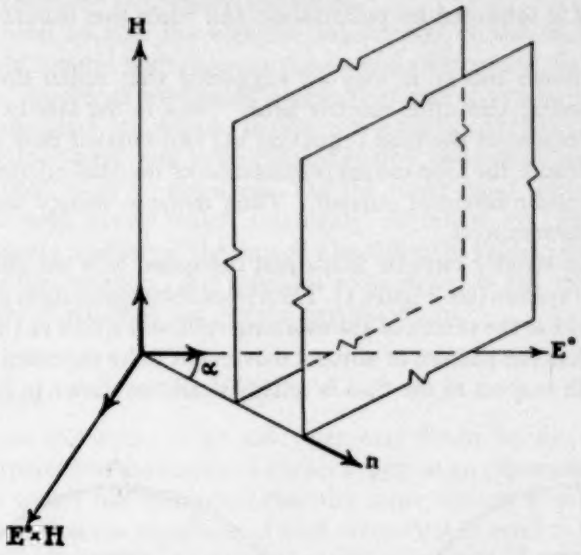

FIG. 4. Schematic representation of an aurora as a plane slab of highly ionized gas (between the parallel planes) parallel to the geomagnetic field **H** in the ionosphere. An electric field $\mathbf{E}^0$ is applied in direction making angle α with unit normal **n** to the aurora.

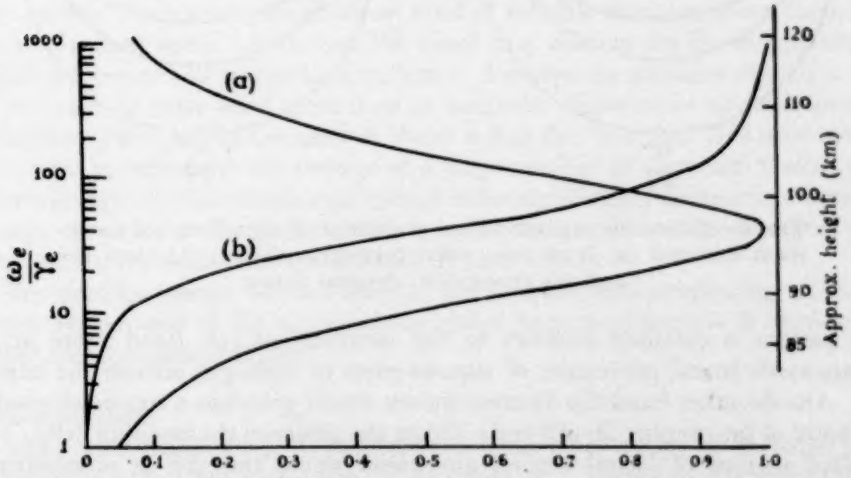

FIG. 5. Approximate plot of (a) $\sigma_3/\sigma_{3\max}$ in an auroral model with constant electron density at all heights; (b) the factor $1/(1+\nu_e\nu_i/\omega_e\omega_i)$ as functions of ω_e/ν_e assuming with Baker and Martyn (1953) that $(\omega_e/\nu_e)(\omega_i/\nu_i) = 1\,650$.

provided the electric field has a component (horizontally) *along* the aurora, whilst equation (15) shows that current flows horizontally along the aurora providing there is a component of electric field in that direction.

Let us represent one of the *Ds* loops as the circumference of a circle with high line density of ionization. If a radial electric field is applied (as in the case of supposed solar wind generation) then in the steady state there will be neither current along nor movement of the loop (by equations 13, 14 above). This occurs because the Pedersen current is inhibited by polarization and when this occurs all current flow ceases.

According to dynamo theory it may be suggested that radial flow of wind would occur thus causing azimuthal electric field. Thus in the steady state there would be radial movement of the loop (equation 13) and current flow around the loop. This occurs because the loop causes polarization of the Hall current which in turn builds up the circumferential current. Thus dynamo theory seems better able to explain the observations.

Let us modify the strictly circular loops just discussed into the (filamentary) loops of a *Ds* (aurora) system (see Figure 1). Then from solar generation one expects a source of electric field at the centre of the morning cells and a sink at the centre of the evening cells. Thus the pattern of auroral movement to be expected in a frame of reference fixed with respect to the Sun is schematically as shown in Figure 6(a).

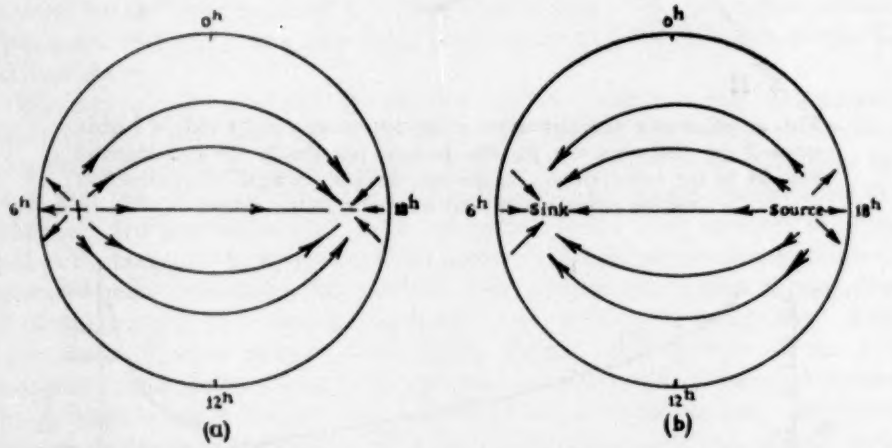

FIG. 6.—Schematic representation of pattern of lateral auroral movement expected (a) from solar wind generation theory; (b) from the author's atmospheric dynamo theory.

This pattern is certainly contrary to the observations (cf. Bond 1960) of the equatorwards lateral movement of auroras prior to midnight outside the auroral zone. On the other hand the dynamo theory would postulate a source of wind at the centre of the evening *Ds* cell and a sink at the centre of the morning cells. The expected pattern of lateral auroral movement would then be as schematically presented in Figure 6(b) (in a frame of reference fixed with respect to the Sun). Observations available so far do not contradict this scheme.

A difficulty with an ionospheric electric field of the type involved in Section 3(b) above is that of explaining the uniformity of auroral movement at all heights. For by equations (13) and (14), since $\mathbf{E}^0$ would be practically constant at all heights, both $\mathbf{V} \cdot \mathbf{n}$ and j_p' would vary considerably with height (cf. Figure 4). This difficulty is avoided in dynamo theory (Cole 1960) for there the operative electric field and movement is determined by a limited height range.

Dynamo theory is not without its difficulties. Piddington (1960) has enumerated some of these. Basic difficulties are explanation of the mechanism of establishment of the necessary upper atmosphere wind system and its rotation with the Sun, and of the necessary patterns of ionization.

It may well be that the ultimate explanation of the morphology of *Ds* and auroras could involve both dynamo theory and electrostatic field theory. Certainly both appear capable of explaining magnetic effects of similar orders of magnitude. Winds of adequate magnitude in the atmospheric dynamo region are certainly observed (Elford 1959) and some electrodynamic consequences of the type analysed by Cole (1960) must be expected. On the other hand there are features of the electrostatic field theory which are highly attractive, viz. its explanation of dependence on the position of the Sun and its ability to explain discontinuous changes in magnetic disturbance. But it has its roots in an, as yet, unobserved solar wind the existence of which is not proved beyond doubt.

5. Discussion

Elsewhere the writer (Cole 1961) has cast doubt on the existence of a "solar wind" interpreted in the theory of Parker (1957) as an expansion of the solar corona. Rather the writer has suggested that the inner corona is a hydromagnetic wave generator and that the expulsion of such waves would tend to inhibit its expansion. However, the above theory of "solar wind" generation of geomagnetic disturbance is not at variance with the concept of hydromagnetic wave emission by the Sun. For, assuming an Alfvén speed of about 10^8 cm/s in interplanetary space, waves of periods $\gtrsim 100$ s would have wavelengths $\gtrsim 10$ Earth diameter. All periods of waves up to a day or more may be represented in the emission spectrum of the inner corona. Such waves would cause wind of variable direction about the Earth in interplanetary space. Such variable winds may account for the complexity of auroral movement and magnetic disturbance. Perhaps the strongest objection that can be made to solar wind generation of magnetic disturbance as developed by Piddington (1960) and in the analysis above is that the "average" *Ds* system which it attempts to explain is the average of a large number of elemental disturbance systems (Nagata & Fukushima 1952) which differ significantly in structure from the average. A physical theory must explain both the element and its average. This seems within the bounds of atmospheric dynamo theory.

The need for precise determination of the instantaneous morphology of the *Ds* current system and of the simultaneous global pattern of auroras is vital to the further development of theory.

Acknowledgments

The author thanks Dr J. H. Piddington for the use of a copy of his paper prior to publication and for discussion of its contents. However, Dr Piddington's agreement with the above analysis is not necessarily to be inferred. Thanks for helpful suggestions with the presentation are extended to Dr F. Jacka, Chief Physicist of this Division.

Antarctic Division,
Department of External Affairs,
Melbourne:
1961 *March.*

References

Baker, W. G. & Martyn, D. F., 1953. *Phil. Trans. Roy. Soc. A*, **246**, 281.
Bond, F. R., 1960. *Aust. J. Phys.* **3**, 477.
Cole, K. D., 1959. Proceedings of Antarctic Symposium, Buenos Aires.
Cole, K. D., 1960. *Aust. J. Phys.*, **3**, 484.
Cole, K. D. & Jacka, F., 1961. *J. Geophys. Res.*, **66**, 1584.
Cole, K. D., 1961. *Nature*, **189**, 31.
Cowling, T. G., 1957. Magneto hydrodynamics (Interscience Publishers, Inc., New York).
Davis, T. N. & Kimball, D. S., 1960. Scientific Report No. 4, NSF Grant No. Y/22.6/327, University of Alaska.
Davis, T. N., 1960. *J. Geophys. Res.*, **65**, 3497.
Denholm, J. V. & Bond, F. R., 1961. *Aust. J. Phys.*, **14**, 193.
Elford, W. G., 1959. Proceedings of Antarctic Symposium, Buenos Aires.
Fukushima, N. & Oguti, T., 1953. *Rep. Ionosphere Res. Japan*, **7**, 137.
Heppner, J. P., 1954. Thesis, California Institute of Technology. D.R.B. Canada Rep. No. DR135.
Johnson, F. S., 1960. *J. Geophys. Res.*, **65**, 3049.
Nagata, T. & Fukushima, N., 1952. *Rep. Ionosphere Res. Japan*, **6**, 85.
Parker, E. N., 1958. *Ap. J.*, **128**, 664.
Piddington, J. H., 1960. *Geophys. J.*, **3**, 314.
Welch, J. A. & Whittaker, W. A., 1959. *J. Geophys. Res.* **64**, 909.

Small Corrections in the Theory of Surface Waves

Harold Jeffreys

(Received 1961 April 13)

Summary

Rayleigh's principle is used to derive expressions for the group velocities of Love and Rayleigh waves without numerical differentiation. It is also used to find expressions, accurate to the first order, for the effects of small changes of the elastic properties on the wave and group velocities.

1. Introduction

The standard method of determining group velocities of surface waves is to assume values of the wave-velocity c and of κ, where $2\pi/\kappa$ is the wavelength; solve the differential equations; and for each κ or c interpolate a value of the other so that the boundary conditions are satisfied. Then the group-velocity C is determined from

$$C = \frac{d}{d\kappa}(\kappa c) = \frac{d}{dc}(\kappa c)\Big/\frac{d\kappa}{dc}.$$

One disadvantage of this procedure is that for any new suggested structure the whole process must be carried out *ab initio*, becoming more complex with each additional complication suggested. Another disadvantage is that the differentiation to give C has to be carried out numerically. But the whole range of c is small, and the intervals used cannot be less than 0·1 of the range of c to give an adequate determination of the behaviour of C; in practice two figures are lost in the differentiation.

E. Meissner (1926; see also Jeffreys 1959, p. 110) gave a method for Love waves, based on Rayleigh's principle, that avoids numerical differentiation. This method could be adapted to Rayleigh waves, but this does not appear to have been done. Rayleigh's principle can also be used to estimate the effects of small changes of the distributions of density and elastic moduli. Since it is fairly easy to work out the solution for a model that can be regarded as a useful first approximation, it appears that such a method should permit rapid testing of any reasonable suggested structure.

2. Love waves

If the displacement is

$$u_1, u_2, u_3 = 0, v(z)\cos(\gamma t - \kappa x), 0 \qquad (1)$$

we have, apart from constant factors,

$$2T = \int \rho\gamma^2 v^2\, dz, \quad 2V = \int \mu(\kappa^2 v^2 + v'^2)\, dz, \tag{2}$$

and by equating T and V,

$$I_0\gamma^2 = I_1\kappa^2 + I_2 \tag{3}$$

where

$$I_0 = \int \rho v^2\, dz, \qquad I_1 = \int \mu v^2\, dz, \qquad I_2 = \int \mu v'^2\, dz. \tag{4}$$

Then Rayleigh's principle says that if we work out (4) using a slightly incorrect form of v, then for given κ (3) will give γ^2 with an error of the second order.

If we change κ_0 to $\kappa_0 + \delta\kappa$ but use for $\kappa = \kappa_0 + \delta\kappa$ the form of v calculated for κ_0, this has a first order error, but

$$I_0(\gamma_0 + \delta\gamma)^2 = I_1(\kappa_0 + \delta\kappa)^2 + I_2 + O(\delta\kappa)^2 \tag{5}$$

whence to the first order in $\delta\kappa$

$$I_0\gamma_0\delta\gamma = I_1\kappa_0\delta\kappa. \tag{6}$$

But since $\mu/\kappa = c$, $d\gamma/d\kappa = C$, this is

$$cC = I_1/I_0. \tag{7}$$

This is Meissner's result, which is exact. It replaces numerical differentiation by the integration of two known functions.

But in the same way, if we also vary ρ and μ, and retain the same values of v, we shall have

$$(I_0 + \delta I_0)(\gamma_0 + \delta\gamma)^2 = (I_1 + \delta I_1)(\kappa_0 + \delta\kappa)^2 + I_2 + \delta I_2 + O((\delta\rho)^2, (\delta\mu)^2, (\delta\kappa)^2) \tag{8}$$

where δI_0, δI_1, δI_2 are independent of κ. Hence if $\delta\kappa = 0$,

$$(I_0 + \delta I_0)(\gamma_0 + \delta\gamma)^2 = (I_1 + \delta I_1)\kappa_0^2 + I_2 + \delta I_2, \tag{9}$$

determining c with a second-order error for a fixed κ; and from (7)

$$(c_0 + \delta c)(C_0 + \delta C) = (I_1 + \delta I_1)/(I_0 + \delta I_1), \tag{10}$$

giving C also with an error of the second order.

A method of mine (Jeffreys 1928) used Rayleigh's principle to allow for increase of the velocity of S with depth in the lower layer, by means of (5); but C was then determined as usual by numerical differentiation.

3. Rayleigh waves

The displacement is

$$u_1, u_2, u_3 = u(z)\sin(\gamma t - \kappa x),\ 0,\ w(z)\cos(\gamma t - \kappa x). \tag{1}$$

We find

$$2T = \int \rho\gamma^2(u^2 + w^2)\, dz \tag{2}$$

$$2V = \int \{\lambda(w' - \kappa u)^2 + 2\mu(\kappa^2 u^2 + w'^2) + \mu(u' + \kappa w)^2\}\, dz \tag{3}$$

and

$$\gamma^2 I_0 = \kappa^2 I_1 + 2\kappa I_2 + I_3 \tag{4}$$

where

$$\left.\begin{aligned} I_0 &= \int \rho(u^2+w^2)\,dz \\ I_1 &= \int \{(\lambda+2\mu)u^2+\mu w^2\}\,dz \\ I_2 &= \int (-\lambda w'u+\mu u'w)\,dz \\ I_3 &= \int \{(\lambda+2\mu)w'^2+\mu u'^2\}\,dz. \end{aligned}\right\} \tag{5}$$

Varying κ as for Love waves we have

$$I_0 cC = I_1 + I_2/\kappa. \tag{6}$$

If we vary ρ, λ and μ, without varying κ or the trial solution, we have

$$(I_0+\delta I_0)(\gamma_0+\delta\gamma)^2 = (I_1+\delta I_1)\kappa^2 + 2(I_2+\delta I_2)\kappa + (I_3+\delta I_3) \tag{7}$$

to the first order, and hence

$$(I_0+\delta I_0)(c_0+\delta c)^2 = I_1+\delta I_1 + 2(I_2+\delta I_2)/\kappa + (I_3+\delta I_3)/\kappa^2. \tag{8}$$

4. Conclusions

The use of these results would be that it would be possible to examine the effects of small changes of ρ, λ, μ over non-overlapping intervals of z, and hence to use observed group-velocities to identify more closely the intervals where such changes are needed. They do for surface waves what Bullen's transformation (1960) does for bodily waves.

160 *Huntingdon Road*,
Cambridge,
1961 *April* 12.

References

Meissner, E., 1926. *Proc. 2nd Congr. Appl. Math.*, Zürich, pp. 3–11.
Jeffreys, H., 1928. *Mon. Not. R. Astr. Soc. Geophys. Suppl.* **2**, 101–111.
Jeffreys, H., 1959. *The Earth* (4th edition), (Cambridge: University Press).
Bullen, K. E., 1960. *Geophys. J.*, **3**, 258–269.

The Nature of the Mohorovičić Discontinuity

E. C. Bullard and D. T. Griggs

(Received 1961 August 4)

Summary

It has been suggested that the Mohorovičić discontinuity represents a change in crystal structure and not a change in chemical composition. Three objections to this view are discussed and it is concluded that it is unlikely to be correct. The objections are (1) that the stability relations are such that the continental and oceanic discontinuities cannot both have the heavier material below them; (2) that the small variation of the depth of the discontinuity with heat flow cannot be accounted for and (3) that the transition should not be sharp in a rock which is not composed of a single well defined chemical substance.

1. Introduction

It has often been supposed that the Mohorovičić discontinuity, or Moho, represents not the boundary between two different materials, but a change in crystal structure induced by increase of pressure with depth (Fermor 1914, 1938, Holmes 1927, Lovering 1958, Kennnedy 1959). This view is attractive since it suggests a mechanism that can cause widespread vertical movements. It is also plausible in that changes in crystal structure are observed in many silicates at about the pressures and temperatures occurring at the Moho. Unfortunately there are three serious objections, which it is the purpose of this paper to discuss.

The first objection concerns the comparison between the variation of temperature with depth in the Earth and the variation of the transition temperature with pressure. It is shown in Section 2 that the oceanic and continental transitions can not both result in the high pressure form lying beneath the Moho.

The second objection (Section 3) is that the variations of Moho depth from place to place are less than would be expected from the variations in heat flow.

The third objection (Section 4) is that a Moho produced by a phase change would be spread over a range of depth.

2. The pressure–temperature relations

The mean heat flow in the Atlantic and Pacific oceans away from the mid-ocean ridges has been estimated at $1{\cdot}08 \pm 0{\cdot}05$ μcal/cm^2 s (Bullard 1961). This may be a little low since unpublished measurements by Von Herzen show higher values over a considerable area off the coast of California. On land the mean usually quoted is $1{\cdot}2$ μcal/cm^2 s, this may also be a little low since several recent measurements have been above it. We will assume $1{\cdot}2$ μcal/cm^2 s as a mean for both oceans

and continents. Beneath a continent the pressure and temperature have been computed on the assumption that the depth of the Moho is 35 km and that the material above it has a thermal conductivity of 0·006 cal/cm s °C. Two extreme assumptions are considered, (1) that all the heat comes from below the Moho and (2) that it is all produced by heat sources uniformly distributed through the crust. The results are given in Table 1 which shows that the temperature at the Moho is likely to be between 350 and 700 °C. As a rough approximation we take 500 ± 150 °C, this is equivalent to assuming that 57 per cent of the heat is produced in the crust. The temperature, T, at any depth, D, in the crust is then given by

$$T = 20D - 0{\cdot}163D^2. \qquad (1)$$

Table 1

	Depth km	Thickness km	Density g/cm³	Thermal condy. cal/cm s °C	Pressure kg/cm²	Gradient °C/km	Temperature (1) °C	Temperature (2) °C
Continent	0				0	20	0	0
		35	2·8	0·006				
	35				9800	8·6	700	350
Ocean	0·0				0		—	
Water		5·0	1·0	—		—		
	5·0				500		0	
Sed.		0·5	2·1	0·0023		52		
	5·5				600		26	
Hard Rock		4·5	2·8	0·006		20		
	10·0				1860		116	

The relation between temperature and pressure, p (in kg/cm²), is

$$T = 0{\cdot}0714p - 2{\cdot}08 \times 10^{-6}p^2;$$

this gives the line *Continent* in Figure 1, C representing the Moho. Under the ocean, above the Moho and below the sediments,

$$T = 16{\cdot}8 + 0{\cdot}0714p;$$

this gives the line *Ocean* in Figure 1 where O represents the Moho.

If the continental and oceanic Mohos are caused by the same transition, the temperature–pressure relation for the transition must be represented by some line through C and O. A straight line is shown in Figure 1; this line cuts the continental pressure temperature relation so that the denser material is stable below the Moho as it should be; under the ocean, however, the denser material is the stable phase at the ocean floor and the transition to the less dense form occurs at O. Provided that the continental and oceanic heat flows are approximately equal, this result does not depend critically on the numerical constants used nor on the transition curve being a straight line. It is a consequence of the topology of Figure 1 and requires only that the continental and oceanic temperature curves intersect above the continental Moho. It can be shown that this will happen if the continental and oceanic heat flows are approximately equal and if more than 5 per cent of the continental heat flow is generated in the crust.

If the transition line were strongly curved, as in Figure 2, it would intersect the oceanic pressure–temperature line in two points. The denser form of the material

would then be stable below the Moho, but would change again to the lighter form at a greater depth, O'. There is no evidence for such an "anti-Moho" and it does not seem likely that it exists. The only escape from the conclusion that the continental and oceanic Mohos cannot represent the same change in crystal structure appears to be in the not very plausible assumption that the measured oceanic heat flows are greatly disturbed by the intrusion of lava at shallow depths.

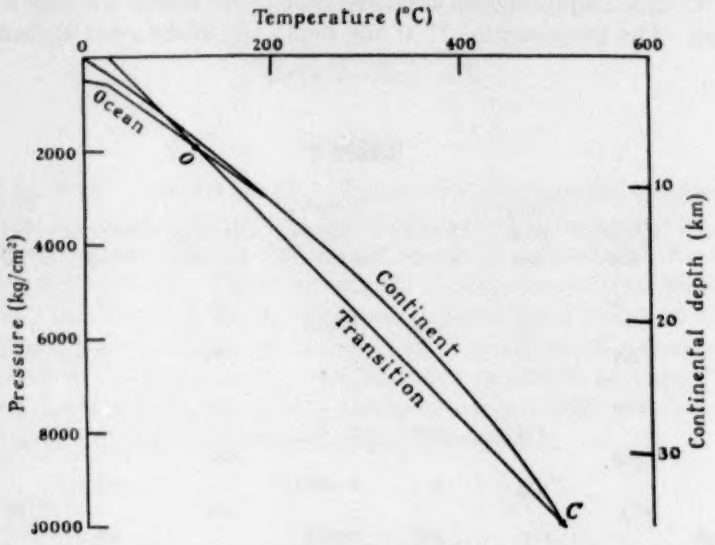

FIG. 1.—The pressure–temperature relations in the crust and the transition line.

3. The variation of Moho depth with heat flow

The observed heat flows in non-volcanic districts on the continents vary from about 0·6 to 3·0 μcal/cm^2 s; there are considerable areas where the mean heat flows are as low as 0·8 and as high as 2·4 μcal/cm^2 s. There appear to be no measurements of Moho depth in areas where the heat flow is known to be exceptionally high or low. It is very desirable that such measurements be made, but in their absence we assume that the usual spread of the observed values from 30 to 45 km has in fact covered some places of anomalous heat flow.

If it is assumed that the temperatures in a continental region with heat flow H can be obtained from those given in Figure 1 by multiplying by $H/1{\cdot}2$, the depth of the Moho can be found for any heat flow. For heat flows less than 1·05 μcal/cm^2 s the temperature–pressure curve does not intersect the transition line of Figure 1 and there is no solution. For larger heat flows the Moho depths are:

Heat flow	1·1	1·2	1·6	2·0	2·4	μcal/cm^2 s
Moho depth	25	35	58	(71)	(80)	km

For heat flows above 1·8 the solutions give temperatures decreasing with depth and are therefore presumably unacceptable. In an effort to widen the range of heat flows which can be accommodated, we drop the restriction that all temperature–depth curves in the crust must be similar and assume only that some part of the

heat is derived from radioactivity uniformly spread through the crust and that the rest comes from below the Moho. The variation of temperature with pressure is then

$$T = Bp - Cp^2.$$

The coefficient B is fixed by the surface heat flow, H_0, and the density, ρ, and thermal conductivity, k, of crustal rocks,

$$B = H_0/\rho k.$$

The coefficient C then determines how great a proportion of the heat comes from below the Moho, it must be positive and not so large that the temperature at the Moho decreases downwards.

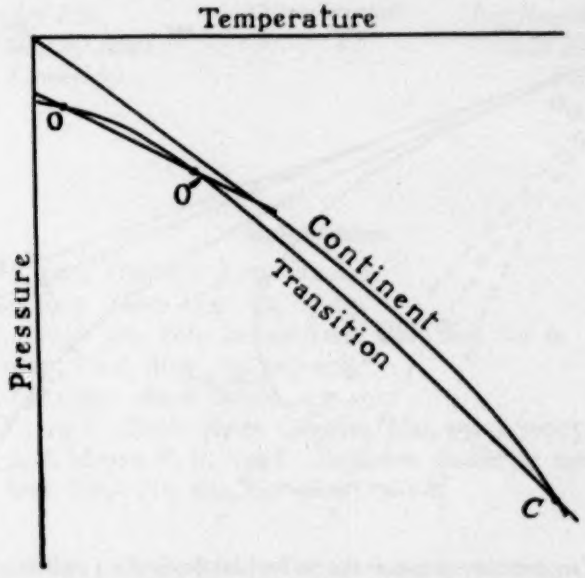

FIG. 2.—Continental and oceanic Mohos with strongly curved transition line.

Families of temperature pressure curves for $H_0 = 0{\cdot}8$ and $2{\cdot}4$ are given in Figure 3 assuming h to be $0{\cdot}006$ μcal/cm^{2}s° C and ρ to be $2{\cdot}8$ g/cm^3. The transition curve must go near the point O, whose position is not seriously in doubt and must be cut by one curve from each family in the pressure range appropriate to the continental Moho (8 400 to 12 600 kg/cm^2 for depths between 30 and 45 km). The curves must have a positive slope at the points of intersection. From Figure 3 it is seen that no such line exists even if moderate departures from straightness are permitted.

The only way to avoid this difficulty appears to be to assume that in areas of high heat flow the sources of heat are at shallow depths in the crust and that in areas of low heat flow most of the heat comes from below the crust. These assumptions would be quite arbitrary and do not seem particularly plausible when applied to such areas as Tasmania or Hungary where there are high heat flows and no signs of recent vulcanism. Measurements of Moho depths in these places are particularly desirable.

4. The sharpness of the transition

The phase rule shows that if a pure substance exists in two crystal forms, the two forms can be in equilibrium along a line in the pressure temperature diagram as in Figure 1. That is, at a fixed temperature the transition takes place at a definite pressure. If the substance is capable of a continuous range of composition, as, for example, is the isomorphous series forsterite-fayalite, the two forms can be in equilibrium over an area in the pressure–temperature diagram. There is then no definite transition pressure, even if the temperature is held constant. The situation is analogous to the melting of water. Pure water at atmospheric pressure freezes sharply at 0 °C, but if a salt solution is cooled, ice forms and remains in equilibrium with the brine over a range of temperature.

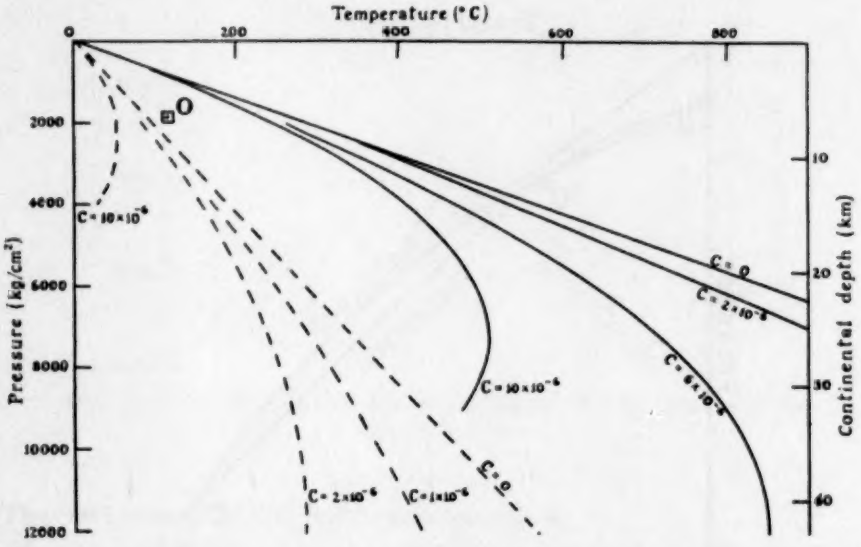

FIG. 3.—Temperature–pressure curves for heat flows of 2·4 (full lines) and 0·8 μcal/cm² s (dashed lines). *O* is the point representing the oceanic Moho from Figure 1.

Since silicate minerals are nearly all members of isomorphous series, and are not compounds with a fixed composition, their structural transitions as the pressure is raised should not occur sharply, but should be spread over a range of pressure. Thus if the Moho represents a change in crystal structure it would not occur at a definite depth, but would be spread over a range, probably of many kilometres. Several workers claim to have observed reflections of seismic waves from the Moho (Steinhort & Meyer 1961), if these are genuine the interface cannot be spread over more than 2 or 3 kilometres. A more critical examination of these reflections is very desirable both on land and at sea. If they are genuine it is difficult to believe that the Moho represents a phase change.

5. Conclusions

The state of the material at inaccessible depths within the Earth is necessarily subject to great uncertainty, and a wide range of assumptions can be made without

contradicting any observation. It does seem, however, that the most natural interpretation of the Moho as a phase change is untenable and that it is more likely that it represents a change in chemical composition. It is possible that some unexpected complication may vitiate the arguments of this paper, for example it might be that the material beneath the continental Moho is different from that beneath the oceanic Moho. Such doubts cannot be profitably discussed till we have more information, which should be provided in the foreseeable future by the drilling of oceanic Moholes.

Just as this paper was being sent to press we received an MS of a paper by Dr G. Wetherill which is to be published in the *J. Geophys. Res.* and which contains many of the same ideas.

Dept. of Geodesy & Geophysics,
Madingley Rise,
Madingley Road,
Cambridge:
1961 *July*

Institute of Geophysics,
Los Angeles Laborataries,
Los Angeles,
Cal., U.S.A.

References

Bullard, E. C., 1961. *Geophys. J.*, **4**, 282–292.
Fermor, L. L., 1914. *Geol. Mag.*, **51**, 65–67.
Fermor, L. L., 1938. Sp. Pub. Indian Assn. Cult. Sci. No. 6.
Holmes, A., 1927. *Geol. Mag.*, **64**, 263–278.
Kennedy, G. C., 1959. *Amer. Scient.*, **47**, 491.
Lovering, J. F., 1958. *Trans. Amer. Geophys. Un.*, **39**, 947–955.
Steinhort, J. S. & Meyer, R. P., 1961. *Explosion studies of continental structure*, Carnegie Inst. Publ. No. 622, pp. 58–68.

Deformation of the Japanese Islands as inferred from Rock Magnetism

N. Kawai,* H. Ito† and S. Kume*‡

(Received 1960 December 21)

Summary

Results are presented of the directions of magnetization for twenty-eight sets of rocks collected from different parts of Japan. The directions for rocks of Pre-Tertiary age from south-west Japan differ systematically from those from north-east Japan. It is suggested that the difference is due to the deformation of the Japanese Islands in the late Mesozoic or early Tertiary. Because of the deformation, it is not possible to infer the accurate position of the geomagnetic dipole with respect to Japan for Pre-Tertiary times.

1. Introduction

Oriented rock samples have been collected over a wide area of the Japanese Islands of Hokkaido, Honshu, Shikoku and Kyushu. The collecting sites are

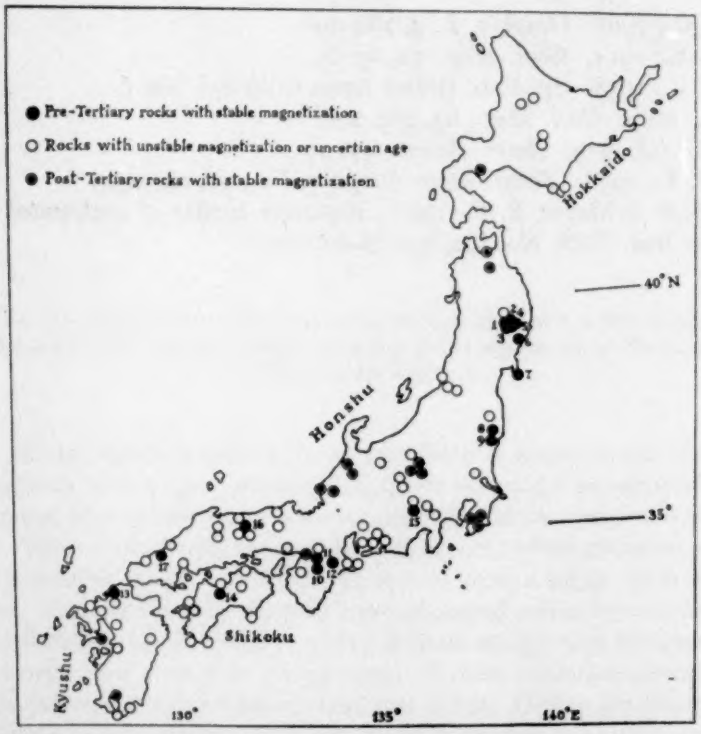

FIG. 1.—The location of sites where rocks were collected. The numbered sites are for rocks of Pre-Tertiary age and the numbers correspond to those given in Table 1 and Figures 2 and 3.

* Geological and Mineralogical Institute, Kyoto University, Japan.
† Institute of Earth Science, Kyoto University, Japan.
‡ Physics Dept., King's College, University of Durham, England.

Table 1

N.R.M. of Pre-Tertiary rocks

	Locality	Rock type	Geological period	D	I	S	α	K	J_r	J_i
			From north-east parts of Japan							
1.	Miyamori (Iwate)	Serpentine	Mesozoic	N 4 W	+51	7	9·3	43·4	87·30	24·70
2.	Tono (Iwate)	Gabbro	Mesozoic	N 106 W	+58	9	6·9	57·3	50·30	79·30
3.	Tono (Iwate)	Serpentine	Mesozoic	N 28 W	+57	5	16·8	21·7	220·00	35·90
4.	Hitokabe (Iwate)	Granite	Mesozoic	N 32 W	+74	10	16·2	9·9	3·14	1·86
5.	Yamaya (Iwate)	Granite	Mesozoic	N 28 W	+53	12	7·7	33·1	11·20	9·89
6.	Takata (Iwate)	Grano-diorite	Mesozoic	N 1 W	+56	12	9·1	23·5	12·60	13·72
7.	Kinkazan (Miyagi)	Granite	Mesozoic	N 57 E	+53	10	9·0	29·6	8·49	11·40
8.	Tono (Fukushima)	Gabbro	Mesozoic	N 53 W	+38	10	10·2	23·3	1·75	0·17
9.	Nakoso (Fukushima)	Gabbro	Mesozoic	N 53 W	+51	12	6·5	45·0	50·30	14·60
			From south-west parts of Japan							
10.	Kohse (Nara)	Serpentine	Late Palaeozoic or Early Mesozoic	N 74 E	+35	7	3·7	265·5	—	—
11.	Sakurai (Nara)	Gabbro	Late Palaeozoic or Early Mesozoic	N 52 E	+43	7	11·7	27·6	5·97	0·44
12.	Taki (Mie)	Gabbro	Late Palaeozoic or Early Mesozoic	N 9 E	+56	5	4·4	306·7	4·21	2·61
13.	Sasakuri (Fukuoka)	Serpentine	Mesozoic	N 29 E	+55	9	17·4	13·0	13·70	6·38
14.	Niihama (Ehime)	Serpentine	Late Palaeozoic or Early Mesozoic	N 13 E	+40	10	18·3	7·9	94·30	66·20
16.	Ishigoshi (Okayama)	Granite	Mesozoic	N 6 W	+42	10	7·1	47·8	3·45	4·50
17.	Nijo (Shimane)	Grano-diorite	Mesozoic	N 34 E	+38	15	14·5	7·9	4·61	10·41

D = Declination. I = Inclination (deg). S = Number of rock samples. α = Radius of 95 per cent circle of confidence (deg) (Fisher 1953). K = Fisher's precision factor. J_r = intensity of remanent magnetization, J_i = intensity of induced magnetization(10^{-3} emu/g).

shown in Figure 1. The rocks range in age from late Palaeozoic to Quaternary and include a variety of rock types.

2. Directions of natural remanent magnetization

Laboratory measurements of natural remanent magnetization (n.r.m.) are summarized in Tables 1 and 2. The method of measurement and accuracy to be expected for individual measurements have been given by Kawai (1951). For the interpretation given later, it is convenient to group the results from north-east and south-west Japan separately. The directions of n.r.m. for different sites are shown on Schmidt's equal area projections in Figures 2 to 5. Figures 2 and 3 show the directions for Pre-Tertiary rocks from north-east and south-west Japan respectively and Figures 4 and 5 those for Tertiary and Quaternary rocks from north-east and south-west Japan.

Table 2

N.R.M. of Tertiary and Quaternary Rocks

	Locality	Rock type	D	I	S	α	K
		From north-east parts of Japan					
18.	Asama (Nagano)	Andesite	N 5°E	+37°	17	8·1°	20·6
19.	Asama (Nagano)	Andesite	N 10E	+49	24	4·9	37·3
20.	Showashinzan (Hokkaido)	Basalt	N 10E	+57	4	8·5	117·6
21.	Arafune (Nagano)	Porphyrite	N 24E	+49	8	3·9	205·9
22.	Towada (Aomori)	Andesite	N 0	+56	18	4·8	—
		From south-west parts of Japan					
23.	Tomuro (Ishikawa)	Basalt	N 1E	+48	22	9·2	12·3
24.	Tomoru (Ishikawa)	Andesite	N 7W	+50	12	7·2	37·8
25.	Shigisan (Nara)	Andesite	N 4W	+59	20	3·5	84·3
26.	Sakurajima (Kagoshima)	Andesite	N 7E	+45	49	5·5	14·8
27.	Tojimbo (Fukui)	Andesite	N 18E	+54	44	15·9	19·5
28.	Sugiyama (Fukui)	Andesite	N 39E	+49	10	6·4	57·5
29.	Ibaragi (Osaka)	Tuff	3 6W	−51	15	5·4	58·6
30.	Genbudo (Hyogo)	Basalt	S 13W	−35	10	6·1	63·8

D = Mean declination of n.r.m.
I = Mean inclination of n.r.m. (deg).
S = Number of rock samples.
α = Radius of 95 per cent circle of confidence (deg) (Fisher 1953).
K = Fisher's precision factor.

Consideration of all the data for rocks likely to possess a stable magnetization and whose ages are known reveals three interesting facts. First, all rocks of Tertiary

and Quaternary age have directions of magnetization nearly parallel or anti-parallel to the present dipole field. These are shown in Figures 6c and 6d where all the results are plotted as normal directions. Secondly, the mean directions of magnetization of Pre-Tertiary (Mesozoic and late Palaeozoic) rocks from the north-eastern part of Japan are found to be north-westerly (Figure 6a) and thirdly, the mean direction for rocks of late Palaeozoic and early Mesozoic age from the south-west part of Japan are found to be north-easterly (Figure 6b). The mean directions of magnetization are summarized in Figure 6e. It is seen that whilst the mean directions of magnetization of rocks of Tertiary and Quaternary ages from both north-east and south-west Japan are close to the axis of the present dipole field, those of pre-Tertiary age from north-east Japan differ in declination from those in south-west Japan by about 40°.

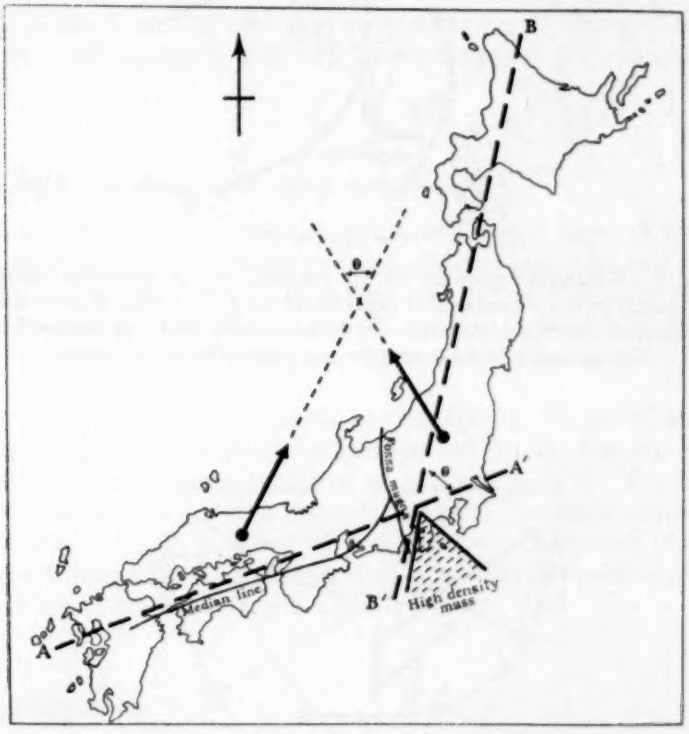

FIG. 7.—Map of the Japanese Islands. AA′ and BB′ are the axes of the south-west and north-east parts of Japan and the arrows represent the mean directions of n.r.m. of Pre-Tertiary rocks sampled from these two regions.

3. Interpretation of results

It is suggested that the difference in declination of 40° for the n.r.m. of rocks collected from south-west and north-east Japan is due to the deformation of the Japanese Islands. Figure 7 shows the position of a zone of plastic deformation known in Japan as the "fossa magna". There are striking differences in geological structure on either side of the "fossa magna" and earthquakes and volcanism are associated with this zone.

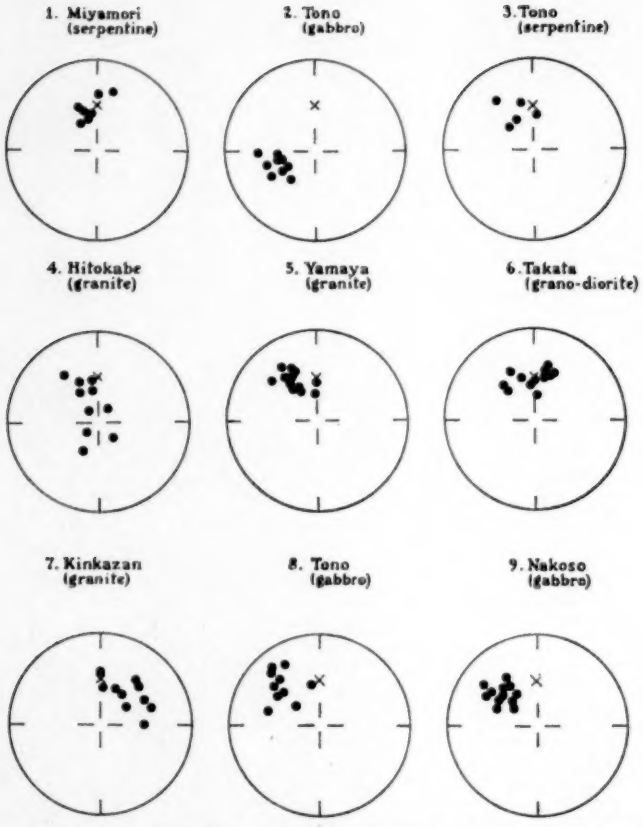

FIG. 2.—Directions of n.r.m. of Pre-Tertiary (Mesozoic) rocks collected from the north-eastern part of Japan. Schmidt equal-area projections are used throughout and points are plotted on the lower hemisphere.

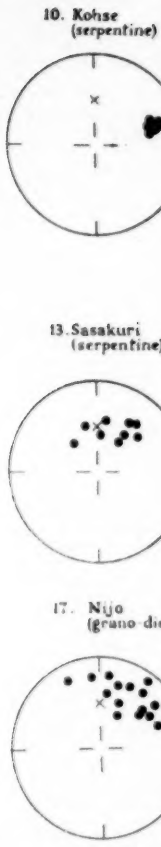

FIG. 3.—Directions
Mesozoic) rocks

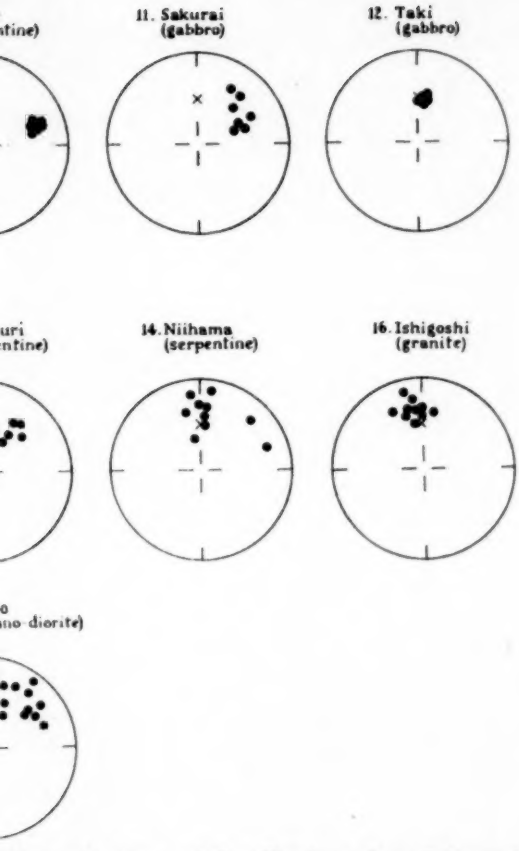

tions of n.r.m. of Pre-Tertiary (late Palaeozoic and
ocks collected from the south-western part of Japan.

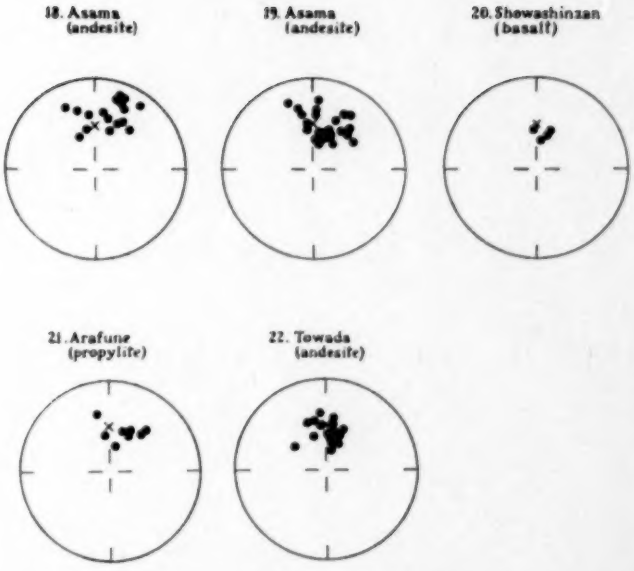

FIG. 4.—Directions of n.r.m. of Tertiary and Quaternary rocks colle
from the north-eastern part of Japan.

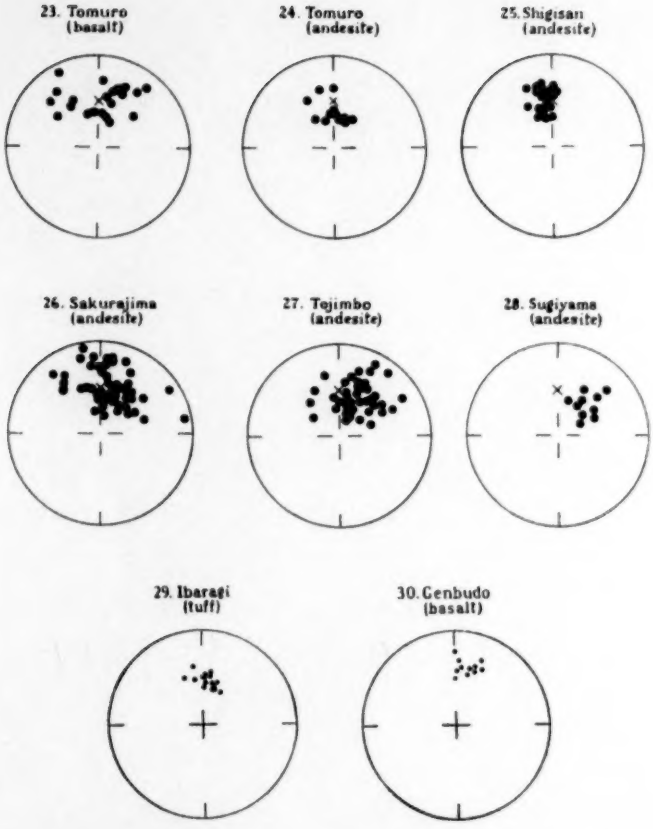

FIG. 5.—Directions of n.r.m. of Tertiary and Quaternary rocks collected from the south-western part of Japan.

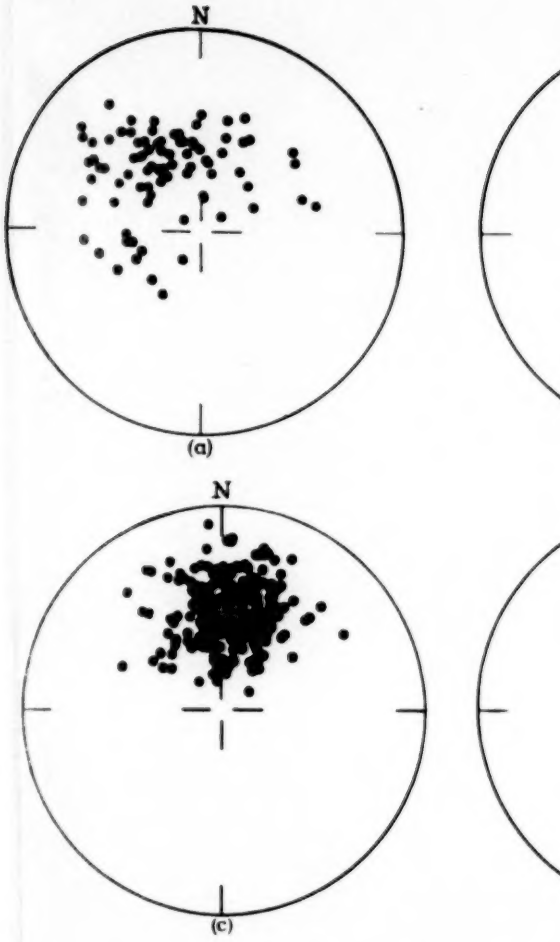

FIG. 6.—Directions of r
east and south-west pa
Tertiary and Quaterna
(c and d) and mean dire

- ● Mean direction of th part of Japan.
- ○ Mean direction of western part of Jap
- ⊙ Mean direction of from north-eastern
- ◎ Mean direction of from south-western
- × Direction of the pr

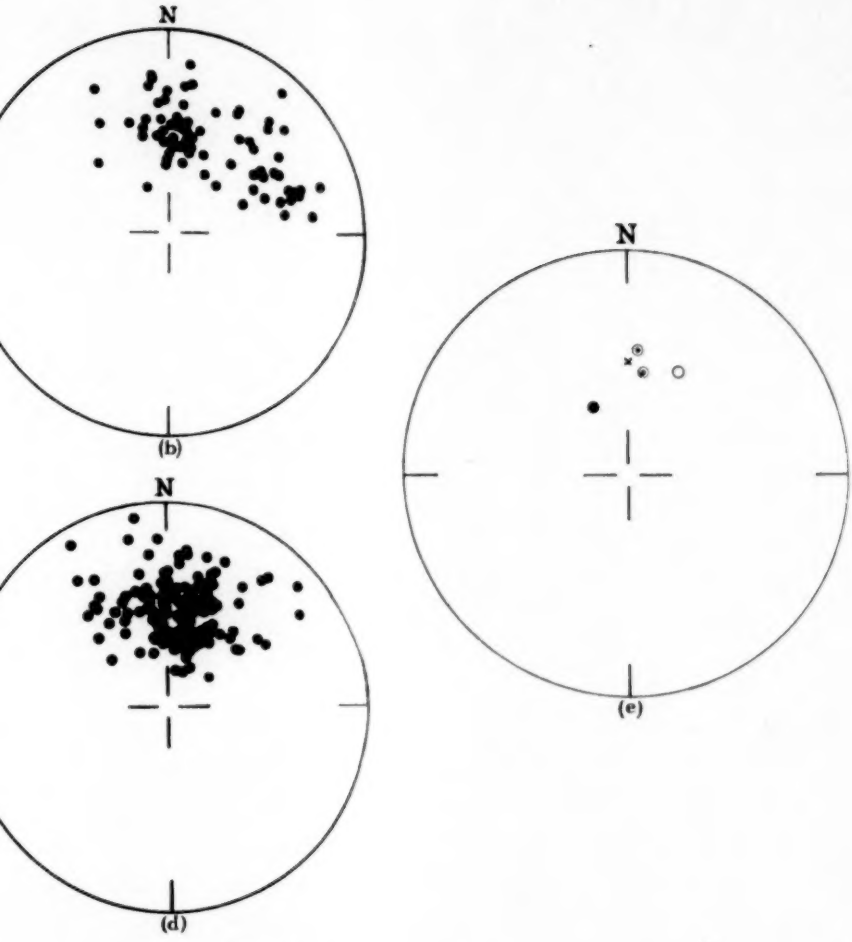

of n.r.m. for rocks of Pre-Tertiary age from north-
t parts of Japan (a and b), directions for rocks of
ernary age from north-east and south-west Japan
directions for the four groups (e).

of the n.r.m. of Pre-Tertiary rocks from north-eastern

n of the n.r.m. of Pre-Tertiary rocks from south-
f Japan.

n of the n.r.m. of Tertiary and Quaternary rocks
tern part of Japan.

n of the n.r.m. of Tertiary and Quaternary rocks
stern part of Japan.

he present dipole field for Japan.

[*Facing page 126*

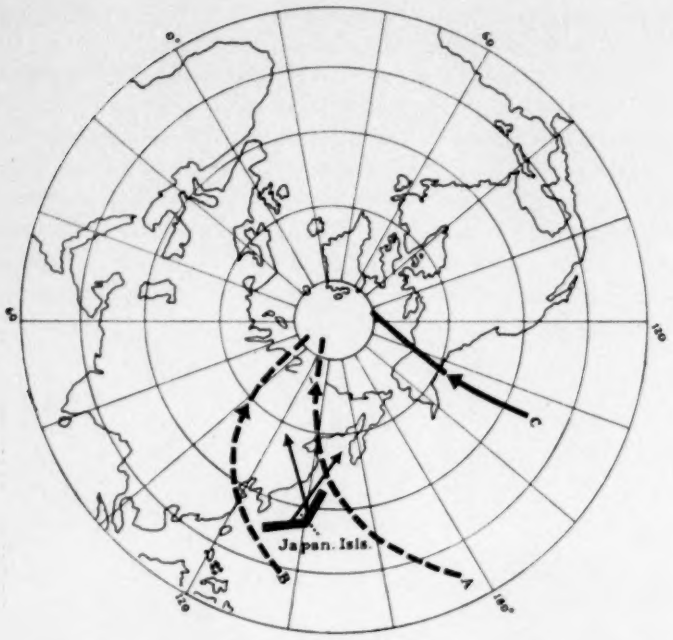

FIG. 8.—Schematic diagram of the bending of the Japanese Islands in relation to the hypothesis of polar wandering. (A) Polar wander path as deduced for North America (B) Polar wander curve as deduced for Europe and (C) polar wander curve as deduced for Japan.

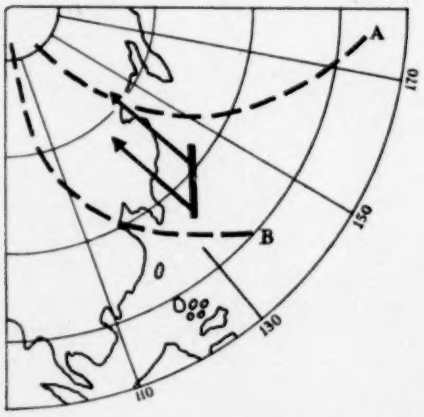

FIG. 9.—A possible interpretation of the direction of magnetization in Pre-Tertiary times by correcting for the bending of the Japanese Islands.

Tamaki (1955) in an analysis of earthquake data has shown the existence of high density material near the Izu Peninsula, that is, near the "fossa magna". This high density sector may be considered to be a mass of basic rocks intruded into the fracture zones which resulted from the bending of the Japanese Islands along this line. Further, Ehara (1961) found gabbro and granodiorite associated with the andesitic magma extruded at Oshima Island confirming the existence of high density material. The region is also associated with positive gravity anomalies (Matsuyama 1936, and Kumagai 1940 and 1953).

Two lines, AA′ and BB′ in Figure 7 represent the mean axes of south-west and north-east Japan respectively. The angle between these lines (θ) is approximately equal to the difference in the mean directions of magnetization for rocks of pre-Tertiary age collected from these two parts of Japan. It is suggested that the difference in direction of magnetization for rocks from north-east and south-west of Japan is due to the bending of the Japanese Islands along the line of the "fossa magna" and in agreement with the geological evidence. Further, it is possible to infer from the rock magnetism data that the bending took place in early Tertiary times.

4. Implications for studies of polar wandering

In view of this rotational movement of the different parts of the Japanese Islands, it is very difficult to infer the position of the geomagnetic pole with respect to Japan for pre-Tertiary times. If the amount of polar wander between the Mesozoic and early Tertiary is assumed to be small, it is possible to infer that the amount of relative rotation of north-east and south-west Japan is of the order of 40°.

The polar wander curve for Japan as deduced by Nagata & others (1959) differs greatly from those deduced for Europe and North America by Creer & others (1954) and by Runcorn (1959) as shown in Figure 8. The discrepancy might be considerably reduced if the bending of the Japanese Islands is taken into consideration. Figure 9 shows one possible interpretation of removing the effect of the bending of the Japanese Islands and the difficulty of defining the polar wander curve for Japan in pre-Tertiary times.

5. Acknowledgments

The authors wish to thank Professor N. Kumagai of Kyoto University for his continuous encouragement throughout this study. Their thanks are also due to Dr R. W. Girdler of Durham University for his kind suggestions and correction of English.

Physics Dept., King's College,
University of Durham,
Newcastle-upon-Tyne:
1960 *December.*

References

Creer, K. M., Irving E., & Runcorn, S. K., 1954. *J. Geomag. & Geoelect.*, **6**, 163.
Ehara, S., 1961. *Geogr. Rev., Jap.*, **34**, 1.
Fisher, Sir Ronald, 1953. *Proc. Roy. Soc. A*, **217**, 295.
Kawai, N., 1951. *J. Geophys. Res.*, **56**, 73.
Kumagai, N., 1940. *Jap. J. Astron. Geophys.* **17**, 477.
Kumagai, N., 1953. *Rep. Jap. Geod. Commis.*, No. 4.
Matsuyama, M., 1936. *Proc. Imp. Acad. Jap.*, **12**, 93.
Nagata, T., Akimoto, S., Shimizu, Y., Kobayashi, K. and Kuno, H., 1959. *Proc. Jap. Acad.*, **35**, 378.
Runcorn, S. K., 1959. *Science*, **129**, 1002.
Tamaki, I., 1955. *Zisin*, **7**, 226.

Geophysical Journal

RECOMMENDATIONS TO AUTHORS

1. Authors are advised to follow the general suggestions for the preparation of scientific papers given in *Notes on the preparation of papers to be communicated to the Royal Society* and in *The printing of mathematics* by T. W. Chaundy, P. R. Barrett and C. Batey (Oxford University Press, 1954). In particular the abbreviations for the names of periodicals used in the *Geophysical Journal* are those given in *Notes on the preparation of papers . . .* and the symbols, signs and abbreviations are those recommended for British scientific publications by the Symbols Committee of the Royal Society.

2. Papers should be typewritten with double spacing and on one side of the paper only. Two copies, one of them the top copy, should be submitted. All papers must be accompanied by a summary; summaries are not required for *Letters to the Editor*.

3. Tables are printed without rules. They should be numbered serially with Arabic numerals. Table headings should be brief. Units should be placed at the head of the column. Tables should be typed on separate sheets and their positions in the text indicated on the copy.

4. Illustrations, especially photographs, should be kept to a minimum, and the same information should not in general be given in both tables and illustrations. Line drawings should be in dense black ink on smooth white board or transparent tracing film. Original drawings must not be lettered; lettering should be indicated on copies or photoprints which must be supplied in addition to the originals. Wherever possible, lettering should be kept outside the diagram so that it may be set in type. Diagrams should be drawn at twice to three times the size at which they will be printed. The maximum dimensions for diagrams, when reduced and with their lettering and captions, are 8 in by 5 in. A wide variety of flat tints of dots, lines and shadings can be applied to line drawings by the blockmaker. Photographs for reproduction should be unmounted glossy prints and should be accompanied by lettered prints.

5. References should be quoted in the form recommended by the Royal Society but authors may also quote titles of papers if they wish. References in the text are made in the form (Smith 1949).

6. Authors whose work involves much mathematics should answer carefully the recommendations in *The Printing of Mathematics*.

7. The Editors will be glad to advise authors on any special points of difficulty arising in the preparation of papers for the Journal.

References

Creer, K. M., Irving E., & Runcorn, S. K., 1954. *J. Geomag. & Geoelect.*, **6**, 163.
Ehara, S., 1961. *Geogr. Rev., Jap.*, **34**, 1.
Fisher, Sir Ronald, 1953. *Proc. Roy. Soc. A*, **217**, 295.
Kawai, N., 1951. *J. Geophys. Res.*, **56**, 73.
Kumagai, N., 1940. *Jap. J. Astron. Geophys.* **17**, 477.
Kumagai, N., 1953. *Rep. Jap. Geod. Commis.*, No. 4.
Matsuyama, M., 1936. *Proc. Imp. Acad. Jap.*, **12**, 93.
Nagata, T., Akimoto, S., Shimizu, Y., Kobayashi, K. and Kuno, H., 1959. *Proc. Jap. Acad.*, **35**, 378.
Runcorn, S. K., 1959. *Science*, **129**, 1002.
Tamaki, I., 1955. *Zisin*, **7**, 226.

Geophysical Journal

RECOMMENDATIONS TO AUTHORS

1. Authors are advised to follow the general suggestions for the preparation of scientific papers given in *Notes on the preparation of papers to be communicated to the Royal Society* and in *The printing of mathematics* by T. W. Chaundy, P. R. Barrett and C. Batey (Oxford University Press, 1954). In particular the abbreviations for the names of periodicals used in the *Geophysical Journal* are those given in *Notes on the preparation of papers* . . . and the symbols, signs and abbreviations are those recommended for British scientific publications by the Symbols Committee of the Royal Society."

2. Papers should be typewritten with double spacing and on one side of the paper only. Two copies, one of them the top copy, should be submitted. All papers must be accompanied by a summary; summaries are not required for *Letters to the Editors*.

3. Tables are printed without rules. They should be numbered serially with Arabic numerals. Table headings should be brief. Units should be placed at the head of the column. Tables should be typed on separate sheets and their positions in the text indicated on the copy.

4. Illustrations, especially photographs, should be kept to a minimum, and the same information should not in general be given in both tables and illustrations. Line drawings should be in dense black ink on smooth white board or transparent tracing film. Original drawings must not be lettered; lettering should be indicated on copies or photoprints which must be supplied in addition to the originals. Wherever possible, lettering should be kept outside the diagram so that it may be set in type. Diagrams should be drawn at twice to three times the size at which they will be printed. The maximum dimensions for diagrams, when reduced and with their lettering and captions, are 8 in by 5 in. A wide variety of flat tints of dots, lines and shadings can be applied to line drawings by the blockmaker. Photographs for reproduction should be unmounted glossy prints and should be accompanied by lettered prints.

5. References should be quoted in the form recommended by the Royal Society but authors may also quote titles of papers if they wish. References in the text are made in the form (Smith 1940).

6. Authors whose work involves much mathematics should answer carefully the recommendations in *The Printing of Mathematics*.

7. The Editors will be glad to advise authors on any special points of difficulty arising in the preparation of papers for the *Journal*.